NASA NAG5-760 Final Report

Satellite Laser Ranging and Gravity Field Modeling Accuracy

George W. Rosborough*

Abstract

Gravitational field mismodeling produces errors in the estimated orbital motion of near Earth satellites. This effect is studied using a linear perturbation approach following the analysis of Kaula. The perturbations in the orbital position as defined by either orbital elements or Cartesian components are determined. From these perturbations it is possible to ascertain the expected signal due to gravitational mismodeling that would be present in station-to-satellite laser ranging measurements. This expected signal has been estimated for the case of the Lageos satellite and using the predicted uncertainties of the GEM-T1 and GEM-T2 gravity field models. The results indicate that observable signal still exists in the laser range residuals given the current accuracy of the range measurements and the accuracy of the gravity field models.

*Department of Aerospace Engineering Sciences, Campus Box 429, University of Colorado, Boulder, Colorado 80309

1 Introduction

Satellites in Earth orbit are affected by a wide range of gravitational and non-gravitational perturbations. An accurate modeling of these perturbations is required if the full scientific benefits of geodetic satellites, such as Lageos, are to be obtained. This modeling is sometimes limited by a lack of understanding of the physical processes producing the perturbations, but it is more often limited by the accuracy of the parameters that are needed in the model definition. A particular example of this latter scenario is the modeling of the Earth's gravity field. The mathematical form of the gravitational perturbation due to the Earth is well defined (using spherical harmonics) but the constants used in the model are of varying accuracy. This leads to a mismodeling of the gravitational effect and a resulting mismodeling of the predicted satellite motion. This mismodeling is observable if accurate tracking measurements of the satellite exist; such as laser range tracking.

To ascertain the level of mismodeling of the gravity field existing in current models, a linear perturbation analysis has been applied. This approach makes it possible to predict the expected magnitude of orbit error due to gravity field modeling error and it also has been extended to determine the expected signal that would be observed with laser range tracking.

The application of using spherical harmonics for modeling the Earth's gravity field is first summarized. This is followed by a discussion of satellite dynamics and the resulting orbital motion due to the presence of a nonspherical gravity field. The perturbation approach, based on the method of Kaula, is then presented. Perturbations in orbital elements and satellite position are included. From these results, the expected perturbation in a station-to-satellite range measurement is then derived. These linear perturbation results facilitate a covariance analysis based on the expected uncertainties of present day gravity field models. Numerical results are presented for the case of the Lageos satellite and the GEM-T1 and GEM-T2 gravity field models.

2 Gravitational Field

2.1 Spherical Harmonic Model

The common approach for modeling the gravitational field of a planetary body is through the spherical harmonic representation,

$$U = \frac{\mu}{r} \sum_{\ell=0}^{\infty} \left(\frac{a_e}{r}\right)^{\ell} \sum_{m=0}^{\ell} P_{\ell m}(\sin\phi) \left[C_{\ell m} \cos m\lambda + S_{\ell m} \sin m\lambda\right] \tag{1}$$

where: μ is the product of the universal constant of gravitation G and the mass of the Earth M; a_e is the semi-major axis of the Earth's reference ellipsoid; r, ϕ, λ are the satellite distance, latitude, and longitude, respectively, in a body-fixed coordinate system; $C_{\ell m}$, $S_{\ell m}$ are spherical harmonic coefficients of degree ℓ and order m; and $P_{\ell m}$ are the Associated Legendre Functions of degree ℓ and order m. A gravitational model consists of a set of constants that specify μ, a_e and the $C_{\ell m}$, $S_{\ell m}$ coefficients. It should also be noted that such a set of constants also implicitly defines a body-fixed coordinate system. The coordinate system defined is precisely that which was used in the solution of the spherical harmonic coefficients.

This representation of the geopotential can be thought of as consisting of three constituent parts,

$$U = U_0 + U_1 + U_2 \tag{2}$$

The first part is simply the leading term of the expansion corresponding to the degree and order zero term. The Associated Legendre Function, P_{00} has a value of one as does the C_{00} coefficient. So the leading term is simply,

$$U_0 = \frac{\mu}{r} \tag{3}$$

This is the familiar potential resulting from treating the body as point mass and that used for deriving the fundamental results of two body motion.

The second part of the spherical harmonic representation are those terms (besides the above two body term) which do not have a longitude dependence. These are the terms corresponding to $m = 0$ and are denoted as the zonal contribution to the potential,

$$U_1 = \frac{\mu}{r} \sum_{\ell=1}^{\infty} \left(\frac{a_e}{r}\right)^{\ell} P_{\ell,0}(\sin\phi) C_{\ell,0} \tag{4}$$

The degree 2 zonal term models the contribution due to the planetary oblateness. As such, it is the second largest contributor to the overall potential following the central body contribution. (The degree 1 term is zero assuming that the center of the Earth-fixed coordinate system coincides with the center of mass of the Earth.) The notation J_ℓ is often used for the zonal coefficients instead of the above $C_{\ell,0}$. The two notations simply differ in sign,

$$J_\ell = -C_{\ell,0} \tag{5}$$

so that the zonal part of the potential could also be written in the form,

$$U_1 = -\frac{\mu}{r}\sum_{\ell=1}^{\infty}\left(\frac{a_e}{r}\right)^{\ell} P_{\ell,0}(\sin\phi)J_\ell \tag{6}$$

The C notation will be used throughout this report.

The remaining part of the spherical harmonic representation is that part depending on longitude,

$$U_2 = \frac{\mu}{r}\sum_{\ell=1}^{\infty}\left(\frac{a_e}{r}\right)^{\ell}\sum_{m=1}^{\ell} P_{\ell m}(\sin\phi)\left[C_{\ell m}\cos m\lambda + S_{\ell m}\sin m\lambda\right] \tag{7}$$

The largest longitudinal contributor to the potential is usually the degree 2 and order 2 terms. These terms represent the amount that the planet is "out of round" about the equator. (As with the degree 1 zonal coefficient, the degree 1 and order 1 coefficients will be zero under the assumption that the center of the coordinate system coincides with the center of mass.)

The spherical harmonic representation of the potential (equation (1)) can then also be written as,

$$\begin{aligned} U &= \frac{\mu}{r} \\ &+ \frac{\mu}{r}\sum_{\ell=1}^{\infty}\left(\frac{a_e}{r}\right)^{\ell} P_{\ell,0}(\sin\phi)C_{\ell,0} \\ &+ \frac{\mu}{r}\sum_{\ell=1}^{\infty}\left(\frac{a_e}{r}\right)^{\ell}\sum_{m=1}^{\ell} P_{\ell m}(\sin\phi)\left[C_{\ell m}\cos m\lambda + S_{\ell m}\sin m\lambda\right] \end{aligned} \tag{8}$$

In the general case, where temporal variations in the potential exist (e.g., tides), the spherical harmonic representation is still valid though the geopotential coefficients ($C_{\ell m}$, $S_{\ell m}$) then become time dependent.

2.2 Normalized Spherical Harmonic Model

The spherical harmonic coefficients ($C_{\ell m}$, $S_{\ell m}$) appearing in equation (1) are unnormalized. These coefficients tend to very small values as the degree increases. This is partly a consequence of the nature of the Earth's gravity field but is for the most part due to the fact that the Associated Legendre Functions tend to large values as degree increases. Thus it is numerically advantageous to normalize the Associated Legendre Functions and the coefficients. The normalization is achieved by multiplying the Legendre functions by a scale factor depending on the degree and order of the function. The resulting normalized Associated Legendre Functions maintain the same magnitude with increasing degree. Denoting normalized values by an overbar, the normalized Associated Legendre Functions are,

$$\bar{P}_{\ell m} = \left[(2-\delta_{m0})(2\ell+1)\frac{(\ell-m)!}{(\ell+m)!}\right]^{1/2} P_{\ell m} \tag{9}$$

where the Kronecker delta, δ_{m0}, is equal to 1 if m is zero and equal to 0 if m is greater than zero. The geopotential coefficients, $C_{\ell m}$ and $S_{\ell m}$, are normalized by the inverse of this scale factor,

$$\left\{ \begin{array}{c} \bar{C}_{\ell m} \\ \bar{S}_{\ell m} \end{array} \right\} = \left[\frac{1}{(2-\delta_{m0})(2\ell+1)} \frac{(\ell+m)!}{(\ell-m)!} \right]^{1/2} \left\{ \begin{array}{c} C_{\ell m} \\ S_{\ell m} \end{array} \right\} \tag{10}$$

The spherical harmonic expansion of the geopotential (equation (1)) can now be written in terms of normalized quantities,

$$U = \frac{\mu}{r} \sum_{\ell=0}^{\infty} \left(\frac{a_e}{r} \right)^{\ell} \sum_{m=0}^{\ell} \bar{P}_{\ell m}(\sin\phi) \left[\bar{C}_{\ell m} \cos m\lambda + \bar{S}_{\ell m} \sin m\lambda \right] \tag{11}$$

This is usually the preferred formulation for numerical implementations of the spherical harmonic representation. For some analytical developments it is simpler to work with the unnormalized form (equation (1)).

2.3 Earth Gravity Field Model

Numerous spherical harmonic models of the Earth's gravity field have been developed. These models are primarily based on the Earth-based tracking of low-Earth orbit satellites. Other data types that are valuable in estimating the Earth's gravity field include surface gravity measurements, satellite-to-satellite tracking and more recently, satellite radar-altimeter measurements of the ocean surface. The maximum degree (ℓ) of the spherical harmonic representations of the Earth is more than 300 in some models. Models based solely on satellite tracking data usually have a maximum degree of approximately 50. Indeed, for most satellite applications, high degree models are not needed due to the insensitivity of the satellite motions to the small scale features represented in such models.

A good general purpose model for satellite applications is the GEM-T1 model developed at the NASA Goddard Space Flight Center (GSFC) [*Marsh et al.*, 1988]. This model is based solely on the tracking data of Earth satellites and is complete to degree and order 36. The accuracy of this model is greatly improved with respect to earlier Goddard Earth Models (GEM). In addition to estimating the spherical harmonic coefficients of the gravity field, GSFC also estimates the accuracy of those coefficients. Such accuracy estimates are very valuable when attempting to estimate the orbit error which may be induced when using the model for orbit propagation.

The GEM-T1 model was followed in development by the GEM-T2 model [*Marsh et al.*, 1990]. This model was a result of continual refinement in analysis techniques as well as the inclusion of more and newer observations. The GEM-T2 model is similar to the GEM-T1 model in that it is based solely on the analysis of satellite tracking data. The GEM-T1 and GEM-T2 models were the primary models used in the analyses presented here.

Table 1. The GEM-T1 Gravity Model.
Normalized Zonals $\bar{C}_{\ell 0}$ in units of 1×10^{-9}

ℓ	m	$\bar{C}_{\ell m}$	σ	ℓ	m	$\bar{C}_{\ell m}$	σ	ℓ	m	$\bar{C}_{\ell m}$	σ
2	0	−484164.97	0.4	14	0	−19.73	4.0	26	0	1.84	4.7
3	0	957.24	0.1	15	0	1.87	4.1	27	0	4.12	4.3
4	0	538.73	1.1	16	0	−9.38	4.5	28	0	−5.85	5.0
5	0	68.78	0.3	17	0	20.40	4.0	29	0	−3.91	4.7
6	0	−148.10	1.5	18	0	11.29	4.1	30	0	−0.27	4.6
7	0	90.53	0.8	19	0	−4.61	3.4	31	0	5.12	4.7
8	0	45.90	2.4	20	0	15.31	5.1	32	0	0.08	4.6
9	0	28.38	1.5	21	0	9.78	2.8	33	0	2.23	4.5
10	0	57.22	2.6	22	0	−4.84	4.8	34	0	−2.48	4.0
11	0	−51.26	2.5	23	0	−24.13	2.6	35	0	1.27	4.7
12	0	32.08	3.5	24	0	−0.96	4.9	36	0	0.74	4.1
13	0	42.23	3.5	25	0	6.89	3.4				

The GEM-T1 normalized zonal coefficients, complete to degree 36, are given in Table 1. The nonzonal coefficients are listed in Table 2. Along with the coefficient values in each table, the estimated uncertainty (σ) of the individual coefficients is also given. The gravitational constant and equatorial radius specified for the GEM-T1 model are,

$$\mu = GM = 3.98600436 \times 10^{14}\ \mathrm{m}^3/\mathrm{s}^2 \quad \text{and} \quad a_e = 6378137.\ \mathrm{m} \tag{12}$$

Several points can be made by examining the coefficient values and their uncertainties. Foremost, the value of the second degree zonal coefficient is seen to be more than two orders of magnitude larger than any other coefficient. The next largest coefficients are those of degree 2 and order 2. Analogous to the second degree zonal which represents the oblateness of the Earth, these coefficients correspond to the ellipticity about the equator.

Also evident is that the magnitude of the coefficients decreases significantly as the degree increases (keep in mind that these are normalized coefficients and effectively have equal weight in their total contribution to the gravitational potential). This characteristic has been formalized in the so-called "Kaula's Rule" [*Kaula* 1966]. This rule gives the expected size of the Earth's normalized harmonic coefficients of degree ℓ to be $\pm 10^{-5}/\ell^2$. This rule of thumb allows one to estimate the expected magnitude of a gravitational coefficient if a value is not otherwise known (this is particularly convenient for higher degree coefficients for which accurate estimates have generally not been obtained). The magnitude of the GEM-T1 coefficients (complete to degree and order 36) are plotted in Figure 1 along with Kaula's Rule.

The estimated accuracy of the various coefficients shown in Tables 1 and 2 show that the lower degree coefficients are the best determined and the accuracy degrades as the degree increases. This variation in accuracy is a reflection of the fact that satellite tracking data was used to solve for the coefficients. As discussed in later sections, the sensitivity of the satellites to the harmonic coefficients decreases as the degree increases. That is, the low degree coefficients produce large perturbations to the orbital motion and the high degree coefficients produce much smaller perturbations. The ability to recover high degree coefficients is a direct function of the accuracy of

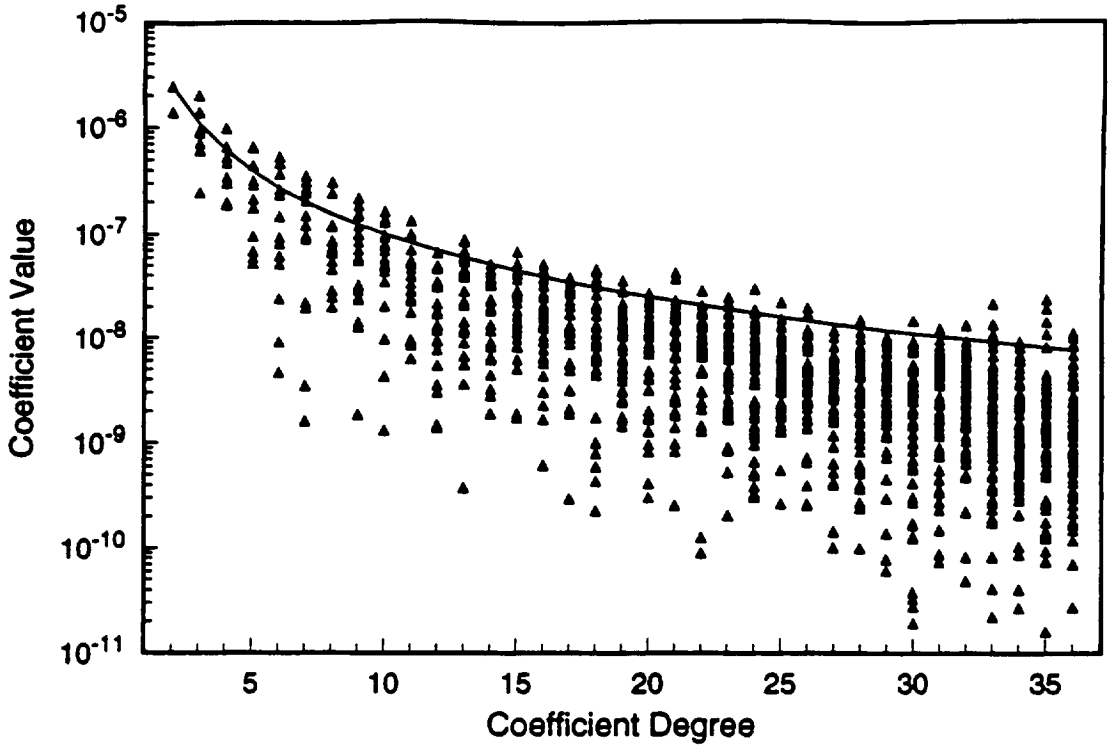

Figure 1: Absolute value of the normalized GEM-T1 coefficients and Kaula's Rule.

the tracking data being utilized and also the geographic distribution of that data. Since the high degree coefficients represent fine scale features in the gravity field it is necessary to have wide geographic coverage, and accurate tracking data, to completely capture such details. The low degree coefficients on the other hand represent the large scale features (continental in size) and it is possible to accurately model such details given sparser geographic coverage.

Overall, the accuracy of the geopotential acceleration is dependent on the constants μ, $\bar{C}_{\ell m}$ and $\bar{S}_{\ell m}$ and the accuracy of the coordinate transformation from body-fixed to inertial coordinates. The accuracy is also clearly dependent on the degree of truncation of the infinite series describing the potential. It should be noted that the quantity a_e enters the potential strictly as a scaling factor and thus does not affect the accuracy of the geopotential computation. Of these possible error sources, the accuracy of the $\bar{C}_{\ell m}$ and $\bar{S}_{\ell m}$ coefficients is currently the limiting factor in precise low-Earth orbit determination.

Table 2. The GEM-T1 Gravity Model. Normalized Sectorials and Tesserals $\bar{C}_{\ell m}$ and $\bar{S}_{\ell m}$ in units of 1×10^{-9}

ℓ	m	$\bar{C}_{\ell m}$	σ	$\bar{S}_{\ell m}$	σ
3	1	2029.77	1.0	249.59	1.1
4	1	−533.43	.9	−475.12	.8
5	1	−58.95	2.5	−95.54	2.8
6	1	−81.38	1.8	23.89	1.7
7	1	277.10	3.9	97.82	4.2
8	1	28.86	3.1	54.72	3.0
9	1	148.04	5.8	24.53	6.0
10	1	76.97	4.4	−138.11	4.3
11	1	9.50	7.0	−27.81	6.6
12	1	−49.26	5.6	−49.65	5.6
13	1	−54.06	6.9	43.46	6.0
14	1	−18.75	6.3	23.22	6.7
15	1	8.29	6.5	14.21	6.5
16	1	31.71	6.2	17.35	6.9
17	1	−30.94	8.0	−26.85	9.0
18	1	−.23	6.1	−45.61	6.8
19	1	−11.59	8.9	5.38	10.2
20	1	14.51	6.7	−21.27	6.9
21	1	−15.39	9.2	41.75	9.6
22	1	8.39	7.5	−14.72	7.3
23	1	.87	8.5	14.60	8.4
24	1	8.12	7.3	−29.20	7.2
25	1	3.71	7.7	4.35	7.6
26	1	4.97	6.9	−17.25	6.8
27	1	.52	7.5	6.61	7.4
28	1	6.53	7.0	−10.03	6.6
29	1	3.47	7.0	2.42	7.0
30	1	−1.62	6.4	−9.09	6.3
31	1	5.18	6.8	2.38	6.6
32	1	−9.15	6.0	−9.25	5.9
33	1	1.27	5.8	2.13	5.7
34	1	−1.56	5.6	−9.10	5.5
35	1	−1.91	5.6	2.01	5.6
36	1	2.88	5.2	−5.84	5.2
3	3	720.99	1.2	1413.17	1.2
4	3	990.98	.9	−200.62	.9
5	3	−448.20	2.0	−215.14	2.1
6	3	61.97	2.5	4.64	2.6
7	3	250.74	4.1	−209.16	4.3
8	3	−19.97	4.6	−86.94	4.7
9	3	−155.37	6.6	−84.02	7.0
10	3	1.31	7.1	−161.48	7.5
11	3	−28.89	8.3	−132.50	8.6
12	3	32.42	8.7	17.94	9.5
13	3	−14.03	8.4	83.66	8.8
14	3	36.93	9.0	22.42	9.6
15	3	44.63	9.2	26.54	9.8
16	3	−32.08	8.3	−45.03	8.5
17	3	10.12	10.9	9.89	11.3
18	3	−1.00	9.6	−7.05	9.6
19	3	1.44	11.0	14.20	11.3
20	3	8.27	10.6	13.72	10.6
21	3	1.99	11.0	22.69	11.0
22	3	6.73	10.2	−8.09	10.4
23	3	−4.56	10.2	−11.95	10.3
24	3	6.91	9.4	−10.59	9.5
25	3	−3.26	9.2	−3.11	9.2
26	3	−.26	8.7	−3.72	8.8
27	3	−5.10	8.7	−1.86	8.7
28	3	−.26	8.1	1.17	8.1
29	3	−4.39	7.8	−1.76	7.9
2	2	2438.93	.3	−1399.84	.3
3	2	903.55	1.1	−620.42	1.2
4	2	347.00	1.5	664.03	1.5
5	2	655.79	2.5	−323.41	2.9
6	2	51.61	3.2	−375.00	3.2
7	2	317.71	4.4	91.61	5.2
8	2	70.38	5.2	68.45	5.1
9	2	31.14	5.9	−32.39	7.4
10	2	−80.52	6.7	−51.34	6.7
11	2	9.05	7.2	−99.24	9.0
12	2	7.64	7.0	34.92	6.9
13	2	53.44	8.7	−57.58	10.3
14	2	−34.81	7.1	−6.07	7.2
15	2	−21.63	9.5	−36.44	10.5
16	2	−15.64	9.0	24.54	9.3
17	2	−5.78	8.8	17.12	9.3
18	2	8.41	9.9	16.84	10.5
19	2	8.44	9.0	−10.47	9.4
20	2	19.88	9.6	3.23	9.9
21	2	.99	9.2	−2.61	9.3
22	2	−14.29	8.7	2.10	8.9
23	2	−.53	9.5	−1.78	9.5
24	2	−5.85	8.6	5.20	8.6
25	2	3.72	9.3	5.21	9.4
26	2	−5.29	8.3	.25	8.3
27	2	10.22	8.3	−2.82	8.4
28	2	−8.43	7.5	−11.55	7.6
29	2	9.46	7.6	−4.33	7.7
30	2	−4.05	7.0	−5.36	7.2
31	2	6.60	6.8	.84	6.8
32	2	1.86	6.4	4.37	6.5
33	2	−1.02	6.3	.95	6.3
34	2	3.58	5.9	5.18	5.9
35	2	−2.55	5.6	1.03	5.6
36	2	.18	5.3	1.29	5.3
4	4	−190.03	.9	308.46	.9
5	4	−294.82	1.7	52.41	1.7
6	4	−92.80	1.9	−473.31	1.9
7	4	−273.74	3.1	−122.02	3.1
8	4	−246.06	3.6	67.75	3.7
9	4	−12.83	5.7	23.26	5.5
10	4	−97.31	6.0	−69.38	6.3
11	4	−33.21	8.9	−70.00	8.7
12	4	−65.30	8.5	−3.01	8.9
13	4	−8.82	10.8	−.37	10.4
14	4	−8.83	10.2	1.88	10.7
15	4	−44.38	10.5	12.64	10.1
16	4	36.51	10.5	43.86	11.0
17	4	12.59	10.2	31.22	10.0
18	4	43.42	9.0	6.09	9.4
19	4	2.57	10.7	7.67	10.8
20	4	−1.80	9.2	.83	9.6
21	4	−.25	10.3	6.99	10.4
22	4	−9.45	9.7	16.71	9.8
23	4	−10.03	9.9	−1.67	9.9
24	4	6.06	9.5	18.11	9.7
25	4	6.35	9.7	−1.53	9.7
26	4	5.32	8.9	4.90	9.1
27	4	2.92	8.8	−.64	8.7
28	4	2.88	8.1	−2.49	8.1
29	4	−6.36	7.9	.73	7.8

Table 2. Continued.

ℓ	m	$\bar{C}_{\ell m}$	σ	$\bar{S}_{\ell m}$	σ	ℓ	m	$\bar{C}_{\ell m}$	σ	$\bar{S}_{\ell m}$	σ
30	3	−1.61	7.3	1.48	7.2	30	4	−2.11	7.4	−3.92	7.4
31	3	−1.87	7.1	−4.08	7.1	31	4	−4.95	7.0	−1.64	7.0
32	3	−.67	6.6	3.00	6.6	32	4	2.02	6.6	−3.38	6.6
33	3	−1.70	6.3	−2.88	6.3	33	4	−.24	6.4	.39	6.4
34	3	−.51	5.9	2.21	5.9	34	4	2.85	6.0	−1.88	6.0
35	3	.67	5.7	.69	5.7	35	4	2.74	5.7	1.49	5.7
36	3	−.81	5.4	−1.39	5.4	36	4	1.32	5.4	−.12	5.4
5	5	177.76	2.2	−666.03	2.3						
6	5	−265.76	1.3	−537.75	1.3	6	6	9.06	.8	−236.33	.8
7	5	3.47	2.7	19.65	2.8	7	6	−357.85	.5	150.92	.5
8	5	−24.93	2.8	85.30	2.8	8	6	−66.42	2.0	312.83	1.9
9	5	−14.11	4.3	−60.06	4.4	9	6	70.53	3.2	216.63	3.2
10	5	−50.44	5.3	−43.83	5.5	10	6	−34.74	3.5	−77.72	3.3
11	5	45.91	6.9	55.28	7.3	11	6	8.47	5.0	24.29	5.1
12	5	30.60	8.0	−1.47	8.1	12	6	1.39	6.2	45.83	6.1
13	5	59.62	10.0	57.45	10.5	13	6	−22.39	7.7	−11.84	7.7
14	5	22.80	10.1	−11.61	10.1	14	6	−3.19	9.2	6.51	9.1
15	5	16.07	11.5	10.89	12.1	15	6	27.23	10.5	−51.71	10.4
16	5	−7.72	11.3	−1.68	10.9	16	6	17.99	11.1	−26.78	11.0
17	5	−11.15	10.6	−5.60	11.2	17	6	.29	12.2	−30.42	12.0
18	5	1.74	11.7	21.13	11.4	18	6	31.20	11.0	−8.56	11.0
19	5	−2.45	10.7	17.38	10.8	19	6	−6.25	11.1	3.92	10.8
20	5	−10.42	10.9	.30	10.7	20	6	12.76	10.6	.97	10.6
21	5	17.76	11.1	−15.89	11.2	21	6	4.21	10.1	−8.35	10.0
22	5	−4.63	10.5	−.13	10.5	22	6	14.63	9.7	2.43	9.8
23	5	1.99	10.8	−7.94	10.8	23	6	10.00	9.7	4.96	9.5
24	5	−14.08	9.7	−7.98	9.7	24	6	−.31	9.5	−.66	9.6
25	5	−2.46	9.5	−2.35	9.6	25	6	5.94	9.6	−6.74	9.5
26	5	4.30	8.9	10.65	8.9	26	6	8.54	9.0	3.20	9.1
27	5	−1.59	8.7	3.71	8.7	27	6	1.77	8.8	−2.13	8.8
28	5	2.92	8.3	−.24	8.2	28	6	−8.33	8.1	2.00	8.1
29	5	3.45	7.9	3.54	7.9	29	6	−.30	7.8	−2.47	7.8
30	5	3.39	7.4	.70	7.4	30	6	−3.22	7.4	4.17	7.4
31	5	.91	7.1	1.46	7.1	31	6	−.56	7.0	.77	7.0
32	5	−.05	6.7	−2.79	6.7	32	6	−3.83	6.6	.22	6.6
33	5	−.51	6.3	3.24	6.3	33	6	1.38	6.4	−1.25	6.3
34	5	−1.30	6.0	.04	6.0	34	6	.58	6.0	−.32	6.0
35	5	−.24	5.7	−.74	5.7	35	6	.83	5.7	−1.48	5.7
36	5	−1.18	5.4	.34	5.4	36	6	−.58	5.4	−.90	5.4
7	7	1.60	2.1	22.00	2.0						
8	7	70.42	1.9	74.86	1.9	8	8	−118.88	3.9	122.33	3.8
9	7	−118.62	3.5	−100.55	3.3	9	8	184.50	3.2	−1.85	3.2
10	7	9.75	3.4	−4.29	3.5	10	8	43.75	3.0	−92.48	2.9
11	7	9.61	4.4	−91.89	4.3	11	8	−6.35	4.1	22.58	4.0
12	7	−12.70	5.2	34.83	5.3	12	8	−21.22	3.0	16.90	3.1
13	7	3.57	6.5	−6.62	6.3	13	8	−12.30	5.0	−11.09	5.0
14	7	37.48	7.4	−4.36	7.6	14	8	−32.94	5.1	−13.18	5.0
15	7	66.71	8.8	11.45	8.8	15	8	−40.67	6.7	24.73	6.7
16	7	3.05	10.1	−9.07	10.1	16	8	−13.44	8.0	2.28	7.9
17	7	22.95	10.4	−11.98	10.5	17	8	31.16	9.2	8.77	9.2
18	7	−.80	11.3	6.72	11.3	18	8	45.72	10.8	.43	10.5
19	7	5.14	11.5	−1.66	11.5	19	8	14.86	10.6	−11.33	10.5
20	7	−7.79	11.4	4.90	11.4	20	8	−2.01	10.8	−1.29	10.8
21	7	−12.23	10.8	−1.41	10.7	21	8	−18.10	10.7	2.52	10.6
22	7	12.75	11.1	1.30	11.1	22	8	−9.82	10.2	−6.83	10.1
23	7	−2.33	10.4	2.65	10.3	23	8	4.22	9.6	−6.80	9.5
24	7	−2.51	10.0	5.07	9.9	24	8	−2.43	9.7	7.56	9.7
25	7	.26	9.5	3.46	9.4	25	8	1.43	9.1	−4.12	9.1
26	7	5.45	8.9	2.58	8.9	26	8	3.09	9.1	−2.14	9.1
27	7	6.93	8.5	−2.82	8.4	27	8	−4.18	8.7	−4.41	8.7
28	7	−4.65	8.2	−1.54	8.2	28	8	−.57	8.2	−3.18	8.1
29	7	1.18	7.9	−7.29	7.8	29	8	−6.42	7.7	2.54	7.7

Table 2. Continued.

ℓ	m	$\bar{C}_{\ell m}$	σ	$\bar{S}_{\ell m}$	σ	ℓ	m	$\bar{C}_{\ell m}$	σ	$\bar{S}_{\ell m}$	σ
30	7	−.17	7.3	−.13	7.3	30	8	2.95	7.4	.57	7.3
31	7	1.48	7.0	−1.75	7.0	31	8	.09	7.0	−1.18	7.0
32	7	−3.08	6.7	1.86	6.7	32	8	.88	6.6	3.32	6.5
33	7	−.04	6.3	1.78	6.3	33	8	−.08	6.3	1.58	6.3
34	7	2.31	5.9	.10	5.9	34	8	.71	6.0	−.79	6.0
35	7	.07	5.7	1.53	5.7	35	8	.27	5.7	.18	5.7
36	7	−.17	5.4	−.42	5.4	36	8	−1.05	5.3	−.54	5.3
9	9	−55.55	5.9	97.59	5.7						
10	9	128.18	3.5	−48.19	3.5	10	10	94.56	4.3	−20.10	4.2
11	9	−38.78	4.1	40.28	4.0	11	10	−52.06	4.3	−17.61	4.3
12	9	46.94	4.4	13.22	4.5	12	10	−9.13	2.8	31.68	2.7
13	9	20.38	4.4	45.78	4.4	13	10	43.30	4.7	−38.04	4.7
14	9	37.16	5.1	17.93	5.2	14	10	37.00	2.9	−2.80	2.8
15	9	13.44	5.7	41.02	5.7	15	10	9.59	4.9	16.08	4.9
16	9	−16.58	6.2	−50.98	6.3	16	10	−10.42	4.2	6.61	4.1
17	9	−3.20	6.9	−34.32	7.0	17	10	2.10	5.8	20.12	5.8
18	9	−13.52	8.1	19.24	8.1	18	10	9.01	6.0	−10.86	6.0
19	9	1.76	8.6	8.66	8.6	19	10	−35.35	7.4	−2.66	7.3
20	9	22.81	10.0	7.24	10.2	20	10	−22.42	8.0	−8.09	8.0
21	9	17.32	9.8	−9.39	9.8	21	10	3.65	8.5	1.84	8.5
22	9	12.51	10.2	−9.48	10.3	22	10	5.01	9.2	20.38	9.2
23	9	−4.03	10.1	−10.39	10.1	23	10	19.98	8.8	−3.76	8.8
24	9	−3.89	9.8	−1.43	9.8	24	10	17.35	8.6	9.30	8.6
25	9	−6.03	9.3	9.84	9.3	25	10	5.69	8.5	−4.47	8.5
26	9	2.52	8.7	−.66	8.8	26	10	−4.84	8.5	1.66	8.5
27	9	.40	8.3	2.16	8.3	27	10	−8.31	8.1	6.01	8.1
28	9	2.94	8.0	−3.06	8.0	28	10	−7.28	8.0	1.20	8.0
29	9	−1.64	7.7	2.48	7.7	29	10	.06	7.5	6.01	7.5
30	9	.17	7.3	−3.94	7.3	30	10	1.23	7.2	−1.04	7.2
31	9	−3.89	6.9	−1.70	6.9	31	10	2.52	6.8	−3.74	6.8
32	9	1.95	6.6	.77	6.6	32	10	.83	6.5	−1.95	6.5
33	9	−.29	6.3	1.87	6.3	33	10	.23	6.1	−.94	6.1
34	9	1.27	5.9	1.51	5.9	34	10	−1.49	5.9	−.01	5.9
35	9	1.08	5.6	−2.07	5.6	35	10	−1.43	5.6	−.84	5.6
36	9	−.32	5.4	.55	5.4	36	10	−.36	5.3	.47	5.3
11	11	54.33	6.2	−54.73	6.3						
12	11	5.41	3.0	−9.52	2.9	12	12	−3.53	2.5	−11.80	2.5
13	11	−40.19	4.4	5.50	4.4	13	12	−28.01	2.5	86.41	2.5
14	11	8.08	3.6	−41.36	3.6	14	12	8.97	1.6	−32.07	1.5
15	11	1.72	4.3	28.93	4.2	15	12	−28.33	3.4	12.49	3.4
16	11	14.02	3.9	−6.44	3.9	16	12	20.88	1.6	5.74	1.6
17	11	−17.11	4.7	17.50	4.7	17	12	34.27	4.1	17.26	4.1
18	11	−12.80	4.0	−.60	3.9	18	12	−26.18	2.4	−16.53	2.3
19	11	16.48	4.7	13.47	4.7	19	12	3.20	4.7	4.33	4.7
20	11	11.38	4.4	−23.93	4.3	20	12	−4.06	3.2	17.30	3.1
21	11	9.28	5.1	−36.78	5.1	21	12	2.82	5.2	12.71	5.2
22	11	−9.37	5.4	−18.38	5.3	22	12	7.44	4.0	−7.84	3.9
23	11	3.85	5.9	13.68	6.1	23	12	21.58	5.5	−16.68	5.6
24	11	12.74	6.6	12.12	6.4	24	12	12.34	5.0	−9.52	4.9
25	11	5.58	6.9	−1.28	7.0	25	12	−5.54	5.8	11.01	5.9
26	11	3.20	6.8	5.05	6.7	26	12	−19.65	5.8	5.43	5.7
27	11	−1.19	7.1	−3.10	7.1	27	12	−.42	6.1	−1.72	6.2
28	11	−.62	6.9	−.83	7.0	28	12	.40	6.2	2.43	6.2
29	11	−9.32	6.9	.45	6.8	29	12	−.83	6.3	−4.93	6.3
30	11	−1.62	6.7	5.08	6.7	30	12	3.79	6.2	−3.42	6.2
31	11	−1.66	6.4	5.85	6.5	31	12	.15	6.1	4.62	6.1
32	11	−2.40	6.3	−.65	6.3	32	12	−1.71	5.8	4.19	5.8
33	11	5.56	6.0	−.48	6.1	33	12	5.22	5.5	4.13	5.5
34	11	1.24	5.7	−3.83	5.7	34	12	.45	5.3	2.49	5.3
35	11	.68	5.4	−3.66	5.4	35	12	1.48	5.3	−2.06	5.3
36	11	.59	5.2	−.73	5.3	36	12	−.22	5.1	−1.61	5.1
13	13	−61.55	1.3	68.27	1.3						

Table 2. Continued.

ℓ	m	$\bar{C}_{\ell m}$	σ	$\bar{S}_{\ell m}$	σ	ℓ	m	$\bar{C}_{\ell m}$	σ	$\bar{S}_{\ell m}$	σ
14	13	31.53	.9	44.62	.9	14	14	−50.57	1.8	−6.37	1.8
15	13	−28.11	1.0	−4.98	1.0	15	14	6.17	1.0	−25.61	.9
16	13	13.08	1.1	.61	1.1	16	14	−19.12	.8	−38.29	.8
17	13	16.91	1.2	20.11	1.2	17	14	−13.34	.8	11.76	.8
18	13	−6.58	1.1	−35.16	1.1	18	14	−9.28	1.2	−10.94	1.2
19	13	−6.09	1.6	−29.17	1.6	19	14	−5.12	.7	−12.64	.7
20	13	26.65	1.3	4.89	1.3	20	14	10.32	1.8	−11.76	1.8
21	13	−18.17	2.1	11.60	2.0	21	14	18.78	1.2	8.70	1.2
22	13	−16.95	1.4	17.85	1.4	22	14	8.73	2.2	10.24	2.2
23	13	−10.46	2.8	−7.51	2.8	23	14	4.61	2.2	−3.27	2.2
24	13	−3.62	2.2	−.38	2.2	24	14	−18.64	2.8	1.46	2.8
25	13	7.38	3.5	−15.19	3.5	25	14	−21.94	3.3	13.21	3.3
26	13	2.72	3.2	1.42	3.3	26	14	3.93	3.5	5.63	3.5
27	13	−5.98	4.2	−4.13	4.1	27	14	11.97	4.3	6.64	4.3
28	13	.10	3.8	3.53	3.9	28	14	−2.11	4.3	−6.50	4.3
29	13	−1.15	4.5	−1.98	4.5	29	14	−5.15	4.6	1.94	4.7
30	13	14.67	4.6	−.02	4.6	30	14	−.03	4.8	−2.55	4.8
31	13	5.69	4.6	1.32	4.6	31	14	−7.28	4.4	1.25	4.5
32	13	7.26	5.0	.22	5.0	32	14	4.66	4.6	6.92	4.6
33	13	3.67	4.4	6.78	4.3	33	14	9.23	3.9	2.51	3.9
34	13	−8.08	4.8	1.28	4.9	34	14	−1.04	3.9	−.29	3.9
35	13	−1.18	4.7	4.48	4.7	35	14	−.48	4.2	−.12	4.1
36	13	.77	4.5	3.79	4.5	36	14	−4.84	4.5	−4.07	4.5
15	15	−18.09	3.2	−8.09	3.2						
16	15	−12.53	3.9	−32.30	3.9	16	16	−32.41	7.1	−4.37	7.1
17	15	4.94	1.4	5.75	1.4	17	16	−29.07	5.5	1.88	5.5
18	15	−37.76	3.8	−19.82	3.8	18	16	9.79	4.0	5.00	4.0
19	15	−18.32	2.7	−12.77	2.7	19	16	−19.90	5.0	−11.93	5.0
20	15	−22.73	3.5	−.41	3.5	20	16	−10.67	4.3	1.69	4.3
21	15	16.62	3.5	14.98	3.4	21	16	8.73	4.2	−5.16	4.2
22	15	27.94	3.3	3.10	3.3	22	16	.09	5.0	−4.93	5.0
23	15	17.73	4.1	−2.28	4.0	23	16	4.90	4.5	11.77	4.6
24	15	9.81	3.6	−13.53	3.6	24	16	−.49	6.2	6.28	6.2
25	15	−1.99	4.4	−2.27	4.4	25	16	3.04	5.3	−12.80	5.3
26	15	−11.38	4.8	4.70	4.9	26	16	5.82	6.4	−4.15	6.3
27	15	−4.34	5.3	.10	5.3	27	16	6.58	5.5	−4.11	5.6
28	15	−8.21	5.8	5.38	5.8	28	16	−8.31	6.1	−7.69	6.0
29	15	−1.27	5.6	−2.49	5.7	29	16	−2.20	6.4	−5.53	6.4
30	15	2.81	6.0	−9.28	6.0	30	16	.62	6.3	5.66	6.3
31	15	.45	5.6	−4.37	5.6	31	16	−4.51	6.4	4.80	6.4
32	15	3.91	5.5	−4.94	5.5	32	16	2.92	6.2	4.10	6.2
33	15	−3.01	5.3	2.17	5.3	33	16	−.39	5.7	1.97	5.7
34	15	.76	5.4	3.00	5.4	34	16	1.13	5.6	−2.66	5.6
35	15	.26	5.1	2.83	5.1	35	16	.13	5.4	−1.34	5.4
36	15	−1.82	4.8	1.86	4.8	36	16	1.34	5.2	−2.01	5.2
17	17	−38.31	7.5	−20.62	7.6						
18	17	6.11	7.4	8.77	7.4	18	18	−4.45	11.4	−5.06	11.4
19	17	27.95	4.0	−10.88	4.0	19	18	21.65	9.2	−3.11	9.1
20	17	4.29	7.0	−8.98	7.1	20	18	10.58	6.5	1.30	6.5
21	17	−6.75	6.2	.84	6.2	21	18	16.83	8.2	−6.57	8.2
22	17	13.81	6.4	−11.13	6.4	22	18	7.03	6.8	−10.30	6.7
23	17	−7.21	6.3	−6.60	6.3	23	18	−1.91	6.4	−6.30	6.4
24	17	−8.46	5.9	1.88	5.9	24	18	4.31	6.5	−5.07	6.5
25	17	−8.31	6.4	.55	6.4	25	18	−1.30	6.7	−10.67	6.6
26	17	−4.89	5.9	8.28	5.9	26	18	−9.01	7.2	7.55	7.3
27	17	5.55	6.4	1.59	6.4	27	18	−5.19	6.9	5.94	6.9
28	17	4.52	6.9	−4.26	6.9	28	18	.36	6.7	−.83	6.6
29	17	4.57	6.5	−2.78	6.5	29	18	−2.01	6.3	−.14	6.3
30	17	1.01	6.5	−1.54	6.5	30	18	.30	6.5	.85	6.5
31	17	−5.93	6.4	2.57	6.4	31	18	2.56	6.4	.85	6.4
32	17	−3.66	6.3	1.89	6.3	32	18	2.21	6.2	−1.48	6.2
33	17	−2.14	6.0	3.04	6.0	33	18	.87	6.1	−1.24	6.1

Table 2. Continued.

ℓ	m	$\bar{C}_{\ell m}$	σ	$\bar{S}_{\ell m}$	σ	ℓ	m	$\bar{C}_{\ell m}$	σ	$\bar{S}_{\ell m}$	σ
34	17	.36	5.7	2.58	5.7	34	18	−2.72	5.8	−.09	5.9
35	17	3.39	5.5	−2.44	5.5	35	18	1.50	5.5	−.59	5.5
36	17	2.17	5.3	−.85	5.3	36	18	.07	5.2	.53	5.2
19	19	6.46	10.5	10.42	10.5						
20	19	−7.10	9.4	8.46	9.5	20	20	1.71	13.1	−13.51	13.2
21	19	−20.95	5.7	15.88	5.7	21	20	−19.04	9.9	18.54	9.9
22	19	6.62	8.2	−4.70	8.3	22	20	−13.32	7.6	14.78	7.6
23	19	−8.68	7.9	7.49	8.1	23	20	17.22	8.4	−9.05	8.5
24	19	.53	7.3	−15.02	7.2	24	20	−6.06	8.0	−.33	8.1
25	19	9.18	6.9	2.13	7.0	25	20	−3.73	7.0	−6.62	6.9
26	19	1.63	6.7	.72	6.7	26	20	9.48	6.8	−10.95	6.8
27	19	.93	6.7	−6.23	6.7	27	20	2.95	6.7	3.01	6.7
28	19	4.42	6.7	13.80	6.7	28	20	−.98	7.0	1.13	7.0
29	19	−2.19	6.8	1.51	6.8	29	20	−4.80	6.7	3.16	6.7
30	19	−5.63	6.7	−2.64	6.7	30	20	−.03	6.5	3.57	6.5
31	19	2.02	6.2	2.82	6.3	31	20	1.89	6.3	.56	6.2
32	19	3.09	6.2	−1.51	6.2	32	20	−1.59	6.2	1.42	6.2
33	19	1.68	5.9	.24	6.0	33	20	2.08	5.9	−.75	5.9
34	19	.60	5.7	−1.00	5.7	34	20	.89	5.8	−.40	5.7
35	19	−2.90	5.6	.59	5.6	35	20	−.77	5.5	−.88	5.6
36	19	−.26	5.3	−.07	5.3	36	20	−.91	5.3	−.87	5.3
21	21	2.48	11.3	−6.85	11.3						
22	21	−13.22	10.4	7.60	10.4	22	22	−1.46	12.7	4.72	12.6
23	21	10.82	6.4	7.64	6.4	23	22	−.90	9.5	−2.14	9.5
24	21	10.57	8.2	1.12	8.1	24	22	−1.73	7.9	−1.30	7.9
25	21	5.40	8.0	3.14	8.0	25	22	−1.87	7.5	−1.76	7.5
26	21	−.39	7.3	−2.41	7.3	26	22	10.91	7.8	9.16	7.8
27	21	2.07	6.7	−4.54	6.6	27	22	−.14	6.6	2.93	6.6
28	21	2.49	6.6	.27	6.6	28	22	−4.85	6.5	.51	6.4
29	21	−9.40	6.2	−5.95	6.1	29	22	9.66	6.3	4.44	6.3
30	21	−7.45	6.5	−3.10	6.5	30	22	3.25	6.3	−5.54	6.3
31	21	2.34	6.4	3.58	6.4	31	22	−6.27	6.0	−5.73	6.0
32	21	1.17	6.1	5.88	6.1	32	22	−4.66	6.1	.75	6.1
33	21	.73	5.9	−.84	5.8	33	22	−4.10	5.8	−1.10	5.8
34	21	1.37	5.7	−.66	5.8	34	22	.83	5.6	.42	5.6
35	21	1.38	5.4	2.74	5.4	35	22	.02	5.4	3.30	5.3
36	21	.74	5.2	−2.12	5.2	36	22	.57	5.2	.69	5.2
23	23	.84	10.5	.20	10.5						
24	23	−2.14	9.9	−9.01	9.9	24	24	2.34	11.2	−1.21	11.2
25	23	4.57	6.3	−2.46	6.3	25	24	3.61	8.5	−3.86	8.5
26	23	2.35	7.1	8.95	7.1	26	24	−1.37	6.9	12.18	7.0
27	23	−5.39	7.0	−2.74	7.0	27	24	−1.94	6.1	2.62	6.1
28	23	−2.64	6.7	6.39	6.6	28	24	6.88	6.3	−15.08	6.3
29	23	−5.01	6.0	−.08	6.0	29	24	−2.53	5.4	3.70	5.4
30	23	−1.58	6.0	−5.34	5.9	30	24	−2.51	5.6	−.04	5.6
31	23	9.50	5.4	5.65	5.5	31	24	−3.83	5.5	−1.91	5.4
32	23	3.86	5.8	.48	5.7	32	24	−6.59	5.3	5.33	5.3
33	23	−.63	5.6	−4.40	5.6	33	24	3.99	4.9	−.48	4.9
34	23	−.93	5.5	−2.14	5.5	34	24	6.73	5.3	.85	5.3
35	23	−2.38	5.2	−1.56	5.2	35	24	2.53	5.0	2.20	5.0
36	23	−1.22	5.0	−.55	5.0	36	24	.66	4.9	−1.42	4.9
25	25	4.95	8.5	4.01	8.5						
26	25	−3.99	8.3	8.25	8.4	26	26	3.43	7.6	−4.27	7.5
27	25	11.80	5.5	3.15	5.5	27	26	−5.01	6.4	4.00	6.4
28	25	1.13	6.4	−4.81	6.5	28	26	3.44	5.7	1.68	5.7
29	25	8.31	6.1	3.63	6.0	29	26	6.26	5.0	−3.69	5.1
30	25	8.85	6.0	−5.61	6.0	30	26	−3.21	5.9	8.14	5.9
31	25	−7.74	5.2	−.28	5.2	31	26	−4.69	4.8	.36	4.8
32	25	−13.17	5.1	7.70	5.1	32	26	−1.05	4.9	−1.53	4.9
33	25	−1.26	4.7	−4.82	4.7	33	26	8.13	4.3	5.54	4.3
34	25	6.25	4.9	−8.21	4.9	34	26	1.08	4.6	−9.01	4.6
35	25	−3.39	4.7	1.52	4.7	35	26	−14.34	3.7	−.14	3.7

Table 2. Continued.

ℓ	m	$\bar{C}_{\ell m}$	σ	$\bar{S}_{\ell m}$	σ	ℓ	m	$\bar{C}_{\ell m}$	σ	$\bar{S}_{\ell m}$	σ
36	25	.03	4.9	8.65	4.9	36	26	8.45	3.9	11.08	3.9
27	27	6.89	3.0	3.45	3.1						
28	27	−9.92	5.5	1.33	5.4	28	28	6.77	4.7	1.95	4.7
29	27	−7.47	3.4	−2.15	3.4	29	28	10.32	6.1	−1.96	6.1
30	27	−1.92	4.7	7.82	4.7	30	28	−8.97	4.2	−5.16	4.2
31	27	7.00	3.5	12.25	3.5	31	28	.34	4.1	1.73	4.1
32	27	−3.09	4.4	−3.02	4.4	32	28	1.57	4.4	2.35	4.4
33	27	−10.33	2.6	−2.13	2.6	33	28	−10.89	3.3	1.90	3.3
34	27	6.90	4.0	−.54	4.0	34	28	4.55	3.5	−8.20	3.5
35	27	2.78	1.5	−19.13	1.6	35	28	−10.89	1.9	−23.35	2.0
36	27	−10.19	2.5	4.23	2.6	36	28	6.95	2.0	5.66	2.1
29	29	8.64	7.6	3.16	7.6						
30	29	4.82	6.3	.12	6.2	30	30	−1.51	7.4	−.42	7.4
31	29	−5.42	3.9	−5.95	4.0	31	30	−2.45	6.5	8.42	6.5
32	29	−3.34	4.1	2.50	4.0	32	30	8.29	4.7	1.67	4.7
33	29	−21.32	3.5	.19	3.5	33	30	2.52	4.4	−13.49	4.4
34	29	−3.81	3.1	−4.48	3.0	34	30	−6.12	4.4	.03	4.4
35	29	8.19	3.3	−3.15	3.3	35	30	3.71	4.8	−2.89	4.8
36	29	−1.34	2.9	−2.45	2.9	36	30	−1.56	3.7	−2.03	3.6
31	31	−.23	7.2	−.07	7.2						
32	31	−.76	6.3	−2.71	6.3	32	32	.73	6.8	.51	6.8
33	31	.17	5.6	1.16	5.6	33	32	2.41	6.3	−.02	6.3
34	31	2.35	4.3	2.30	4.3	34	32	−.82	5.4	−1.16	5.4
35	31	1.33	5.1	1.03	5.1	35	32	−3.98	5.3	.57	5.3
36	31	−3.55	4.9	1.36	4.8	36	32	−.88	4.8	−.30	4.8
33	33	−.27	6.5	−.36	6.5						
34	33	1.02	6.0	1.38	6.0	34	34	−.21	6.1	−.60	6.1
35	33	−.29	5.6	1.67	5.6	35	34	−.52	5.7	.12	5.7
36	33	−2.40	4.9	−2.62	4.9	36	34	.83	5.2	1.76	5.2
35	35	.09	5.8	−.14	5.8						
36	35	.22	5.4	−.73	5.4	36	36	.15	5.4	.42	5.4

3 Satellite Dynamics

3.1 Cartesian Equations of Motion

The gravitational acceleration at any given location is obtained by computing the gradient of the potential. Since the potential is given as a function of Earth-fixed spherical coordinates, it is most convenient to compute the gradient in the same system. In Earth-fixed spherical coordinates, this gradient is,

$$\vec{a} = \nabla U = \frac{\partial U}{\partial r}\vec{u}_r + \frac{1}{r}\frac{\partial U}{\partial \phi}\vec{u}_\phi + \frac{1}{r\cos\phi}\frac{\partial U}{\partial \lambda}\vec{u}_\lambda \tag{13}$$

where $\vec{u}_r$, $\vec{u}_\phi$ and $\vec{u}_\lambda$ are unit vectors in the r, ϕ, λ basis. This basis has $\vec{u}_r$ pointing along the radius vector to the satellite, $\vec{u}_\phi$ is in the direction of increasing north latitude and $\vec{u}_\lambda$ is in the direction of increasing east longitude. The acceleration vector obtained from this expression will be the inertial acceleration for the point of interest. Though, as noted, the components of the acceleration are given in the Earth-fixed coordinate system. For most applications it will be desired to have the components of the acceleration expressed in an inertial (nonrotating) coordinate system. This is accomplished by applying the appropriate coordinate transformation from the spherical coordinates to the desired coordinate system. So as a first step, the components of the inertial acceleration in the Earth-fixed (rotating) coordinate system are obtained. Substituting for the gravitational potential (equation (1)) and taking the indicated partials in equation (13) gives the acceleration vector,

$$\begin{aligned}
\vec{a} &= \left\{-\frac{\mu}{r^2}\sum_{\ell=0}^{\infty}(\ell+1)\left(\frac{a_e}{r}\right)^\ell \sum_{m=0}^{\ell} P_{\ell m}(\sin\phi)\left[C_{\ell m}\cos m\lambda + S_{\ell m}\sin m\lambda\right]\right\}\vec{u}_r \\
&+ \left\{\frac{\mu}{r^2}\sum_{\ell=1}^{\infty}\left(\frac{a_e}{r}\right)^\ell \sum_{m=0}^{\ell} \frac{\partial P_{\ell m}(\sin\phi)}{\partial\phi}\left[C_{\ell m}\cos m\lambda + S_{\ell m}\sin m\lambda\right]\right\}\vec{u}_\phi \\
&+ \left\{\frac{\mu}{r^2}\sum_{\ell=1}^{\infty}\left(\frac{a_e}{r}\right)^\ell \sum_{m=1}^{\ell} m\frac{P_{\ell m}(\sin\phi)}{\cos\phi}\left[-C_{\ell m}\sin m\lambda + S_{\ell m}\cos m\lambda\right]\right\}\vec{u}_\lambda
\end{aligned} \tag{14}$$

Notice that the leading term of the radial component (degree and order equal to zero) is simply the expected two-body gravitational acceleration $-\mu/r^2$. Also, if only zonal terms are used ($m = 0$), then the longitudinal component of the acceleration is zero.

Next, the Earth-fixed Cartesian components of the acceleration can be obtained by rotating from the spherical coordinates to the x, y, z basis. Let the components of the acceleration in spherical coordinates be represented by,

$$\vec{a} = a_r\vec{u}_r + a_\phi\vec{u}_\phi + a_\lambda\vec{u}_\lambda \tag{15}$$

where the components a_r, a_ϕ and a_λ are given in equation (14). The acceleration vector in Cartesian coordinates can be written as,

$$\vec{a}_{xyz} = a_x\vec{u}_x + a_y\vec{u}_y + a_z\vec{u}_z \tag{16}$$

where $\vec{u}_x$, $\vec{u}_y$ and $\vec{u}_z$ are the Cartesian unit vectors in the Earth-fixed (rotating) coordinate system. The Cartesian components of the acceleration can be obtained from the spherical coordinate components through the standard transformation,

$$\begin{vmatrix} a_x \\ a_y \\ a_z \end{vmatrix} = \begin{vmatrix} \cos\phi\cos\lambda & -\sin\phi\cos\lambda & -\sin\lambda \\ \cos\phi\sin\lambda & -\sin\phi\sin\lambda & \cos\lambda \\ \sin\phi & \cos\phi & 0 \end{vmatrix} \begin{vmatrix} a_r \\ a_\phi \\ a_\lambda \end{vmatrix} \tag{17}$$

Having obtained the Earth-fixed Cartesian components of the acceleration one further coordinate transformation is necessary to obtain the acceleration components in the defined inertial coordinate system. If the matrix T represents the coordinate transformation from the Earth-fixed system to the inertial coordinate system, then the acceleration components in the inertial system will be,

$$\vec{a}_{XYZ} = T\vec{a}_{xyz} \tag{18}$$

where $\vec{a}_{XYZ}$ is the inertial acceleration vector in inertial coordinates,

$$\vec{a}_{XYZ} = a_X\vec{u}_X + a_Y\vec{u}_Y + a_Z\vec{u}_Z \tag{19}$$

with $\vec{u}_X$, $\vec{u}_Y$ and $\vec{u}_Z$ being the unit vectors of the Cartesian inertial coordinate system. In component form, this final transformation will have the structure,

$$\begin{vmatrix} a_X \\ a_Y \\ a_Z \end{vmatrix} = \begin{vmatrix} T_{11} & T_{12} & T_{13} \\ T_{21} & T_{22} & T_{23} \\ T_{31} & T_{32} & T_{33} \end{vmatrix} \begin{vmatrix} a_x \\ a_y \\ a_z \end{vmatrix} \tag{20}$$

The actual elements of the transformation matrix T depend on the inertial coordinate system being used. In the most general case, this transformation will account for polar motion (the motion of the spin axis with respect to the Earth crust), Earth rotation (the largest effect) and, precession and nutation (the motion of the spin axis with respect to the stars). In the simplest case, all of these effects are neglected except for Earth rotation. This defines a coordinate system with the same z axis as the Earth-fixed system but not rotating with the Earth. For many applications such a system is effectively inertial. The transformation from the Earth-fixed system to this nonrotating system is simply,

$$T = \begin{vmatrix} \cos\theta & -\sin\theta & 0 \\ \sin\theta & \cos\theta & 0 \\ 0 & 0 & 1 \end{vmatrix} \tag{21}$$

where θ is the Greenwich Hour Angle (the angle from a reference direction, usually the Vernal Equinox, to the Greenwich meridian).

3.3 Lagrangian Equations of Motion

The equations of motion for a satellite moving in the gravity field are given by equation (13). These equations are convenient for numerical computation of an ephemeris but not for analytic investigations into the evolution of the orbital elements. Such analyses are more conveniently performed using the Lagrangian equations of motion. These equations are equivalent to equation (13) but directly give the time rates of change of the Kepler orbital elements,

$$\frac{da}{dt} = \frac{2}{na}\frac{\partial V}{\partial M} \tag{22}$$

$$\frac{de}{dt} = \frac{1-e^2}{na^2e}\frac{\partial V}{\partial M} - \frac{(1-e^2)^{1/2}}{na^2e}\frac{\partial V}{\partial \omega} \tag{23}$$

$$\frac{d\omega}{dt} = -\frac{\cos i}{na^2(1-e^2)^{1/2}\sin i}\frac{\partial V}{\partial i} + \frac{(1-e^2)^{1/2}}{na^2e}\frac{\partial V}{\partial e} \tag{24}$$

$$\frac{di}{dt} = \frac{\cos i}{na^2(1-e^2)^{1/2}\sin i}\frac{\partial V}{\partial \omega} - \frac{1}{na^2(1-e^2)^{1/2}\sin i}\frac{\partial V}{\partial \Omega} \tag{25}$$

$$\frac{d\Omega}{dt} = \frac{1}{na^2(1-e^2)^{1/2}\sin i}\frac{\partial V}{\partial i} \tag{26}$$

$$\frac{dM}{dt} = n - \frac{1-e^2}{na^2e}\frac{\partial V}{\partial e} - \frac{2}{na}\frac{\partial V}{\partial a} \tag{27}$$

$$\tag{28}$$

where V is the perturbing gravitational potential, i.e., the gravitational potential excluding the point mass contribution,

$$U = \frac{\mu}{r} + V \tag{29}$$

These equations require that the perturbing gravitational potential V be represented in terms of the orbital elements instead of the spherical coordinates as expressed in equation (1). This conversion has been carried out by *Kaula* [1966],

$$V = \frac{\mu}{a}\sum_{l=1}^{\infty}\left(\frac{a_e}{a}\right)^l \sum_{m=0}^{l}\sum_{p=0}^{l} \bar{F}_{lmp}(i) \sum_{q=-\infty}^{\infty} G_{lpq}(e) S_{lmpq}(\omega, M, \Omega, \theta) \tag{30}$$

where

$$S_{lmpq} = \begin{bmatrix} \bar{C}_{lm} \\ -\bar{S}_{lm} \end{bmatrix}_{l-m\ \text{odd}}^{l-m\ \text{even}} \cos\psi_{lmpq} + \begin{bmatrix} \bar{S}_{lm} \\ \bar{C}_{lm} \end{bmatrix}_{l-m\ \text{odd}}^{l-m\ \text{even}} \sin\psi_{lmpq} \tag{31}$$

and

$$\psi_{lmpq} = (l-2p)\omega + (l-2p+q)M + m(\Omega - \theta) \tag{32}$$

All quantities having been previously defined except for the inclination function $F_{lmp}(i)$ and eccentricity function $G_{lpq}(e)$, which are given by Kaula. In this formulation, the overbar on F_{lmp} indicates it is normalized (in the same fashion that

3.2 Orbital Elements

While it is convenient to express the satellite equations of motion in the Cartesian coordinate system, the evolution of the satellite orbit is more conveniently evaluated in terms of its orbital elements. This is because the satellite motion is nearly Keplerian (i.e., it corresponds closely to the ideal elliptical motion which results from the gravitational motion about a point mass). The orbital elements are a set of six parameters which uniquely define the position and velocity of the satellite. Transformations exist which convert Cartesian position and velocity to orbital elements and vice-versa. The set of elements used in this study are the conventional set of Kepler elements. These six elements are

semi-major axis —a— One-half the length of the major axis of the ellipse. For a circular orbit this would be the radius of the circle.

eccentricity —e— Measure of ellipticity ($0 \leq e \leq 1$). For a circular orbit $e = 0$.

inclination —i— The angle formed by the orbital plane and the equatorial (x-y) plane ($0° \leq i \leq 180°$).

right ascension of the ascending node —Ω— The angle measured in the equatorial (x-y) plane from the x-axis to the point of intersection of the orbital path with the equatorial plane. The orbital path will intersect the x-y plane in two places: once ascending (south to north) and once descending (north to south). The x-axis will normally be defined to be pointing at the vernal equinox (the location of the Sun in the sky on or about March 21).

argument of perigee —ω— The angle measured in the plane of the orbit from the ascending node to the point of the orbit corresponding to closest approach (the distance from the center of the Earth to the satellite is a minimum). This angle will not be defined if the orbit is circular.

mean anomaly —M— A non-physical angle. Defined as $M = n(t - T)$ where T is the time of periapsis passage, t is the current time, and n is the mean motion ($n = 2\pi/P$, where P is the orbital period). Unless the orbit is circular, the satellite does not move with a constant angular rate and thus the actual angle swept out by the satellite (which is the true anomaly) in a given amount of time will not correspond to the mean anomaly. The mean anomaly would be the angle swept out by the satellite if it were moving at a uniform rate.

At any given instant the Cartesian position and velocity of the satellite can be converted to the corresponding set of Kepler orbital elements. These values of the orbital elements will continually change in time due to the various forces affecting the satellite; these instantaneous values for the orbital elements are referred to as the osculating orbital elements. And it is the changes in these osculating orbital elements (due to the acting forces) that is of primary interest here.

the Associated Legendre Functions are normalized via equation (9)). This is required since normalized spherical harmonic coefficients are being utilized.

4 Satellite Motion

4.1 Precessing Ellipse

A satellite moving in the low-Earth orbit environment does not follow the idealized elliptical path resulting from the consideration of the motion of a particle about a point mass. Instead, the satellite will deviate from the idealized elliptical path as the various acting forces perturb the satellite. In this discussion, only the perturbing forces resulting from the Earth's gravity field are considered. Though it should be emphasized that depending on the actual orbital geometry and spacecraft design, other forces (principally, atmospheric drag, solar radiation pressure, and lunar and solar gravity) may be more important.

The general problem of determining the motion of a satellite orbiting in a gravitational field (described by spherical harmonics) can only be solved through numerical integration. The equations presented in section 3 can be used for this purpose. However, it is possible through various degrees of approximation to analytically determine the important characteristics of the motion.

The largest effect on a satellite orbiting the Earth is that due to the oblateness (predominantly the second degree zonal $\bar{C}_{2,0}$). This is not surprising given the size of the second degree zonal with respect to all other coefficients of the gravity field (Tables 1 and 2). The most noticeable effect of the oblateness is to cause the right ascension of the ascending node and argument of periapse of the orbit to vary linearly in time. In the two-body problem these quantities remain constant. The oblateness also causes a small change in the orbital period. Besides these secular effects (linear changes in time) the oblateness causes (relatively) large periodic changes in all of the orbital elements.

The rate of change in the node, periapse, and mean anomaly due to the second degree zonal coefficient are (from *Kaula* [1966]), respectively,

$$\frac{d\Omega}{dt} = \frac{3}{2} n \left(\frac{a_e}{a}\right)^2 \frac{\cos i}{(1-e^2)^2} C_{2,0} \tag{33}$$

$$\frac{d\omega}{dt} = -\frac{3}{4} n \left(\frac{a_e}{a}\right)^2 \frac{(5\cos^2 i - 1)}{(1-e^2)^2} C_{2,0} \tag{34}$$

$$\frac{dM}{dt} = n - \frac{3}{4} n \left(\frac{a_e}{a}\right)^2 \frac{(3\cos^2 i - 1)}{(1-e^2)^{3/2}} C_{2,0} \tag{35}$$

(Note that the unnormalized second degree zonal coefficient is used in these expressions.)

So as a first approximation, a satellite orbiting the Earth can be reasonably represented by a secularly precessing ellipse. This is an ellipse that has constant values for the semi-major axis, eccentricity and inclination, and values that vary linearly in time for the right ascension of the ascending node, argument of periapse and mean anomaly. The actual motion of the satellite then consists of small deviations away from this secularly precessing ellipse. To characterize these deviations away from this precessing ellipse the solution presented by *Kaula* [1966] is very useful.

4.2 Kaula's Solution

Kaula's approach was to define a reference orbital path corresponding to the secularly precessing ellipse. The orbital elements that define this reference orbital path are referred to as mean (or averaged) orbital elements. Kaula determined (to first order) the deviation from these mean orbital elements caused by the spherical harmonic coefficients of the gravity field. That is, it is assumed that the orbital elements can be written in the form,

$$\text{semi-major axis} \qquad a^* = a + \Delta a \tag{36}$$

$$\text{eccentricity} \qquad e^* = e + \Delta e \tag{37}$$

$$\text{inclination} \qquad i^* = i + \Delta i \tag{38}$$

$$\text{right ascension of the ascending node} \qquad \Omega^* = \dot{\Omega}t + \Omega_o + \Delta\Omega \tag{39}$$

$$\text{argument of periapse} \qquad \omega^* = \dot{\omega}t + \omega_o + \Delta\omega \tag{40}$$

$$\text{mean anomaly} \qquad M^* = \dot{M}t + M_o + \Delta M \tag{41}$$

where the star quantities represent the osculating (true) orbital elements of the satellite and the unstarred orbital elements are those that define the reference precessing ellipse. The time t is measured from a reference epoch and Ω_o, ω_o and M_o are the values at the reference epoch. The deviations from the reference ellipse will be purely periodic (assuming the mean orbital elements and rates have been accurately defined).

The resulting deviations in the orbital elements are of the form

$$\Delta\alpha = \sum_{\ell=1}^{\infty} \sum_{m=0}^{\ell} \sum_{p=0}^{\ell} \sum_{q=-\infty}^{+\infty} \Delta\alpha_{\ell mpq} \tag{42}$$

where α represents any one of the six orbital elements. The individual $\Delta\alpha_{\ell mpq}$ can be written in the forms

$$\Delta\alpha_{\ell mpq} = C^{\alpha}_{\ell mpq} S_{\ell mpq} \qquad \text{for } a, e, \text{ and } i \tag{43}$$

$$\Delta\alpha_{\ell mpq} = C^{\alpha}_{\ell mpq} S^{*}_{\ell mpq} \qquad \text{for } \Omega, \omega, \text{ and } M \tag{44}$$

where the $C^{\alpha}_{\ell mpq}$ are constants which depend upon the orbital elements of the reference secularly precessing ellipse; and the $S_{\ell mpq}$ and $S^{*}_{\ell mpq}$ functions are sinusoidal with amplitudes dependent on the values of the gravity field spherical harmonic coefficients. The constant $C^{\alpha}_{\ell mpq}$ coefficients are

$$C^{a}_{\ell mpq} = 2a \left(\frac{a_e}{a}\right)^{\ell} \bar{F}_{\ell mp} G_{\ell pq} (\ell - 2p + q) \frac{n}{\dot{\psi}_{\ell mpq}} \tag{45}$$

$$C^{e}_{\ell mpq} = \left(\frac{a_e}{a}\right)^{\ell} \frac{(1-e^2)^{1/2}}{e} \bar{F}_{\ell mp} G_{\ell pq} \left[(1-e^2)^{1/2}(\ell - 2p + q) - (\ell - 2p)\right] \frac{n}{\dot{\psi}_{\ell mpq}} \tag{46}$$

$$C^{i}_{\ell mpq} = \left(\frac{a_e}{a}\right)^{\ell} \frac{G_{\ell pq}}{(1-e^2)^{1/2}} \bar{F}_{\ell mp} \frac{[(\ell - 2p)\cos i - m]}{\sin i} \frac{n}{\dot{\psi}_{\ell mpq}} \tag{47}$$

$$C^{\omega}_{\ell mpq} = \left(\frac{a_e}{a}\right)^{\ell} \left[\frac{(1-e^2)^{1/2}}{e}\frac{\partial G_{\ell pq}}{\partial e}\bar{F}_{\ell mp} - \frac{G_{\ell pq}}{(1-e^2)^{1/2}}\frac{\cos i}{\sin i}\frac{\partial \bar{F}_{\ell mp}}{\partial i}\right]\frac{n}{\dot{\psi}_{\ell mpq}} \tag{48}$$

$$C^{\Omega}_{\ell mpq} = \left(\frac{a_e}{a}\right)^{\ell} \frac{1}{\sin i}\frac{\partial \bar{F}_{\ell mp}}{\partial i}\frac{G_{\ell pq}}{(1-e^2)^{1/2}}\frac{n}{\dot{\psi}_{\ell mpq}} \tag{49}$$

$$C^{M}_{\ell mpq} = \left(\frac{a_e}{a}\right)^{\ell} \bar{F}_{\ell mp}\left\{\left[2(\ell+1) - 3(\ell-2p+q)\frac{n}{\dot{\psi}_{\ell mpq}}\right]G_{\ell pq} - \frac{(1-e^2)}{e}\frac{\partial G_{\ell pq}}{\partial e}\right\}\frac{n}{\dot{\psi}_{\ell mpq}} \tag{50}$$

The sinusoidal functions $S_{\ell mpq}$ and $S^{*}_{\ell mpq}$ are

$$S_{\ell mpq} = \left[\begin{array}{c}\bar{C}_{\ell m}\\ -\bar{S}_{\ell m}\end{array}\right]_{\ell-m\ \text{odd}}^{\ell-m\ \text{even}} \cos\psi_{\ell mpq} + \left[\begin{array}{c}\bar{S}_{\ell m}\\ \bar{C}_{\ell m}\end{array}\right]_{\ell-m\ \text{odd}}^{\ell-m\ \text{even}} \sin\psi_{\ell mpq} \tag{51}$$

$$S^{*}_{\ell mpq} = \left[\begin{array}{c}\bar{C}_{\ell m}\\ -\bar{S}_{\ell m}\end{array}\right]_{\ell-m\ \text{odd}}^{\ell-m\ \text{even}} \sin\psi_{\ell mpq} - \left[\begin{array}{c}\bar{S}_{\ell m}\\ \bar{C}_{\ell m}\end{array}\right]_{\ell-m\ \text{odd}}^{\ell-m\ \text{even}} \cos\psi_{\ell mpq} \tag{52}$$

The periodicities of the orbital element variations caused by the gravity field are thus,

$$\dot{\psi}_{\ell mpq} = (\ell-2p)\dot{\omega} + (\ell-2p+q)\dot{M} + m(\dot{\Omega}-\dot{\theta}) \tag{53}$$

where $\dot{\theta}$ is the Earth rotation rate, ℓ and m are the spherical harmonic degree and order, p is an integer that can take on the values 0 to ℓ, and q is an integer that can take on the values $\pm\infty$. Kaula's solution is obtained through an expansion in the orbital eccentricity which is the reason the index q has an infinite extent. For orbits with small eccentricities only a small range of q values needs to be considered. High eccentricity orbits require the consideration of much greater range in q and Kaula's solution may not be the best approach in such cases.

4.3 Position Perturbation

Kaula's solution provides a prediction of the expected variation in the Kepler orbital elements due to the gravity field. This formulation is useful for determining the amplitudes and frequencies of the variations in the osculating orbital elements. To determine how these orbital element perturbations are manifested in terms of a position displacement of the satellite (with respect to the reference secularly precessing ellipse) it is necessary to transform the results back into a Cartesian coordinate system. The chosen coordinate system for doing this is the rotating radial, transverse (along-track), and normal (cross-track) system. This coordinate system is defined by the reference secularly precessing ellipse. The radial direction is along the radius vector, transverse is perpendicular to the radius vector (in the orbital plane and positive in the direction of the satellite motion), and normal is perpendicular to the orbital plane (and positive in the direction of the angular momentum vector).

The corresponding position perturbation in the radial, transverse, and normal directions is given by the following relations (*Rosborough and Tapley*, [1987])

$$\Delta r = \frac{\partial r}{\partial a}\Delta a + \frac{\partial r}{\partial e}\Delta e + \frac{\partial r}{\partial M}\Delta M \tag{54}$$

$$\Delta \tau = r\left(\Delta\omega + \frac{\partial f}{\partial M}\Delta M + \Delta\Omega\cos i\right) \tag{55}$$

$$\Delta \eta = r\left[\Delta i \sin(\omega + f) - \Delta\Omega \sin i \cos(\omega + f)\right] \tag{56}$$

where f is the true anomaly as measured along the reference secularly precessing ellipse (the central angle from the point of periapse to the satellite location). Given the expected perturbations in the orbital elements from Kaula's solution it is then possible to compute the corresponding position perturbations using these mapping relations.

In the application at hand, the satellites of interest are established in orbits with small eccentricity. This allows for an accurate evaluation of the expected orbital element variations using a very limited range of q values. This in turn simplifies the evaluation for the position perturbation. Assuming a small eccentricity, the perturbations in the radial, transverse and normal components are approximately given by

$$\Delta r = \sum_{\ell=1}^{\infty}\sum_{m=0}^{\ell}\sum_{p=0}^{\ell} C^{r}_{\ell mp} S_{\ell mp0} \tag{57}$$

$$\Delta \tau = \sum_{\ell=1}^{\infty}\sum_{m=0}^{\ell}\sum_{p=0}^{\ell} C^{\tau}_{\ell mp} S^{*}_{\ell mp0} \tag{58}$$

$$\Delta \eta = \sum_{\ell=1}^{\infty}\sum_{m=0}^{\ell}\sum_{p=0}^{\ell} \left(C^{\eta+}_{\ell mp} S^{*}_{(\ell+1)mp0} - C^{\eta-}_{\ell mp} S^{*}_{(\ell-1)mp0}\right) \tag{59}$$

The constant coefficients $C^{r}_{\ell mp}$, $C^{\tau}_{\ell mp}$, $C^{\eta+}_{\ell mp}$ and $C^{\eta-}_{\ell mp}$ depend upon the orbital elements and rates of the reference secularly precessing ellipse and are given by,

$$C^{r}_{\ell mp} = na\left(\frac{a_e}{a}\right)^{\ell} \bar{F}_{\ell mp}\left[\frac{2(\ell-2p)}{\dot{\psi}_{\ell mp0}} + \frac{4p-3\ell-1}{2\dot{\psi}_{\ell mp1}} + \frac{4p-\ell+1}{2\dot{\psi}_{\ell mp-1}}\right] \tag{60}$$

$$C^{\tau}_{\ell mp} = na\left(\frac{a_e}{a}\right)^{\ell} \bar{F}_{\ell mp}\left[\frac{2(\ell+1) - 3(\ell-2p)\frac{n}{\dot{\psi}_{\ell mp0}}}{\dot{\psi}_{\ell mp0}} + \frac{4p-3\ell-1}{\dot{\psi}_{\ell mp1}} + \frac{\ell-4p-1}{\dot{\psi}_{\ell mp-1}}\right] \tag{61}$$

$$C^{\eta+}_{\ell mp} = \frac{a}{2}\left(\frac{a_e}{a}\right)^{\ell} \frac{n}{\dot{\psi}_{\ell mp0}}\left\{\left[(\ell-2p)\cos i - m\right]\frac{\bar{F}_{\ell mp}}{\sin i} - \frac{\partial \bar{F}_{\ell mp}}{\partial i}\right\} \tag{62}$$

$$C^{\eta-}_{\ell mp} = \frac{a}{2}\left(\frac{a_e}{a}\right)^{\ell} \frac{n}{\dot{\psi}_{\ell mp0}}\left\{\left[(\ell-2p)\cos i - m\right]\frac{\bar{F}_{\ell mp}}{\sin i} + \frac{\partial \bar{F}_{\ell mp}}{\partial i}\right\} \tag{63}$$

5 Perturbations in Laser Range

Of particular interest in this application is the expected orbit error signal that will be observed using satellite laser ranging. The orbit perturbations produced by the gravity field cause a perturbation in position (in three-dimensions) as described in the preceding section. This perturbation in position will result in a perturbation of the expected station-to-satellite range measurement. The final step is to then determine this perturbation in the range observable.

The station-to-satellite range is

$$\rho = \sqrt{(x - x_s)^2 + (y - y_s)^2 + (z - z_s)^2} \tag{64}$$

where x, y, z are the Cartesian coordinates of the satellite and x_s, y_s, z_s are the Cartesian coordinates of the tracking station. The perturbation in the range measurement due to a perturbation in the satellite position is given (to first order) by

$$\Delta\rho = A^T B = \left| \frac{x-x_s}{\rho} \quad \frac{y-y_s}{\rho} \quad \frac{z-z_s}{\rho} \right| \left| \begin{matrix} \Delta x \\ \Delta y \\ \Delta z \end{matrix} \right| \tag{65}$$

$$= \frac{x - x_s}{\rho}\Delta x + \frac{y - y_s}{\rho}\Delta y + \frac{z - z_s}{\rho}\Delta z \tag{66}$$

where Δx, Δy, and Δz are the perturbations in the satellite position. The perturbations in the satellite Cartesian position will now be expressed in terms of the already specified radial, transverse, and normal position perturbations. The transformation between these two orthogonal coordinate systems is

$$D = \left| \begin{matrix} \Delta r \\ \Delta \tau \\ \Delta \eta \end{matrix} \right| = RB = \left| \begin{matrix} R_{11} & R_{12} & R_{13} \\ R_{21} & R_{22} & R_{23} \\ R_{31} & R_{32} & R_{33} \end{matrix} \right| \left| \begin{matrix} \Delta x \\ \Delta y \\ \Delta z \end{matrix} \right| \tag{67}$$

The rows of the R rotation matrix contain the components of the unit vectors in the radial, transverse, and normal directions. That is,

$$R = \left| \begin{matrix} \vec{u}_r \\ \vec{u}_\tau \\ \vec{u}_\eta \end{matrix} \right| = \left| \begin{matrix} \vec{r}/r \\ \vec{u}_\eta \times \vec{u}_r \\ (\vec{r} \times \vec{v})/|\vec{r} \times \vec{v}| \end{matrix} \right| \tag{68}$$

Thus, given the perturbations in the radial, transverse, and normal components, it is possible to compute the corresponding perturbations in the xyz Cartesian system. And the resulting perturbation in the range measurement is

$$\Delta\rho = A^T B = A^T R^T D = A^T R^T \left| \begin{matrix} \Delta r \\ \Delta \tau \\ \Delta \eta \end{matrix} \right| \tag{69}$$

6 Covariance Analysis

The preceding analysis provides the tools for determining the perturbations in the satellite orbit position (in terms of orbital elements or Cartesian position) and the resultant perturbation in a station-to-satellite range measurement. These perturbations describe the effect on the orbit of the perturbing gravitational potential with respect to the reference precessing ellipse. Since the relations are all linear with respect to the gravity spherical harmonic coefficients, one can equally well determine the effect of errors in the coefficients (as opposed to the entire effect). Since a nominal gravity model is used in the analysis of geodetic satellite tracking data, it is in fact the error in the coefficients that is of most interest and not the entire effect (most of which is being accurately modeled by the nominal gravity model). However, the error in the coefficients is obviously not known. But the statistics of the expected error (in the gravity field coefficients) is known. This knowledge of the error statistics is a by-product of the least-squares process used in the estimation of the nominal gravity model, and it is represented by the estimated error covariance matrix.

Define a vector which contains the differences of the true gravity field spherical harmonic coefficients with respect to the nominal gravity model values

$$\delta g = \begin{vmatrix} \bar{C}_{20} - \bar{C}^*_{20} \\ \bar{C}_{21} - \bar{C}^*_{21} \\ \bar{S}_{21} - \bar{S}^*_{21} \\ \bar{C}_{22} - \bar{C}^*_{22} \\ \bar{S}_{22} - \bar{S}^*_{22} \\ \bar{C}_{30} - \bar{C}^*_{30} \\ \bar{C}_{31} - \bar{C}^*_{31} \\ \bar{S}_{31} - \bar{S}^*_{31} \\ \vdots \\ \bar{C}_{40} - \bar{C}^*_{40} \\ \vdots \end{vmatrix} = \begin{vmatrix} \delta\bar{C}_{20} \\ \delta\bar{C}_{21} \\ \delta\bar{S}_{21} \\ \delta\bar{C}_{22} \\ \delta\bar{S}_{22} \\ \delta\bar{C}_{30} \\ \delta\bar{C}_{31} \\ \delta\bar{S}_{31} \\ \vdots \\ \delta\bar{C}_{40} \\ \vdots \end{vmatrix} \tag{70}$$

where the coefficients with an asterisk denote the values used in the nominal gravity field model. The error covariance matrix of the estimated coefficients is then

$$P_g = E[\delta g \delta g^T] \tag{71}$$

where E is the expectation operator. The gravity field coefficient error covariance matrix P_g is an $n \times n$ symmetric matrix where n is the total number of coefficients.

Using the gravity field error covariance and the linear relations between the orbit perturbations and the gravity field coefficients, it is possible to compute the estimated orbit position variance. Similarly, the estimated station-to-satellite range error variance can also be obtained. So for a given uncertainty in the gravity field (as provided by the estimated error covariance matrix P_g) it is possible to determine what the expected uncertainty in the satellite position and/or range measurement will be.

As noted, the relations between the orbit perturbations and the gravity field coefficients are linear, and thus can all be expressed in the form

$$\delta\epsilon = F^T \delta g \tag{72}$$

where F is the vector of coefficients that multiply the gravity field coefficients. The quantity $\delta\epsilon$ can represent any quantity of interest that has been previously derived: orbital element; radial, transverse, normal position component; Cartesian position components; or the range measurement error. In each case, the coefficients in the vector F will differ, but the linear relation with respect to the gravity field coefficients always exist. The lower case δ is used to indicate that the perturbation is resulting from an error in the gravity field coefficients; as opposed to the previously used upper case Δ which was used to denote the full perturbation effect due to the gravity field coefficients.

The variance in the quantity ϵ is then

$$P_\epsilon = E[F^T \delta g \delta g^T F] = F^T E[\delta g \delta g^T] F = F^T P_g F \tag{73}$$

7 Applications

These analytical developments were applied to the particular case of laser range tracking of the Lageos satellite. The problem was to determine the expected magnitude and characteristic of the Lageos orbit error due to gravitational field mismodeling as observed through laser range tracking. In this study the gravity field error covariance for GEM-T1 and GEM-T2 were used to quantify the current uncertainty of the Earth's gravity field. Thus the results presented here are only indicative of the current state of the art as represented by GEM-T1 and GEM-T2. Though the methodology described in this report can continually be applied to new fields that are developed and thus provide another means for quantifying the improved accuracy that such fields provide.

7.1 Lageos and the Tracking Network

The geodetic satellite Lageos is an excellent satellite for analysing the effect of gravity field mismodeling. The satellite is in a high near-circular orbit which decreases its sensitivity to the high degree gravity field coefficients but at the same time it is also minimally effected by nongravitational forces which could mask the gravitational perturbations. So while it does not provide a good test for the entire gravity field model, it does provide a stringent test for the low degree portions of the gravity field (approximately up to degree 20). The orbital elements of the Lageos satellite are given in Table 3.

Table 3. Lageos Orbital Elements.

Orbital Element	Value
semi-major axis	12,271 km
eccentricity	0.0044
inclination	109.84 degrees

Geodetic satellites such as Lageos are tracked by a globally distributed network of laser ranging stations. Some of these stations operate at a fixed location and others are transportable and have operated at a number of locations. This has resulted in observations being obtained at well more than 50 locations. To evaluate the expected Lageos laser range residuals that could result from mismodeling the gravity field, a representative subset of 20 tracking locations have been used in this study. These stations are globally distributed and are listed in Table 4.

Table 4. Subset of Laser Range Tracking Station Locations.

Location	East Longitude	Latitude
Arequipa, Peru	288.5°	−16.5°
Easter Island, Chile	250.6°	−27.1°
Goldstone, USA	243.2°	35.2°
Grasse, France	6.9°	43.8°
Graz, Austria	15.5°	47.1°
Greenbelt, USA	283.2°	39.0°
Haleakala, USA	203.7°	20.7°
Huahine, French Polynesia	209.0°	−16.7°
Kwajalein, USA	192.5°	9.4°
Matera, Italy	16.7°	40.6°
McDonald Observatory, USA	256.0°	30.7°
Monument Peak, USA	243.6°	32.9°
Orroral, Australia	149.0°	−35.6°
Platteville, USA	255.3°	40.2°
Quincy, USA	239.1°	40.0°
Royal Greenwich Observatory, UK	0.3°	50.9°
Shanghai, China	121.2°	31.1°
Simosato, Japan	135.9°	33.6°
Wettzell, Germany	12.9°	49.1°
Yaragadee, Australia	115.3°	−29.0°

7.2 Predicted Range Uncertainty

For each of the tracking station locations listed in Table 4, the expected uncertainty of the station-to-satellite range was determined for the Lageos satellite and using the error covariance matrices of the GEM-T1 and GEM-T2 gravity field models. These uncertainties were computed for every geographic location of the Lageos satellite that placed the satellite at least 20 degrees above the horizon with respect to the tracking station location. Thus, the uncertainty varied depending on the relative orientation of the satellite with respect to the tracking site. The results of these computations are summarized in Table 5 for GEM-T1 and Table 6 for GEM-T2.

Table 5. Station-to-Satellite Range Uncertainty for Lageos.
Based on the GEM-T1 Gravity Field Error Covariance.

	Range Uncertainty in millimeters						
	Ascending			Descending			Overall
Station	Min	Max	RMS	Min	Max	RMS	RMS
Arequipa	11	22	16	13	23	17	16
Easter Island	12	33	20	12	24	17	19
Goldstone	11	25	17	12	20	15	16
Grasse	11	26	18	12	33	22	20
Graz	11	28	18	12	33	22	20
Greenbelt	11	23	16	12	23	16	16
Haleakala	14	31	21	12	21	16	18
Huahine	15	35	23	12	23	17	20
Kwajalein	15	33	22	12	21	16	19
Matera	12	24	18	12	35	22	20
McDonald Observatory	11	23	16	12	21	15	16
Monument Peak	11	24	17	12	20	15	16
Orroral	12	32	21	11	24	17	19
Platteville	11	23	17	11	21	16	16
Quincy	11	25	18	11	21	15	17
Greenwich Observatory	11	27	18	11	30	21	19
Shanghai	13	31	21	13	28	19	20
Simosato	13	33	22	12	26	18	20
Wettzell	11	29	18	12	33	22	20
Yaragadee	12	24	18	11	25	17	18

Table 6. Station-to-Satellite Range Uncertainty for Lageos.
Based on the GEM-T2 Gravity Field Error Covariance.

	Range Uncertainty in millimeters						
	Ascending			Descending			Overall
Station	Min	Max	RMS	Min	Max	RMS	RMS
Arequipa	7	14	10	7	14	10	10
Easter Island	7	19	12	7	15	11	11
Goldstone	7	15	10	7	12	9	10
Grasse	7	15	11	7	17	11	11
Graz	7	15	10	7	17	12	11
Greenbelt	7	14	10	7	14	10	10

Table 6. Continued.

	Range Uncertainty in millimeters						
	Ascending			Descending			Overall
Station	Min	Max	RMS	Min	Max	RMS	RMS
Haleakala	8	17	12	8	13	10	11
Huahine	9	19	13	7	14	10	12
Kwajalein	9	18	12	8	14	10	11
Matera	7	14	10	7	18	12	11
McDonald Observatory	7	14	10	7	12	9	10
Monument Peak	7	15	10	7	12	9	10
Orroral	7	17	12	7	15	11	11
Platteville	7	14	10	7	13	10	10
Quincy	7	15	11	7	13	10	10
Greenwich Observatory	7	15	11	7	15	11	11
Shanghai	7	16	11	8	16	11	11
Simosato	8	16	11	8	14	11	11
Wettzell	7	15	11	7	17	12	11
Yaragadee	7	15	11	7	15	11	11

These results demonstrate the improvement in gravity field modeling provided by GEM-T2 versus GEM-T1. The overall uncertainty in the overall station-to-satellite range uncertainty decreased from approximately 20 mm to 10 mm. In all cases the range uncertainty tends to be largest when the satellite is low on the horizon (relative to the tracking site) and smallest when the satellite is directly overhead of the tracking site. This is not unexpected since the transverse component of the orbital perturbations are much larger than the radial component. And it is the transverse component that is predominantly being observed by the ranging system when the satellite is low in the sky. When the satellite is more directly overhead a more direct detection of the radial orbit error is being made. This geographic variation of the range uncertainty is clearly shown in the figures of the Appendix.

8 Conclusions

The linear perturbation approach, patterned after the method of Kaula [1966], is a powerful analysis technique for evaluating the accuracy of gravity field modeling. Given the expected uncertainty in the spherical harmonic coefficients of a gravity field model, via the error covariance matrix from least squares, the corresponding expected uncertainty in the orbital motion can be determined in a straightforward manner. And these results can then be extended to determine how these orbital modeling errors will be observed through the satellite tracking system.

Analysis of the Lageos satellite and the gravity field models GEM-T1 and GEM-T2 have shown that the orbital motion is being modeled to the 1–2 cm accuracy level in terms of station-to-satellite range measurements. This accuracy is compatible (in an RMS sense) with the current accuracy of laser range measurements. The range uncertainty as a function of geographic location, shows that gravity field mismodeling will still at times be significantly above the laser range measurement accuracy, and thus still can be a limiting factor in Lageos geophysical studies.

References

[1] Kaula, W. M., *Theory of Satellite Geodesy*, Blaisdell Publishing Company, Waltham, Massachusetts, 1966.

[2] Marsh, J. G., F. J. Lerch, B. H. Putney, D. C. Christodoulidis, D. E. Smith, T. L. Felsentreger, B. V. Sanchez, S. M. Klosko, E. C. Pavlis, T. V. Martin, J. W. Robbins, R. G. Williamson, O. L. Colombo, D. D. Rowlands, W. F. Eddy, N. L. Chandler, K. E. Rachlin, G. B. Patel, S. Bhati, and D. S. Chinn, "A New Gravitational Model for the Earth From Satellite Tracking Data: GEM-T1," *Journal of Geophysical Research*, Vol. 93, pp. 6169–6215, June 1988.

[3] Marsh, J. G., F. J. Lerch, B. H. Putney, T. L. Felsentreger, B. V. Sanchez, S. M. Klosko, G. B. Patel, J. W. Robbins, R. G. Williamson, T. L. Engelis, W. F. Eddy, N. L. Chandler, D. S. Chinn, S. Kapoor, K. E. Rachlin, L. E. Braatz, and E. C. Pavlis, "The GEM-T2 Gravitational Model," *Journal of Geophysical Research*, Vol. 95, pp. 22,043–22,071, December 1990.

[4] Rosborough, G. W., and B. D. Tapley, "Radial, Transverse, and Normal Satellite Position Perturbations due to the Geopotential," *Celestial Mechanics*, Vol. 40, pp. 409–421, 1987.

9 Appendix

The attached figures illustrate the variation of the range uncertainty for each of the tracking sites that have been considered. Figures are only presented for the case of using the GEM-T1 gravity field model. The results for the GEM-T2 model are very similar in character and primarily differ by having an overall smaller magnitude. For each of the tracking sites two figures are presented — one figure for the situation of Lageos being tracked while on an ascending pass and the corresponding case for when Lageos is being tracked on a descending pass. The contours of the range uncertainty are computed over a slightly larger geographic extent than the results provided in Tables 5 and 6. Here the range uncertainty is evaluated for station-to-satellite elevations down to 10 degrees (instead of 20 degrees). This larger geographic coverage provides for a slightly better visualization of the character of the range uncertainty.

RANGE STANDARD DEVIATION PREDICTED BY GEM-T1
AREQUIPA TRACKING LAGEOS ALONG ASCENDING PASSES

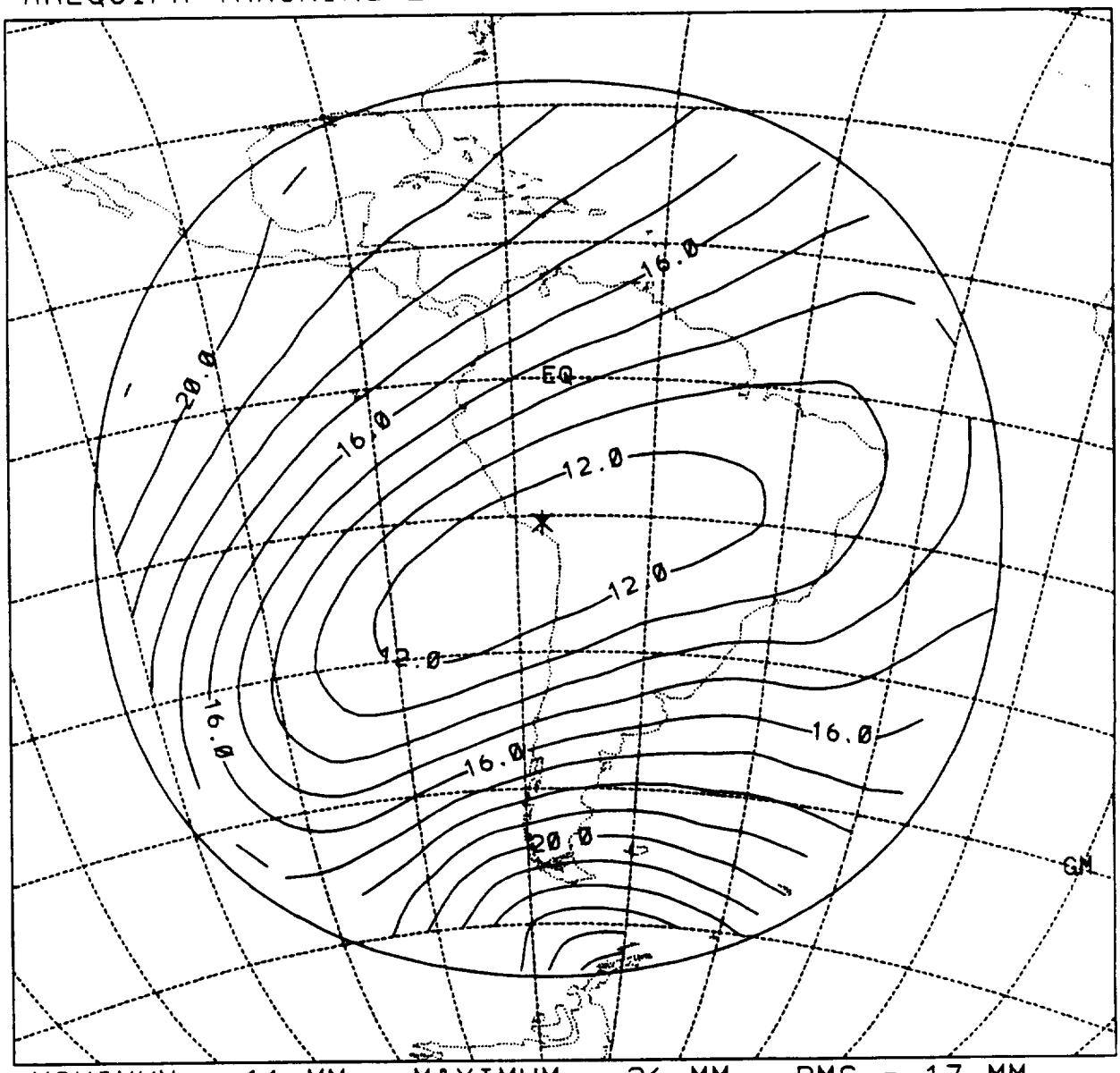

MINIMUM = 11 MM MAXIMUM = 26 MM RMS = 17 MM
CONTOUR INTERVAL = 1 MM

RANGE STANDARD DEVIATION PREDICTED BY GEM-T1
AREQUIPA TRACKING LAGEOS ALONG DESCENDING PASSES

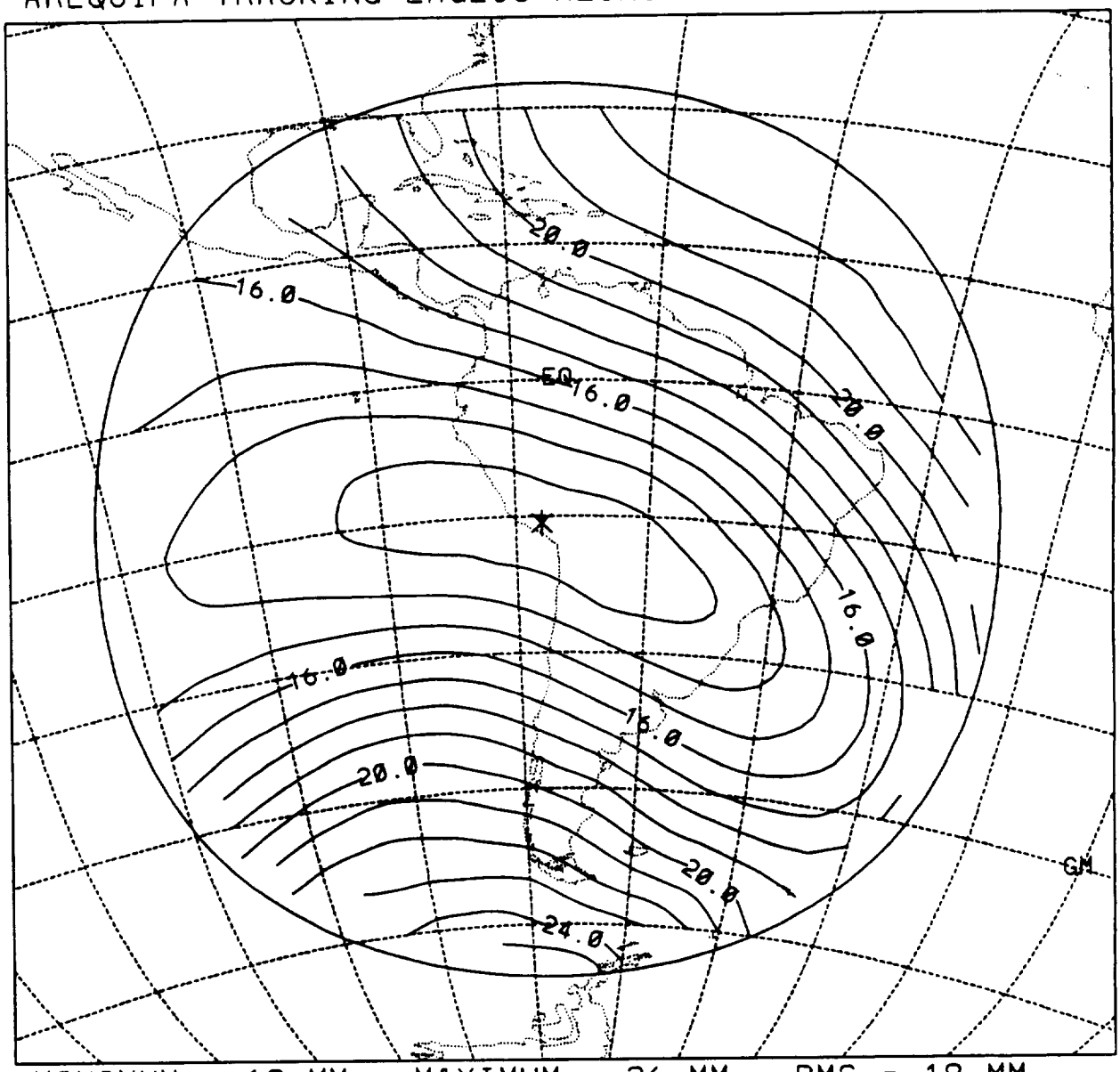

MINIMUM = 12 MM MAXIMUM = 26 MM RMS = 18 MM
CONTOUR INTERVAL = 1 MM

RANGE STANDARD DEVIATION PREDICTED BY GEM-T1
EASTER IS. TRACKING LAGEOS ALONG ASCENDING PASSES

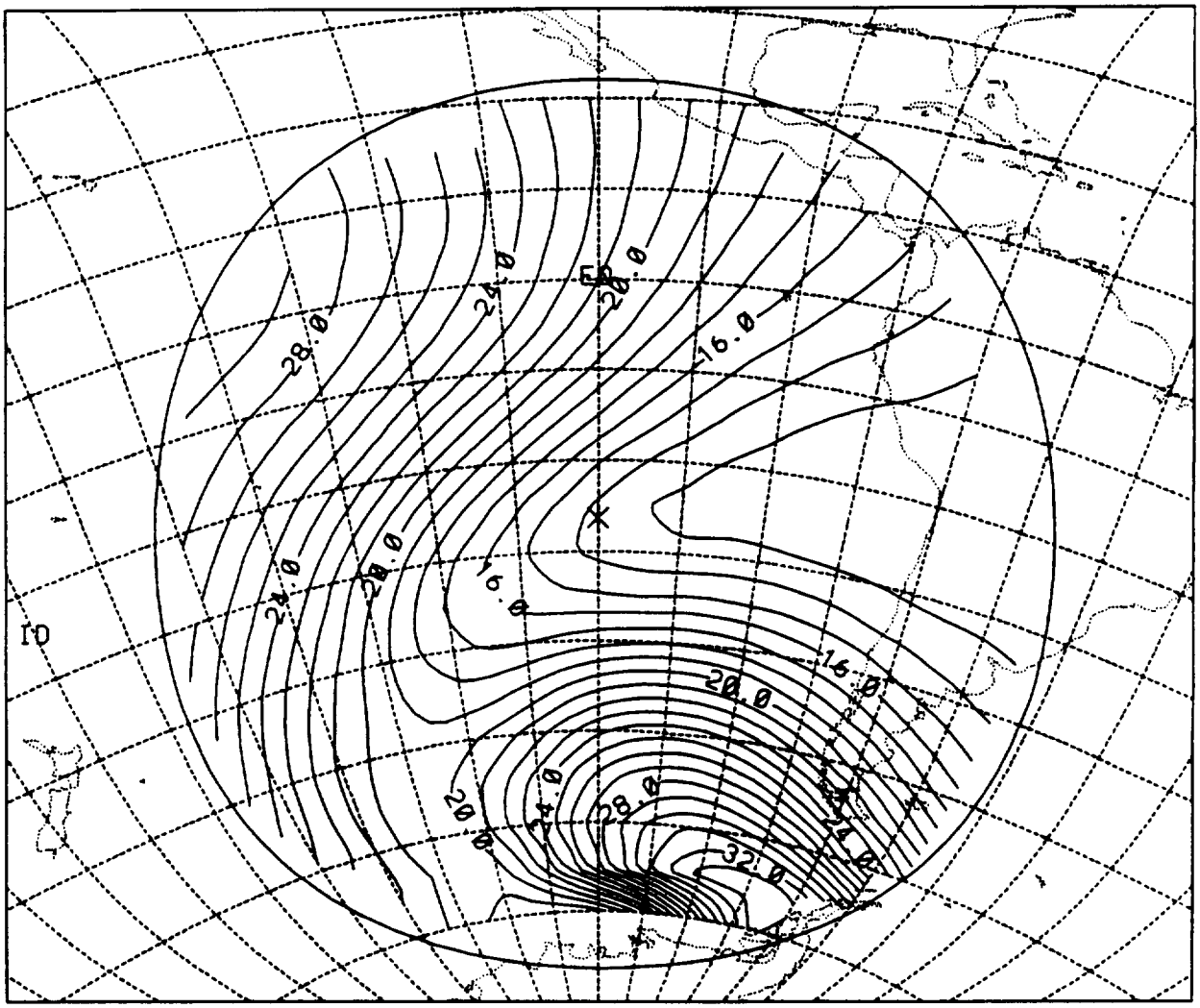

MINIMUM = 12 MM MAXIMUM = 35 MM RMS = 21 MM
CONTOUR INTERVAL = 1 MM

RANGE STANDARD DEVIATION PREDICTED BY GEM-T1
EASTER IS. TRACKING LAGEOS ALONG DESCENDING PASSES

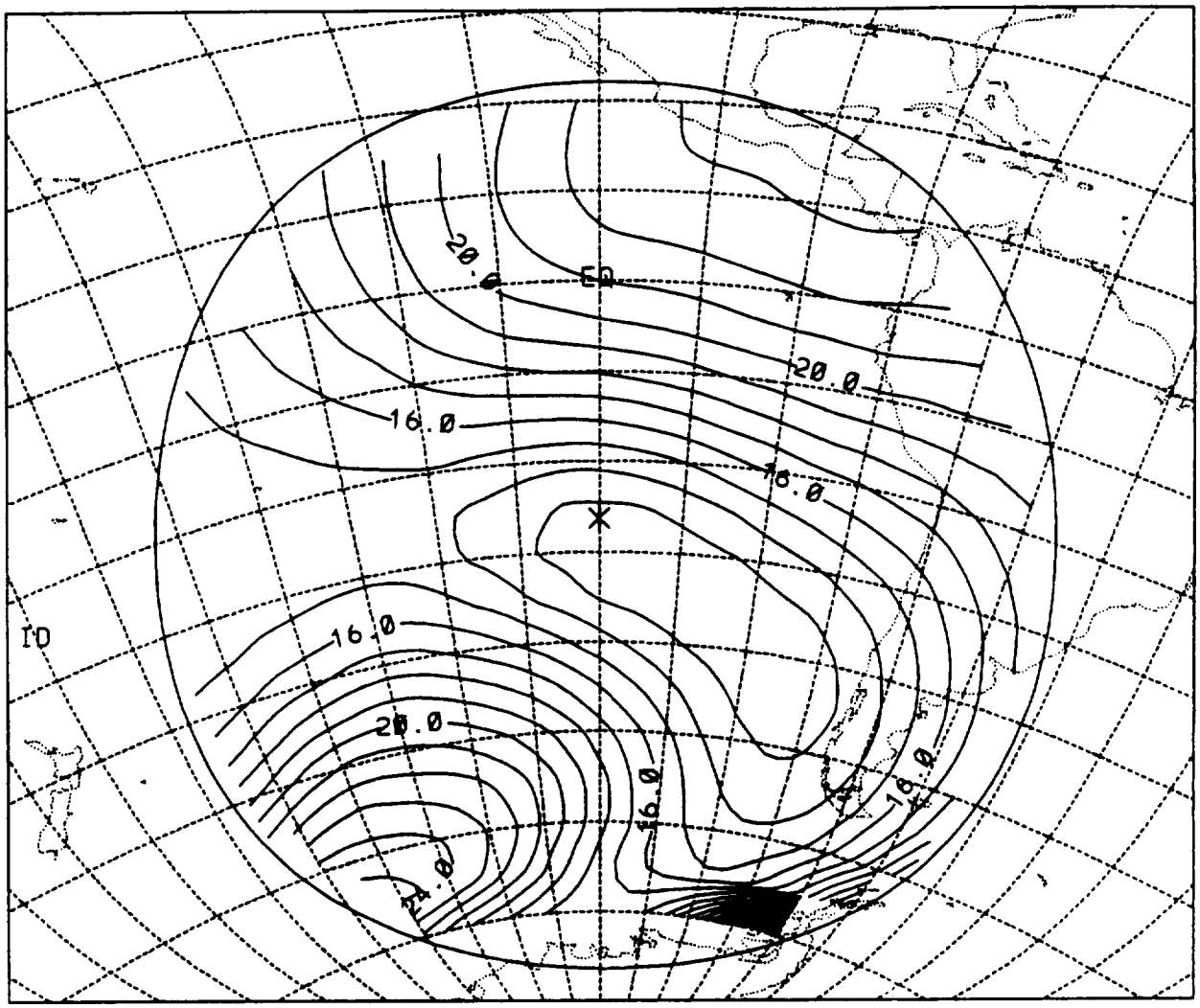

MINIMUM = 12 MM MAXIMUM = 31 MM RMS = 18 MM
CONTOUR INTERVAL = 1 MM

RANGE STANDARD DEVIATION PREDICTED BY GEM-T1
GOLDSTONE TRACKING LAGEOS ALONG ASCENDING PASSES

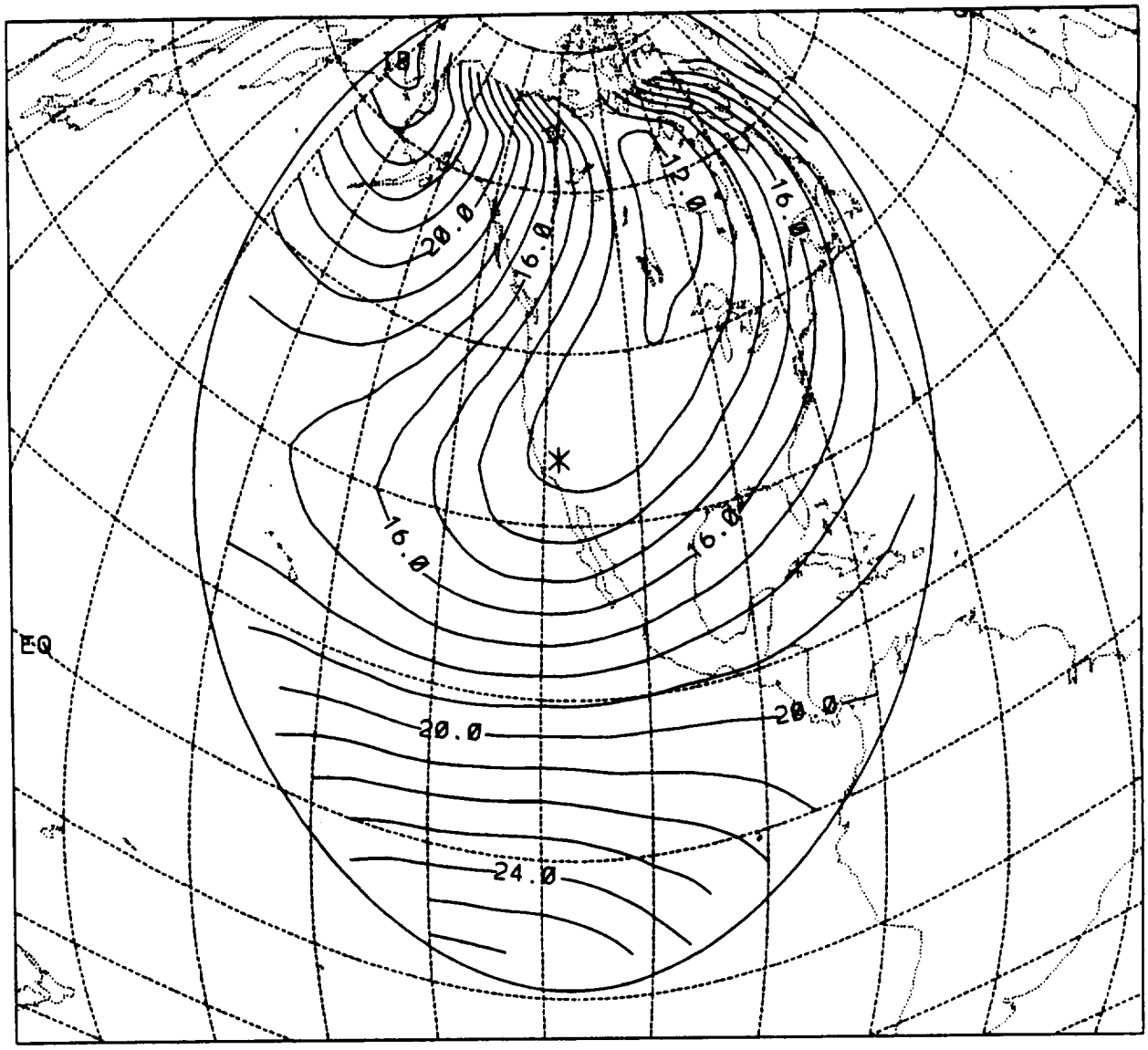

MINIMUM = 12 MM MAXIMUM = 26 MM RMS = 18 MM
CONTOUR INTERVAL = 1 MM

RANGE STANDARD DEVIATION PREDICTED BY GEM-T1
GRASSE TRACKING LAGEOS ALONG ASCENDING PASSES

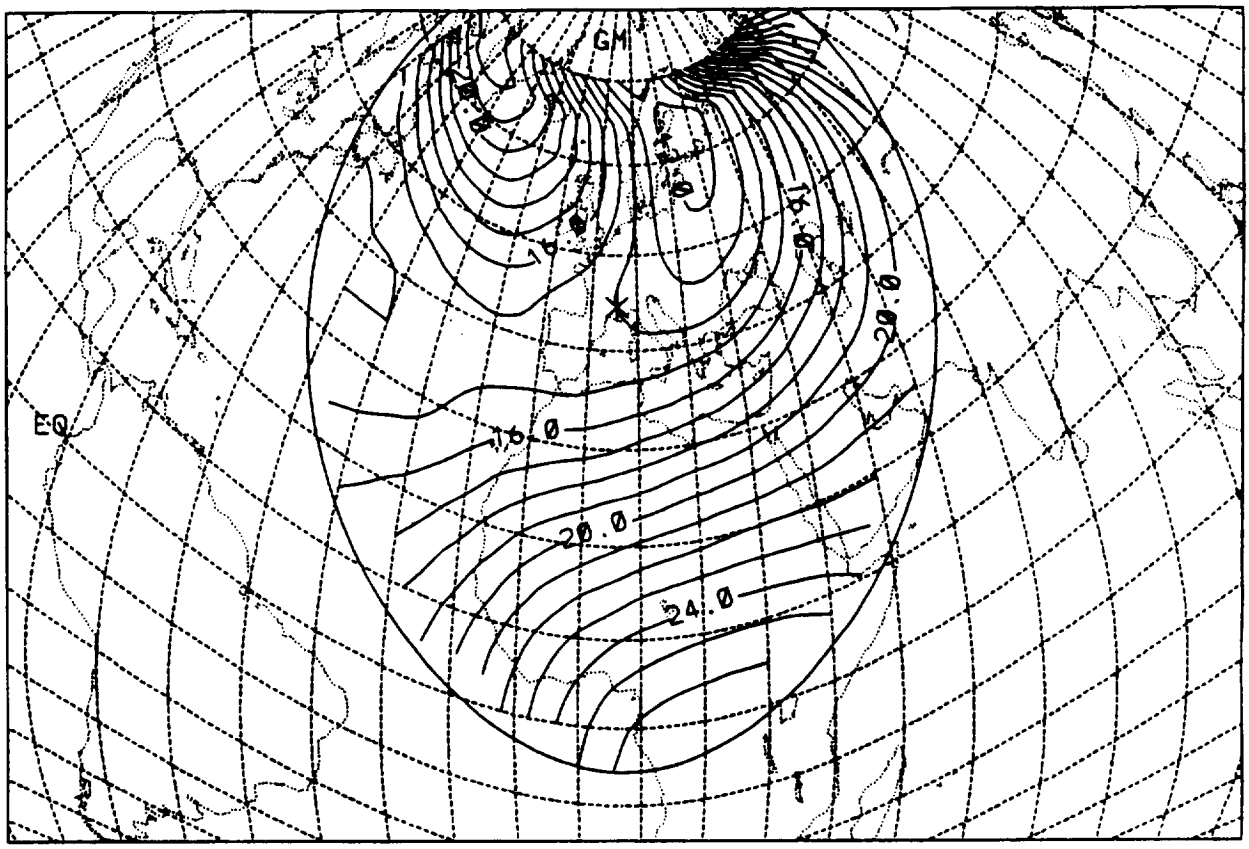

MINIMUM = 11 MM MAXIMUM = 31 MM RMS = 19 MM
CONTOUR INTERVAL = 1 MM

RANGE STANDARD DEVIATION PREDICTED BY GEM-T1
GOLDSTONE TRACKING LAGEOS ALONG DESCENDING PASSES

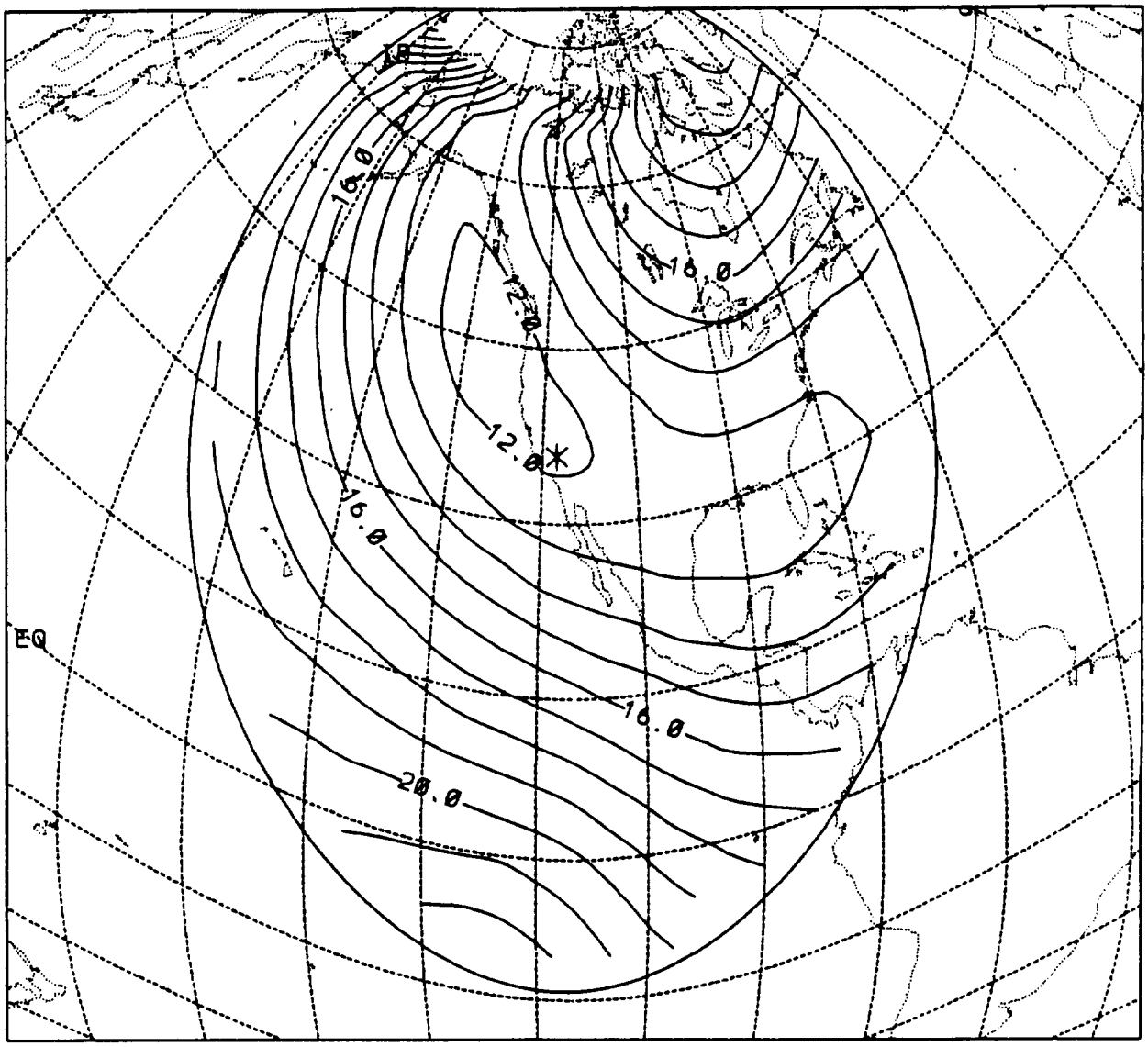

MINIMUM = 11 MM MAXIMUM = 23 MM RMS = 16 MM
CONTOUR INTERVAL = 1 MM

RANGE STANDARD DEVIATION PREDICTED BY GEM-T1
GRASSE TRACKING LAGEOS ALONG DESCENDING PASSES

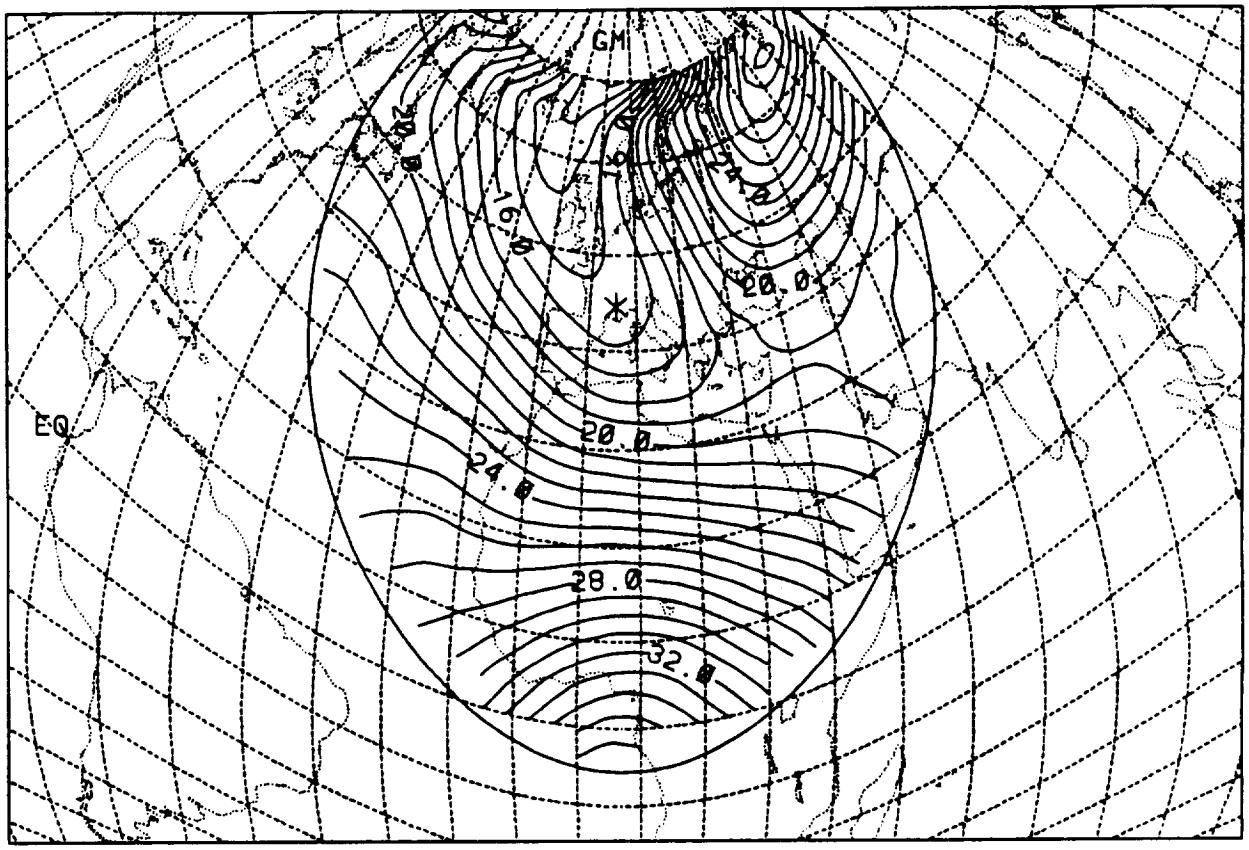

MINIMUM = 12 MM MAXIMUM = 37 MM RMS = 23 MM
CONTOUR INTERVAL = 1 MM

RANGE STANDARD DEVIATION PREDICTED BY GEM-T1
GRAZ TRACKING LAGEOS ALONG ASCENDING PASSES

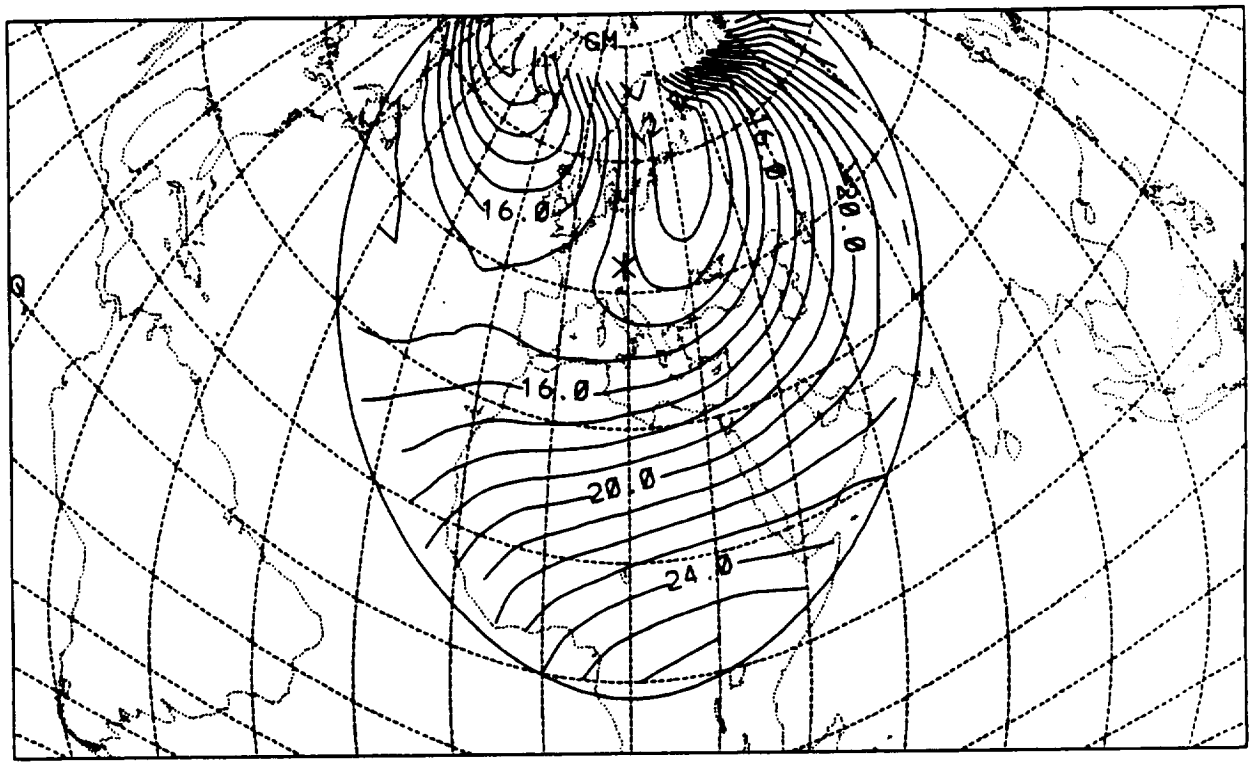

MINIMUM = 11 MM MAXIMUM = 33 MM RMS = 19 MM
CONTOUR INTERVAL = 1 MM

RANGE STANDARD DEVIATION PREDICTED BY GEM-T1
GREENBELT TRACKING LAGEOS ALONG ASCENDING PASSES

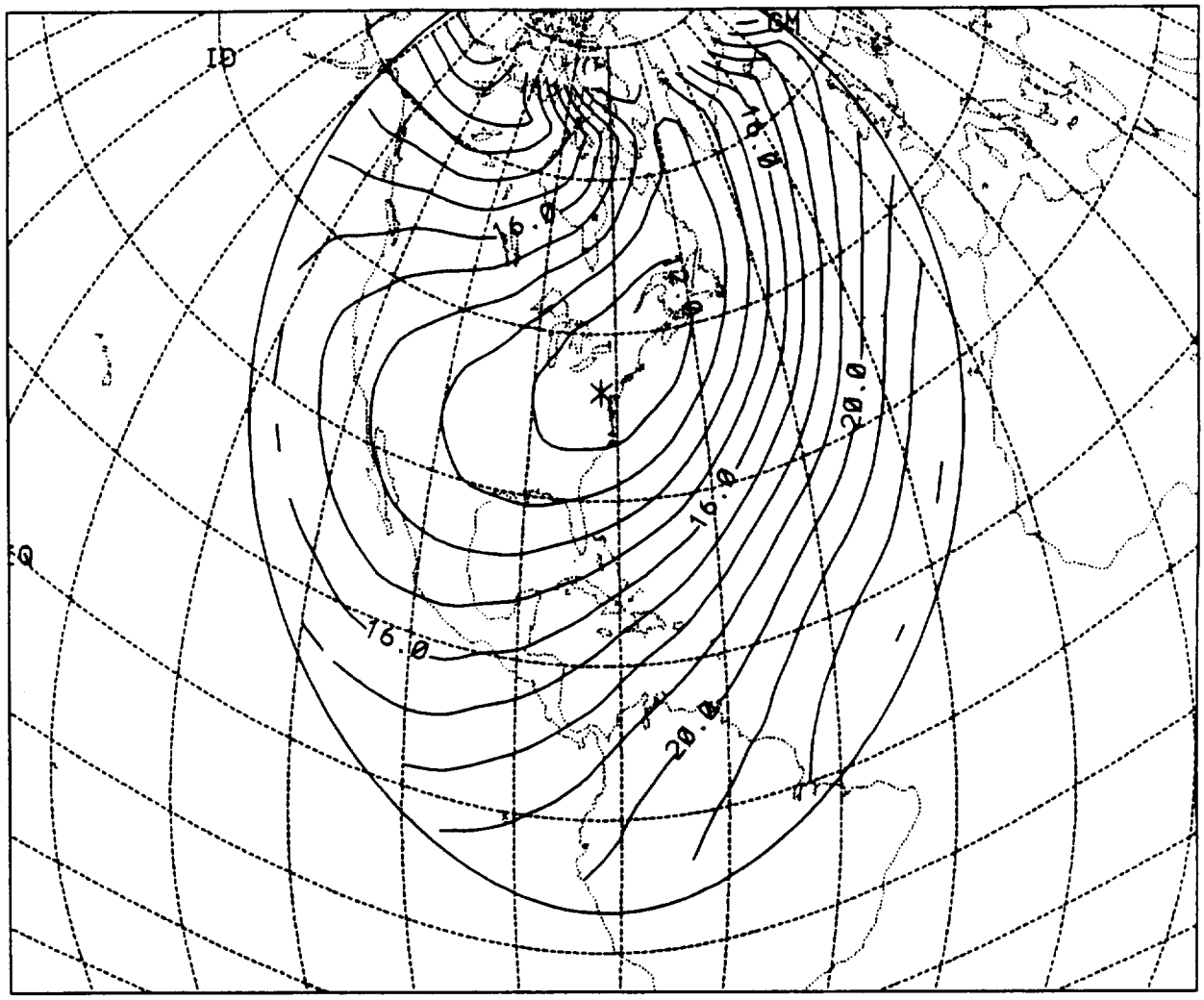

MINIMUM = 11 MM MAXIMUM = 23 MM RMS = 17 MM
CONTOUR INTERVAL = 1 MM

RANGE STANDARD DEVIATION PREDICTED BY GEM-T1
GRAZ TRACKING LAGEOS ALONG DESCENDING PASSES

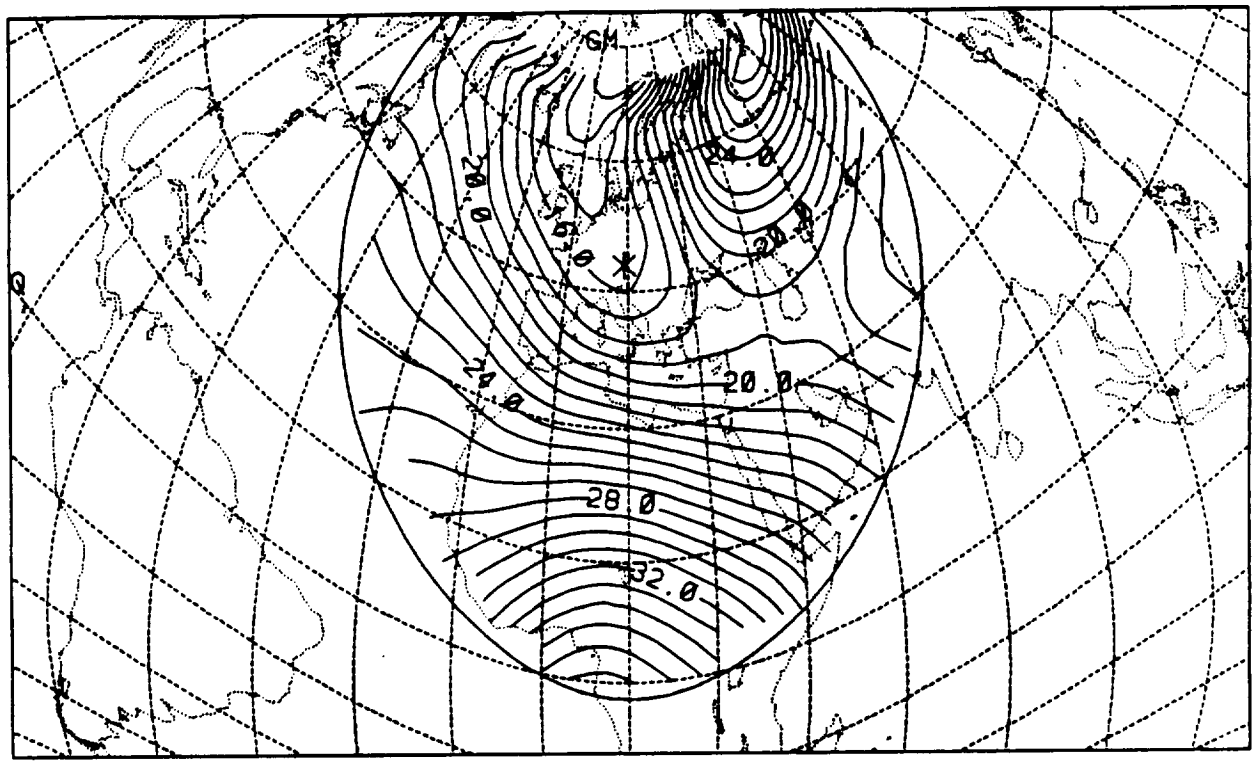

MINIMUM = 12 MM MAXIMUM = 37 MM RMS = 23 MM
CONTOUR INTERVAL = 1 MM

RANGE STANDARD DEVIATION PREDICTED BY GEM-T1
HALEAKALA TRACKING LAGEOS ALONG ASCENDING PASSES

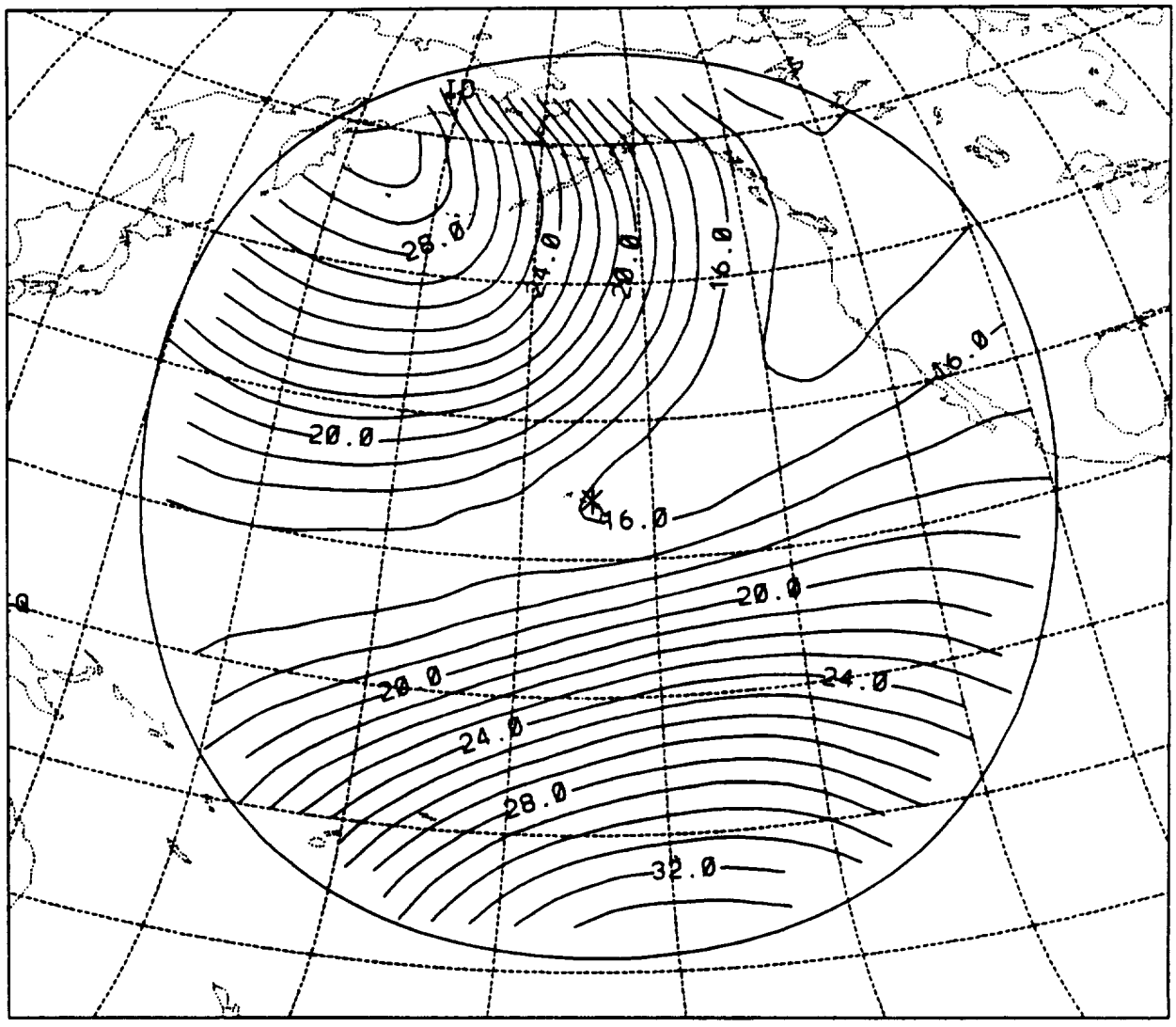

MINIMUM = 13 MM MAXIMUM = 34 MM RMS = 22 MM
CONTOUR INTERVAL = 1 MM

RANGE STANDARD DEVIATION PREDICTED BY GEM-T1
GREENBELT TRACKING LAGEOS ALONG DESCENDING PASSES

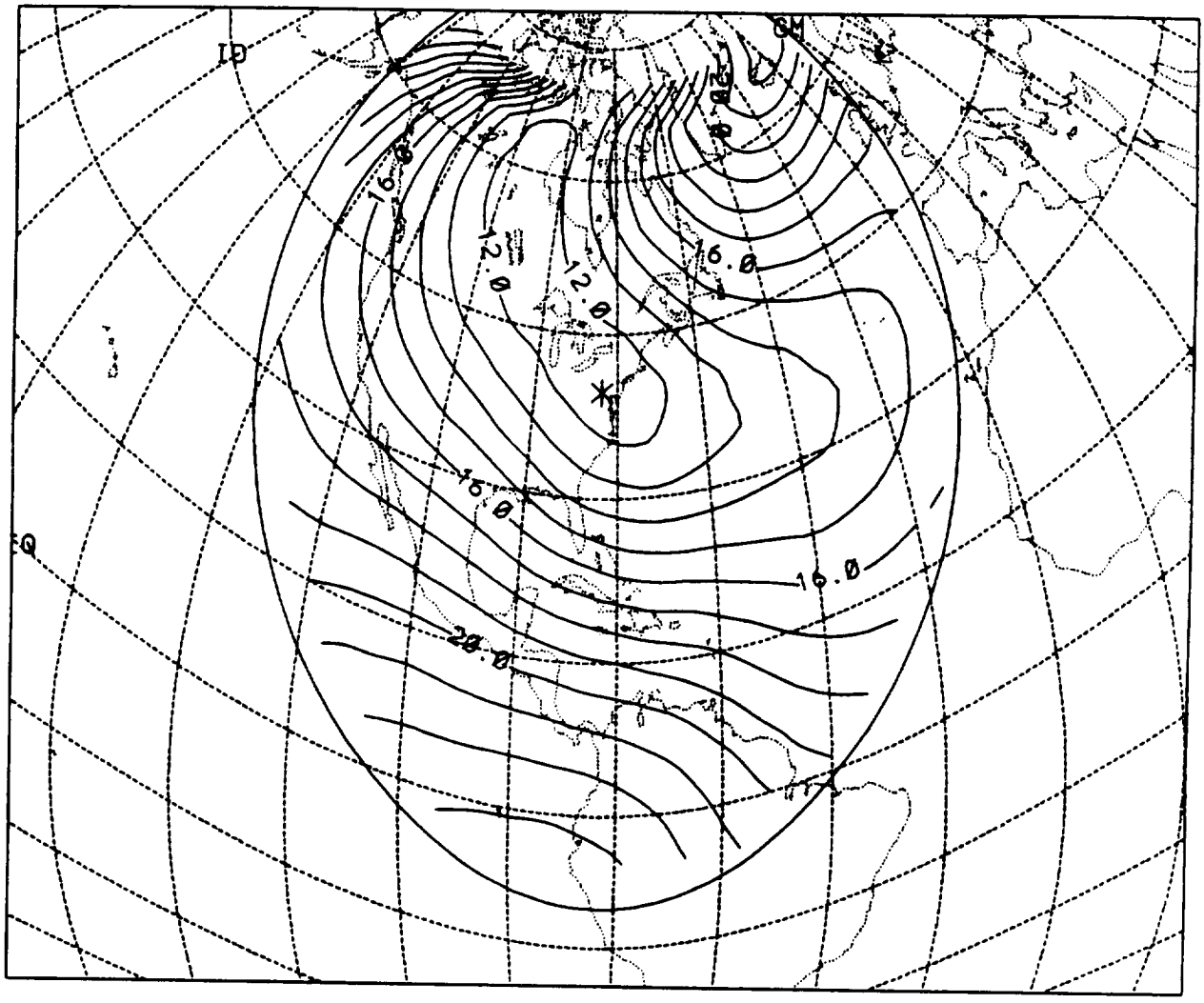

MINIMUM = 11 MM MAXIMUM = 24 MM RMS = 17 MM
CONTOUR INTERVAL = 1 MM

RANGE STANDARD DEVIATION PREDICTED BY GEM-T1
HUAHINE TRACKING LAGEOS ALONG ASCENDING PASSES

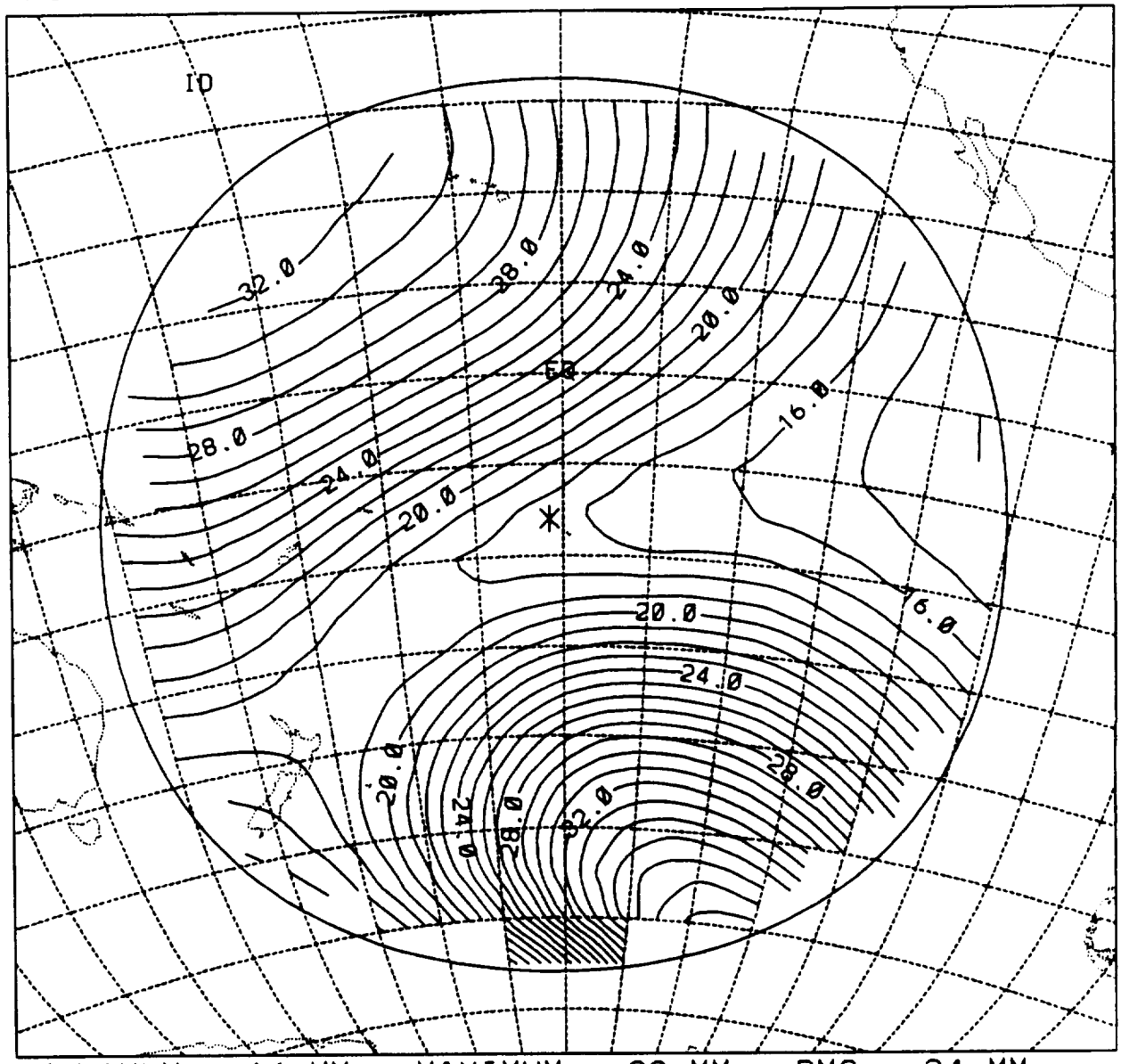

MINIMUM = 14 MM MAXIMUM = 39 MM RMS = 24 MM
CONTOUR INTERVAL = 1 MM

RANGE STANDARD DEVIATION PREDICTED BY GEM-T1
HALEAKALA TRACKING LAGEOS ALONG DESCENDING PASSES

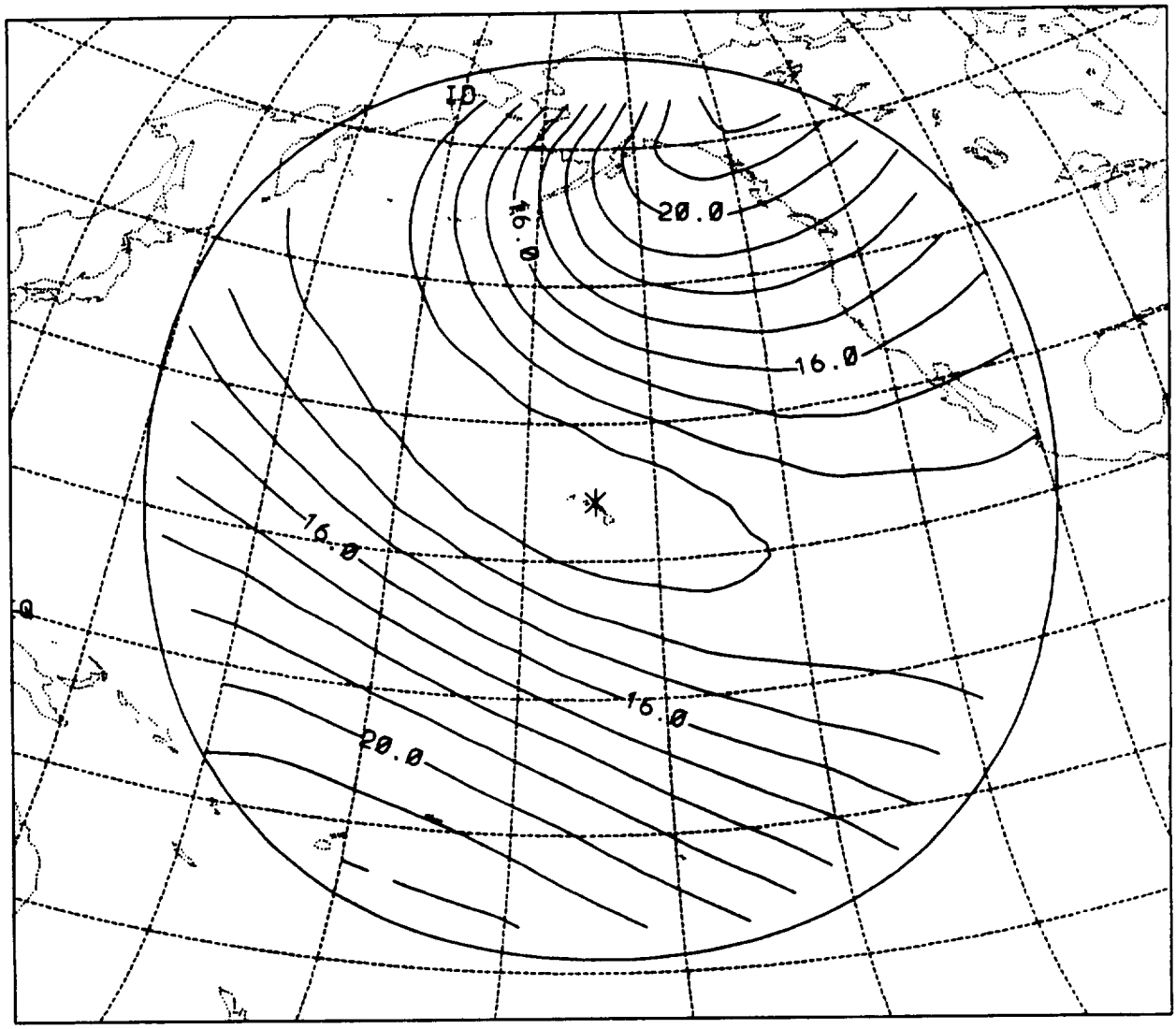

MINIMUM = 12 MM MAXIMUM = 23 MM RMS = 16 MM
CONTOUR INTERVAL = 1 MM

RANGE STANDARD DEVIATION PREDICTED BY GEM-T1
KWAJALEIN TRACKING LAGEOS ALONG ASCENDING PASSES

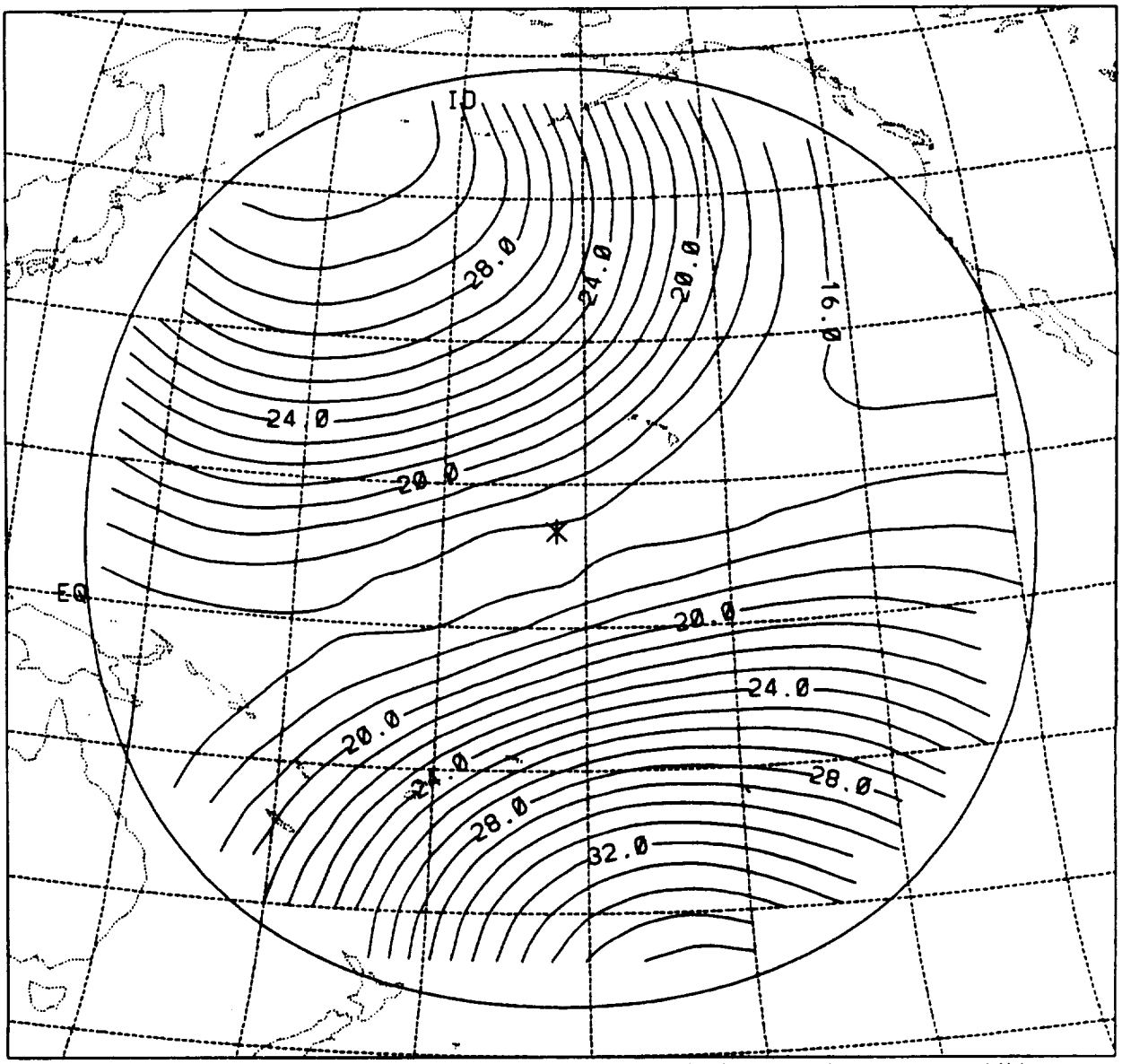

MINIMUM = 15 MM MAXIMUM = 36 MM RMS = 23 MM
CONTOUR INTERVAL = 1 MM

RANGE STANDARD DEVIATION PREDICTED BY GEM-T1
HUAHINE TRACKING LAGEOS ALONG DESCENDING PASSES

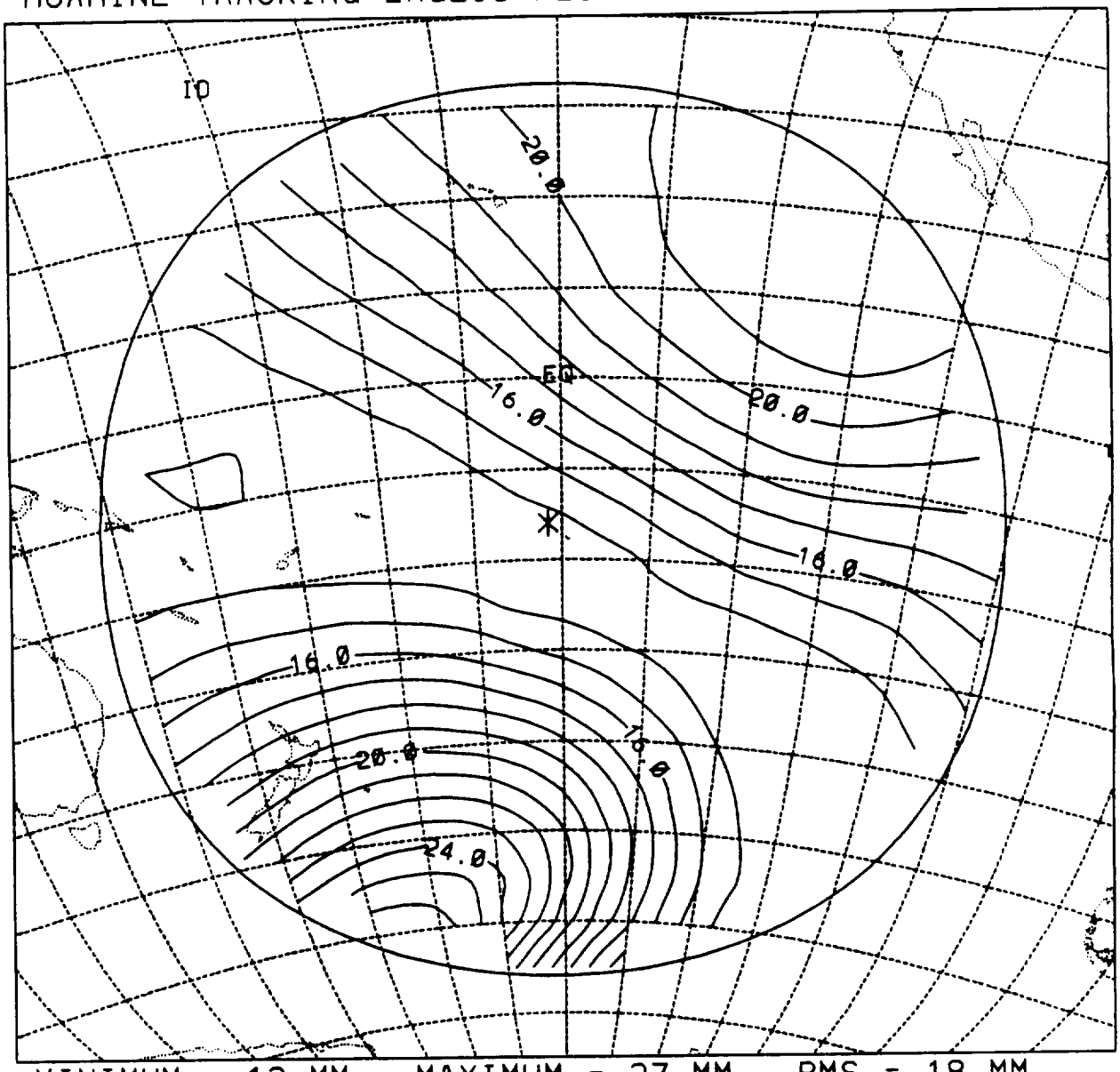

MINIMUM = 13 MM MAXIMUM = 27 MM RMS = 18 MM
CONTOUR INTERVAL = 1 MM

RANGE STANDARD DEVIATION PREDICTED BY GEM-T1
MATERA TRACKING LAGEOS ALONG ASCENDING PASSES

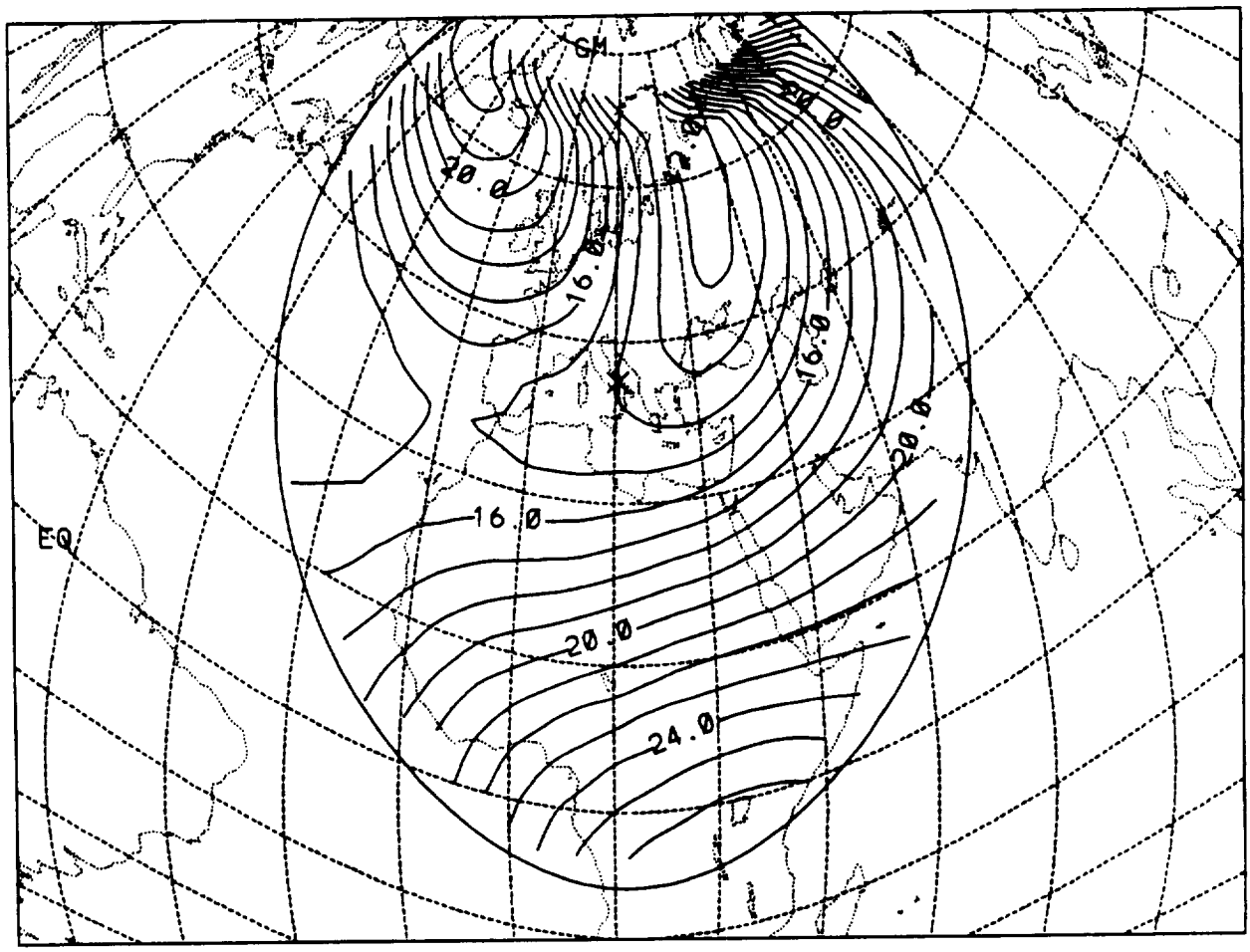

MINIMUM = 12 MM MAXIMUM = 31 MM RMS = 19 MM
CONTOUR INTERVAL = 1 MM

RANGE STANDARD DEVIATION PREDICTED BY GEM-T1
KWAJALEIN TRACKING LAGEOS ALONG DESCENDING PASSES

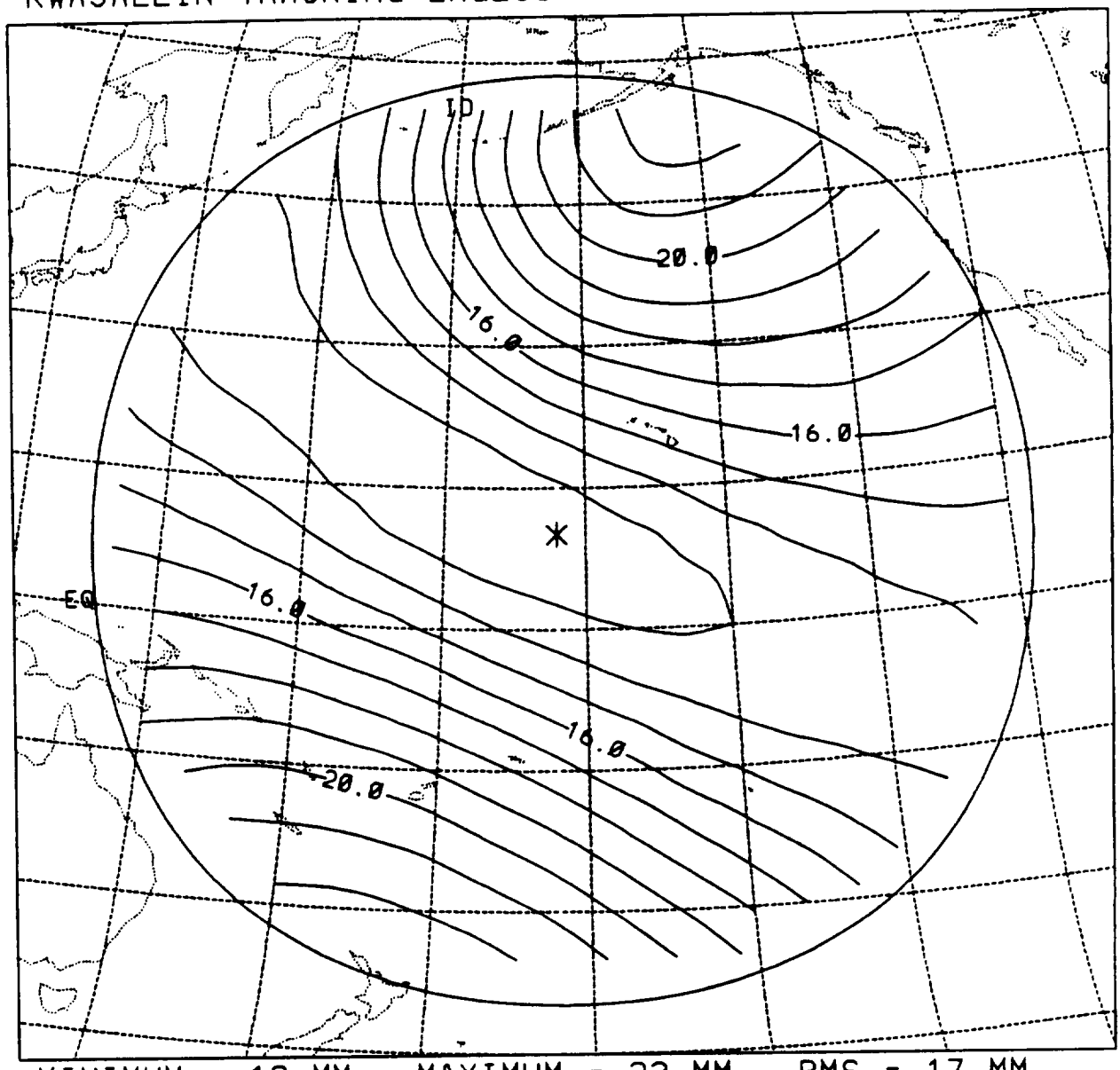

MINIMUM = 12 MM MAXIMUM = 23 MM RMS = 17 MM
CONTOUR INTERVAL = 1 MM

RANGE STANDARD DEVIATION PREDICTED BY GEM-T1
MATERA TRACKING LAGEOS ALONG DESCENDING PASSES

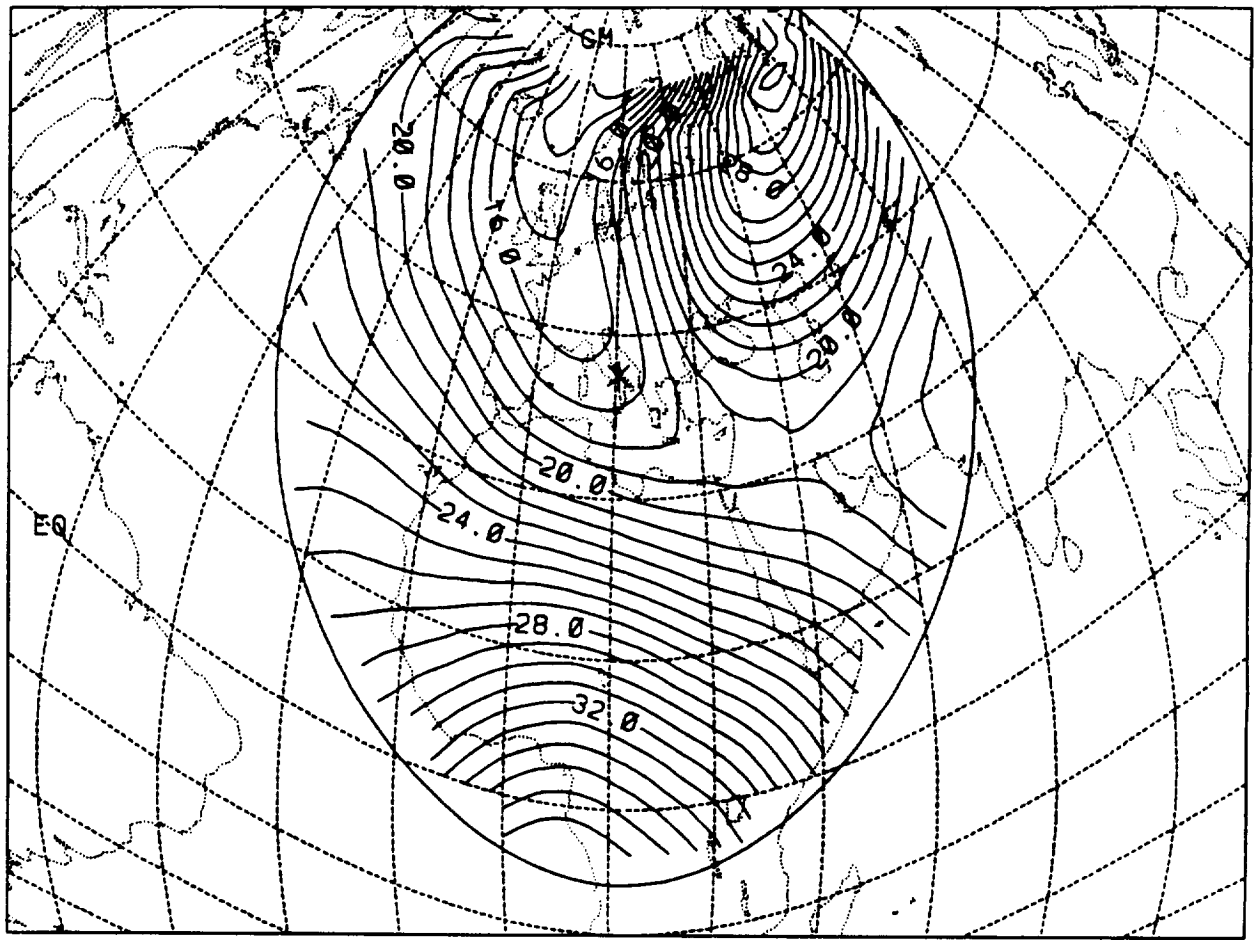

MINIMUM = 12 MM MAXIMUM = 38 MM RMS = 23 MM
CONTOUR INTERVAL = 1 MM

RANGE STANDARD DEVIATION PREDICTED BY GEM-T1
MCDONALD TRACKING LAGEOS ALONG ASCENDING PASSES

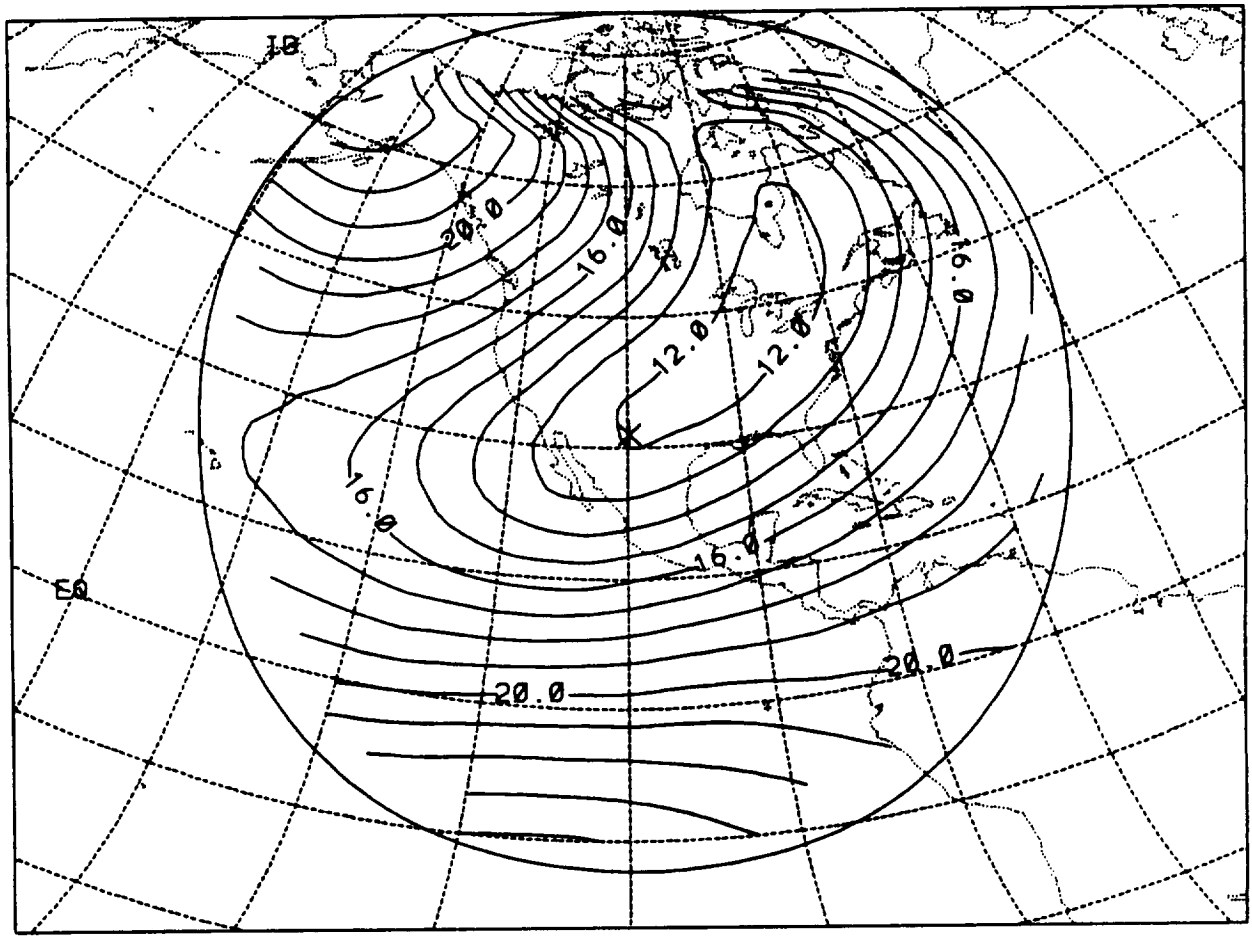

MINIMUM = 12 MM MAXIMUM = 24 MM RMS = 17 MM
CONTOUR INTERVAL = 1 MM

RANGE STANDARD DEVIATION PREDICTED BY GEM-T1
MONUMENT PK TRACKING LAGEOS ALONG ASCENDING PASSES

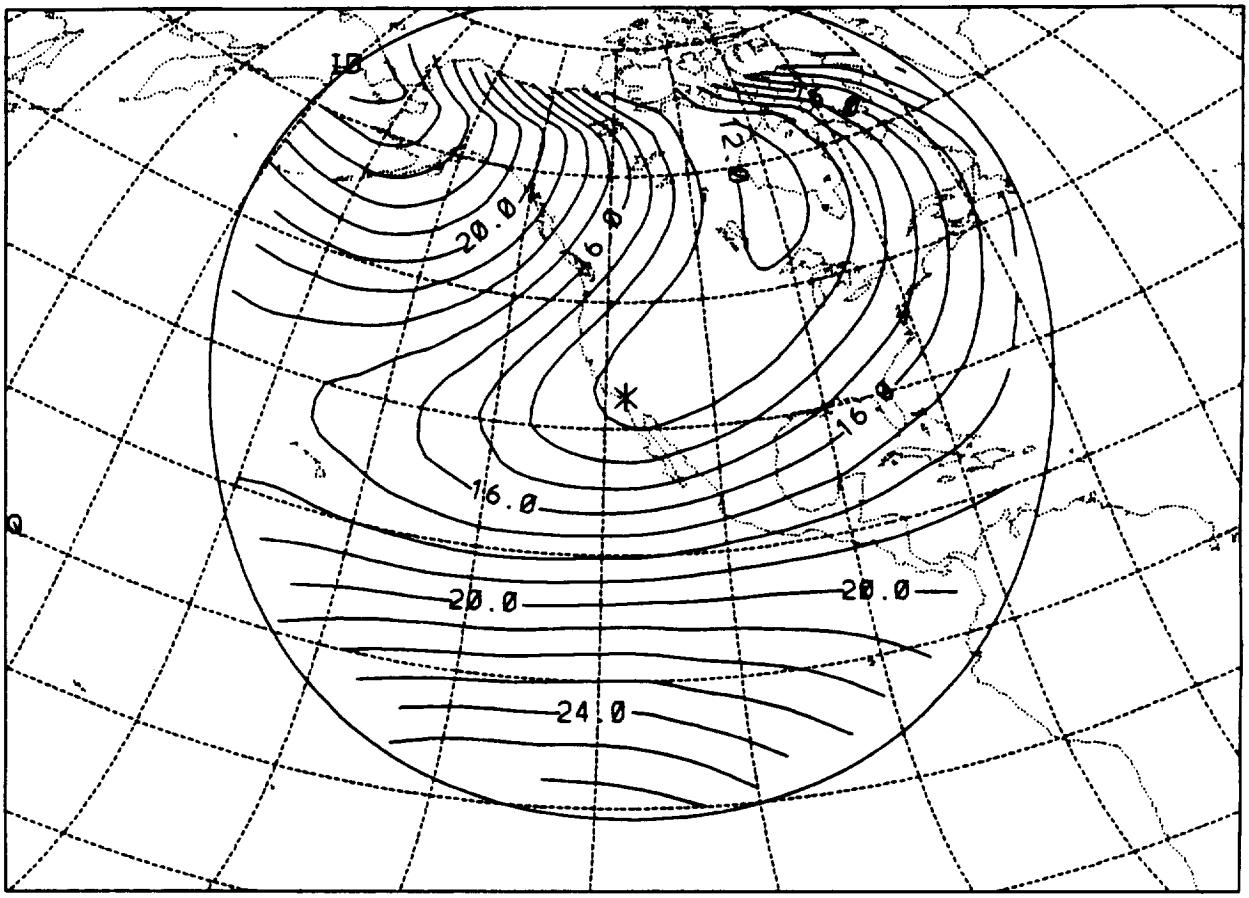

MINIMUM = 12 MM MAXIMUM = 27 MM RMS = 18 MM
CONTOUR INTERVAL = 1 MM

RANGE STANDARD DEVIATION PREDICTED BY GEM-T1
MCDONALD TRACKING LAGEOS ALONG DESCENDING PASSES

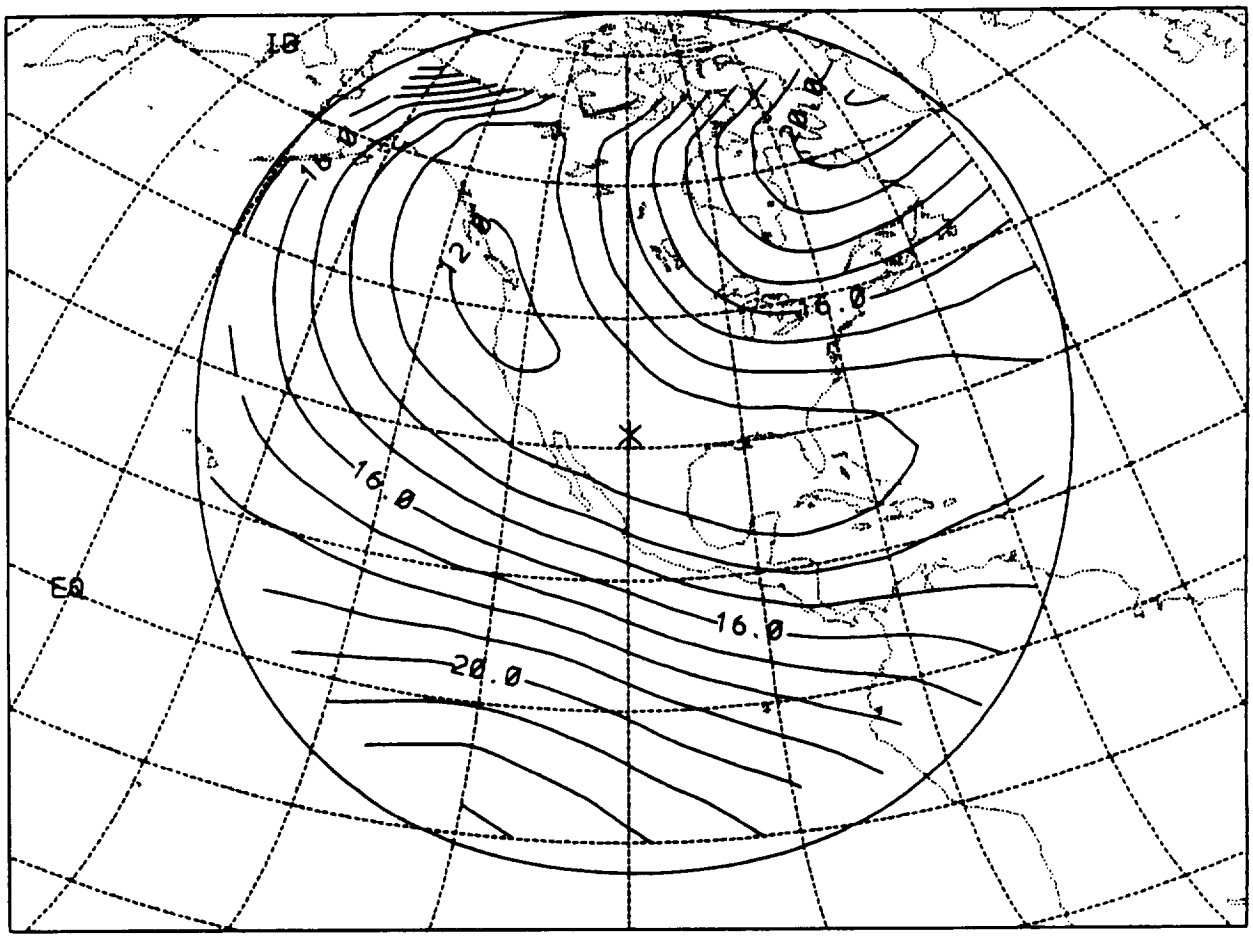

MINIMUM = 12 MM MAXIMUM = 23 MM RMS = 16 MM
CONTOUR INTERVAL = 1 MM

RANGE STANDARD DEVIATION PREDICTED BY GEM-T1
ORRORAL TRACKING LAGEOS ALONG ASCENDING PASSES

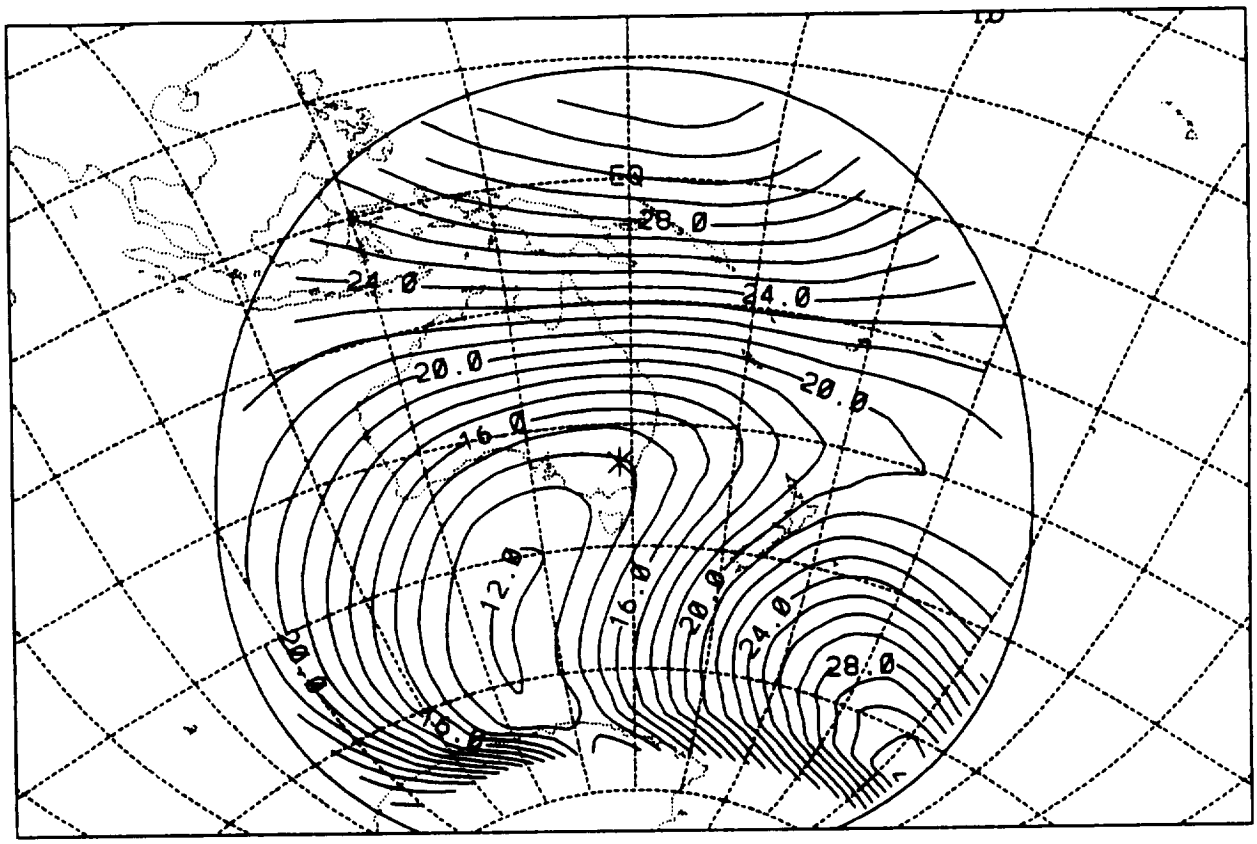

MINIMUM = 12 MM MAXIMUM = 33 MM RMS = 22 MM
CONTOUR INTERVAL = 1 MM

RANGE STANDARD DEVIATION PREDICTED BY GEM-T1
MONUMENT PK TRACKING LAGEOS ALONG DESCENDING PASSE

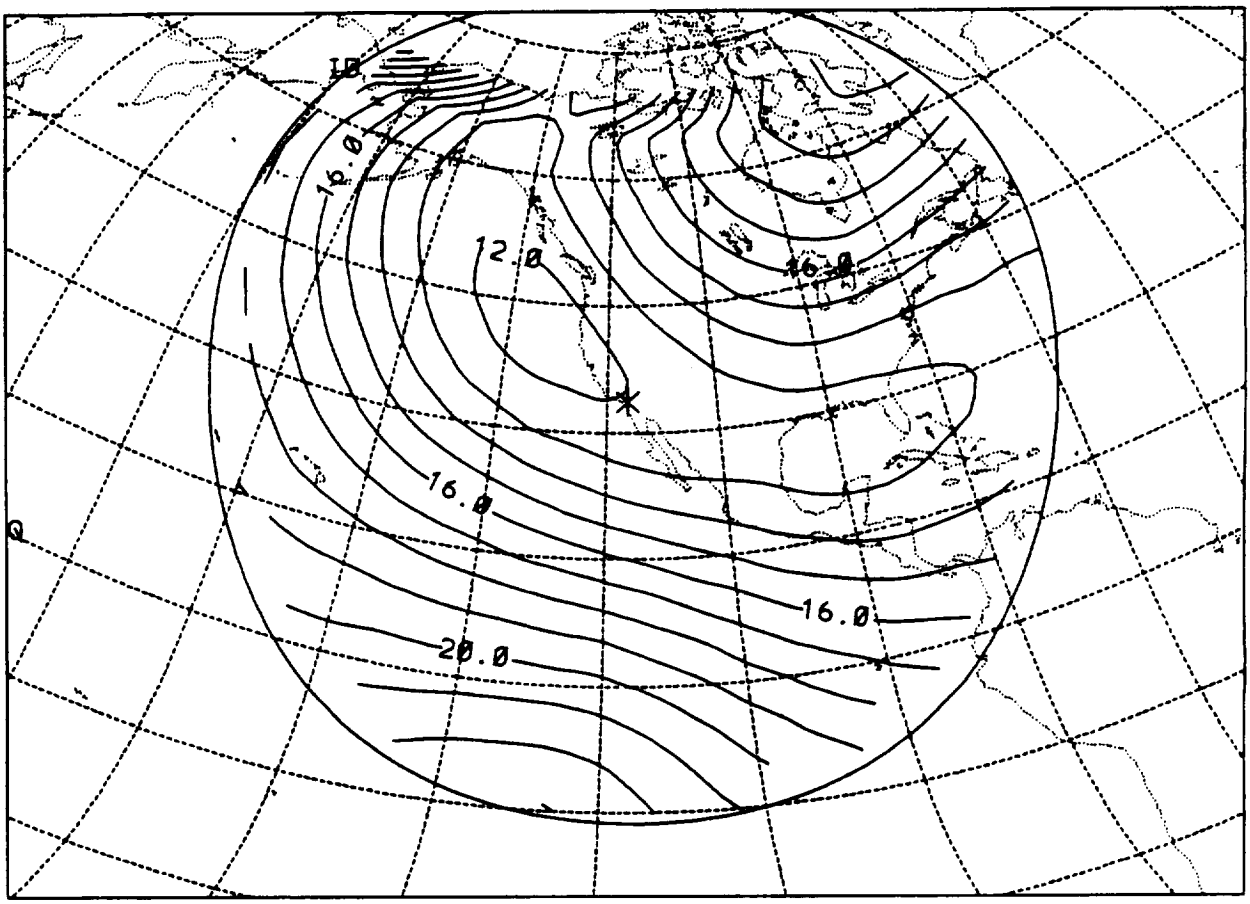

MINIMUM = 12 MM MAXIMUM = 23 MM RMS = 16 MM
CONTOUR INTERVAL = 1 MM

RANGE STANDARD DEVIATION PREDICTED BY GEM-T1
PLATTEVILLE TRACKING LAGEOS ALONG ASCENDING PASSES

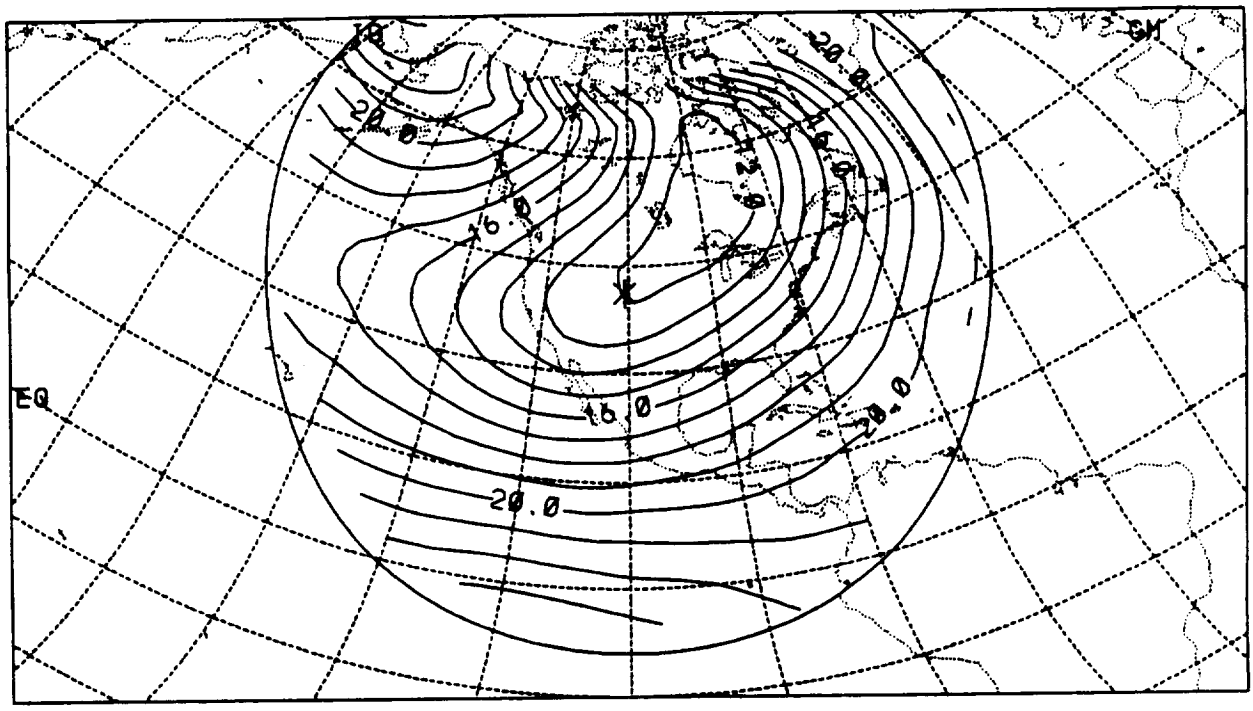

MINIMUM = 11 MM MAXIMUM = 24 MM RMS = 18 MM
CONTOUR INTERVAL = 1 MM

RANGE STANDARD DEVIATION PREDICTED BY GEM-T1
ORRORAL TRACKING LAGEOS ALONG DESCENDING PASSES

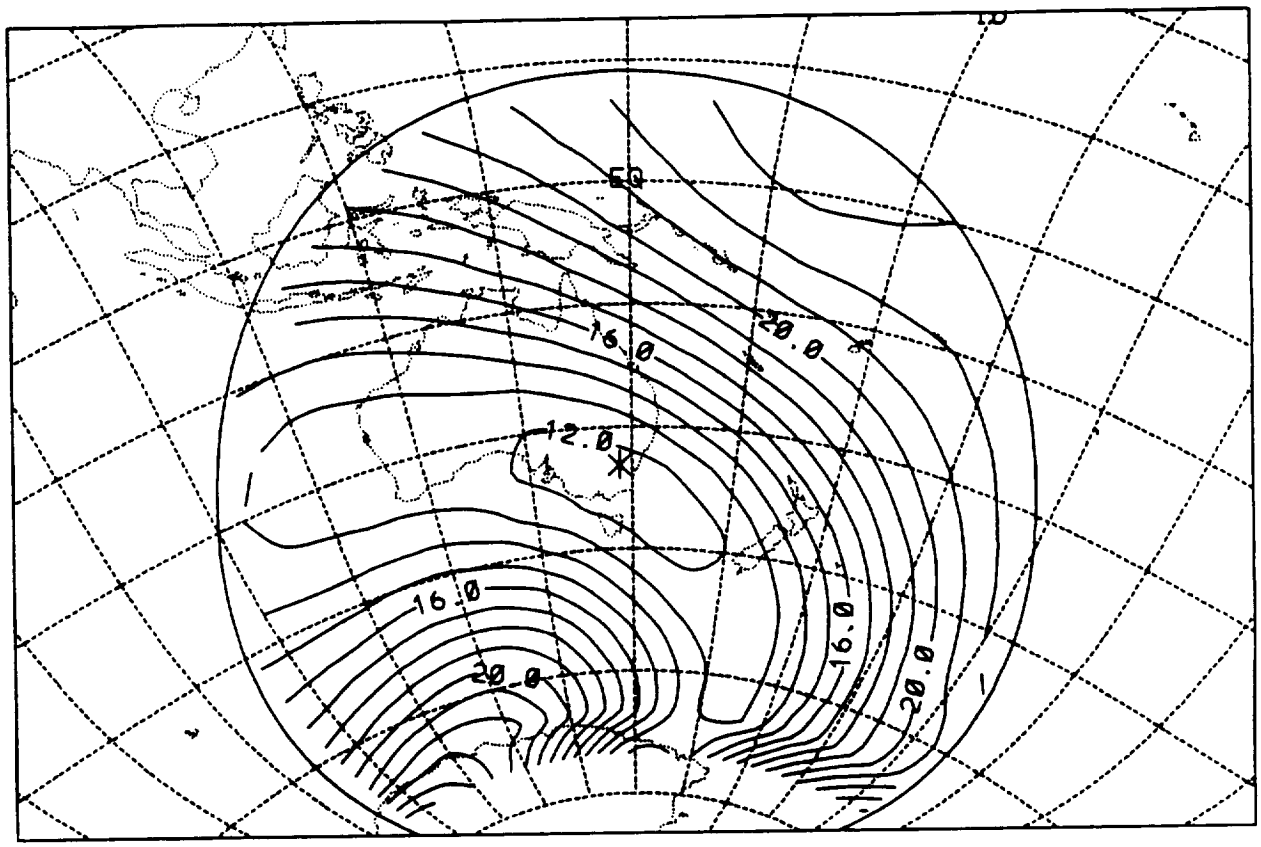

MINIMUM = 11 MM MAXIMUM = 25 MM RMS = 18 MM
CONTOUR INTERVAL = 1 MM

RANGE STANDARD DEVIATION PREDICTED BY GEM-T1
QUINCY TRACKING LAGEOS ALONG ASCENDING PASSES

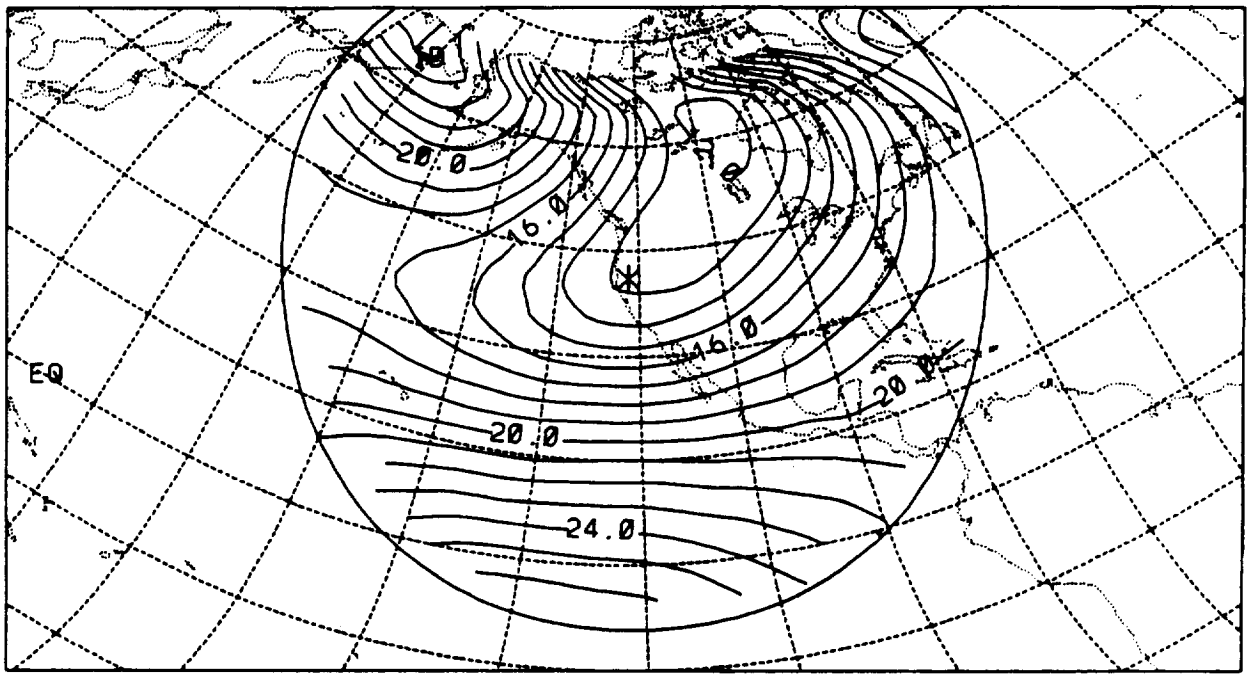

MINIMUM = 12 MM MAXIMUM = 27 MM RMS = 19 MM
CONTOUR INTERVAL = 1 MM

RANGE STANDARD DEVIATION PREDICTED BY GEM-T1
PLATTEVILLE TRACKING LAGEOS ALONG DESCENDING PASSE

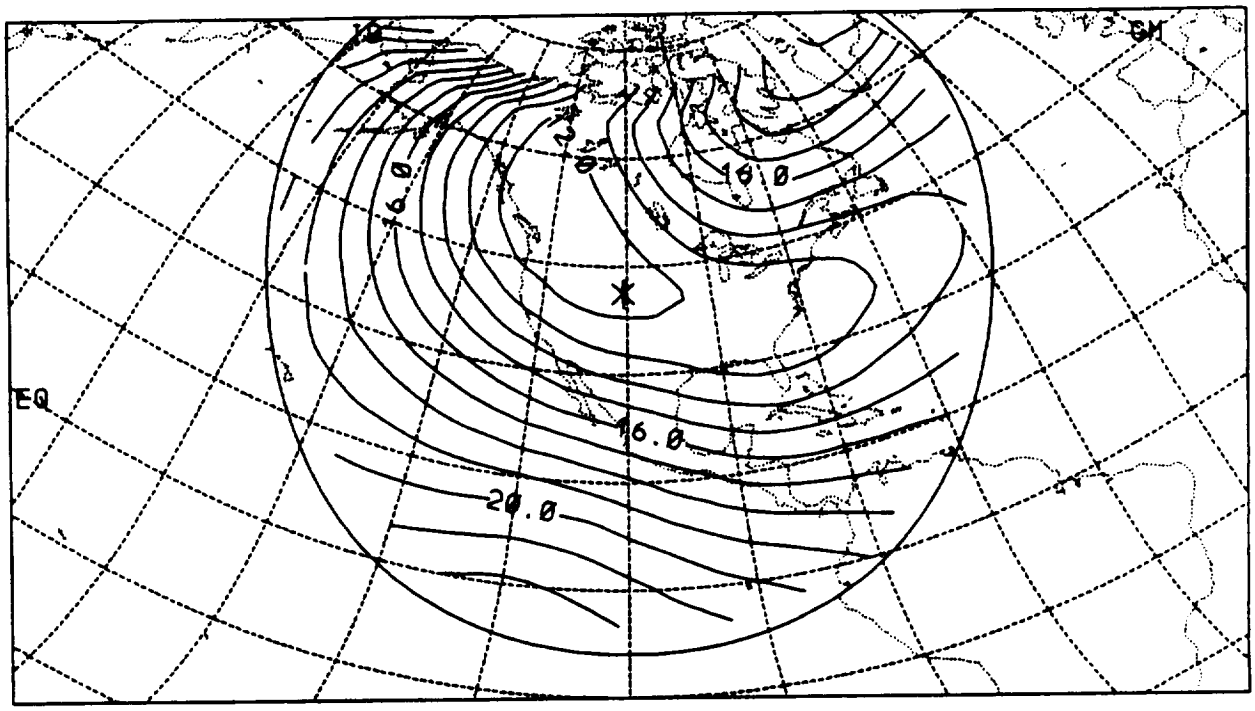

MINIMUM = 11 MM MAXIMUM = 24 MM RMS = 17 MM
CONTOUR INTERVAL = 1 MM

RANGE STANDARD DEVIATION PREDICTED BY GEM-T1
RGO TRACKING LAGEOS ALONG ASCENDING PASSES

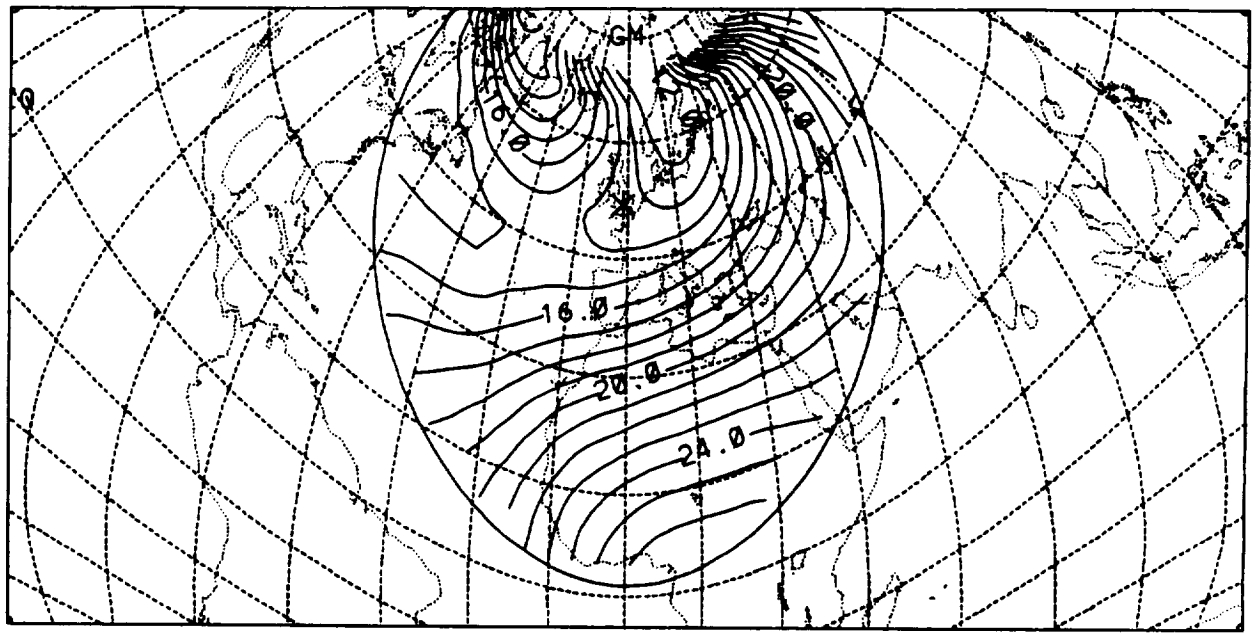

MINIMUM = 11 MM MAXIMUM = 31 MM RMS = 19 MM
CONTOUR INTERVAL = 1 MM

RANGE STANDARD DEVIATION PREDICTED BY GEM-T1
QUINCY TRACKING LAGEOS ALONG DESCENDING PASSES

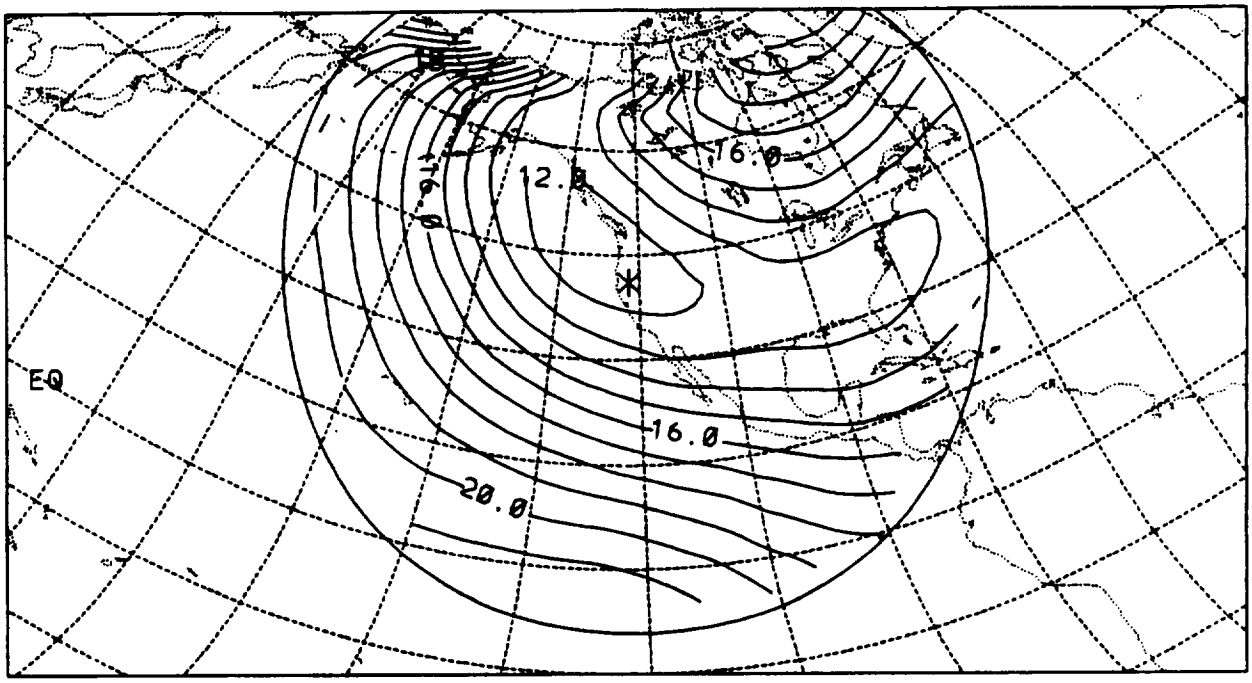

MINIMUM = 11 MM MAXIMUM = 26 MM RMS = 17 MM
CONTOUR INTERVAL = 1 MM

RANGE STANDARD DEVIATION PREDICTED BY GEM-T1
SHANGHAI TRACKING LAGEOS ALONG ASCENDING PASSES

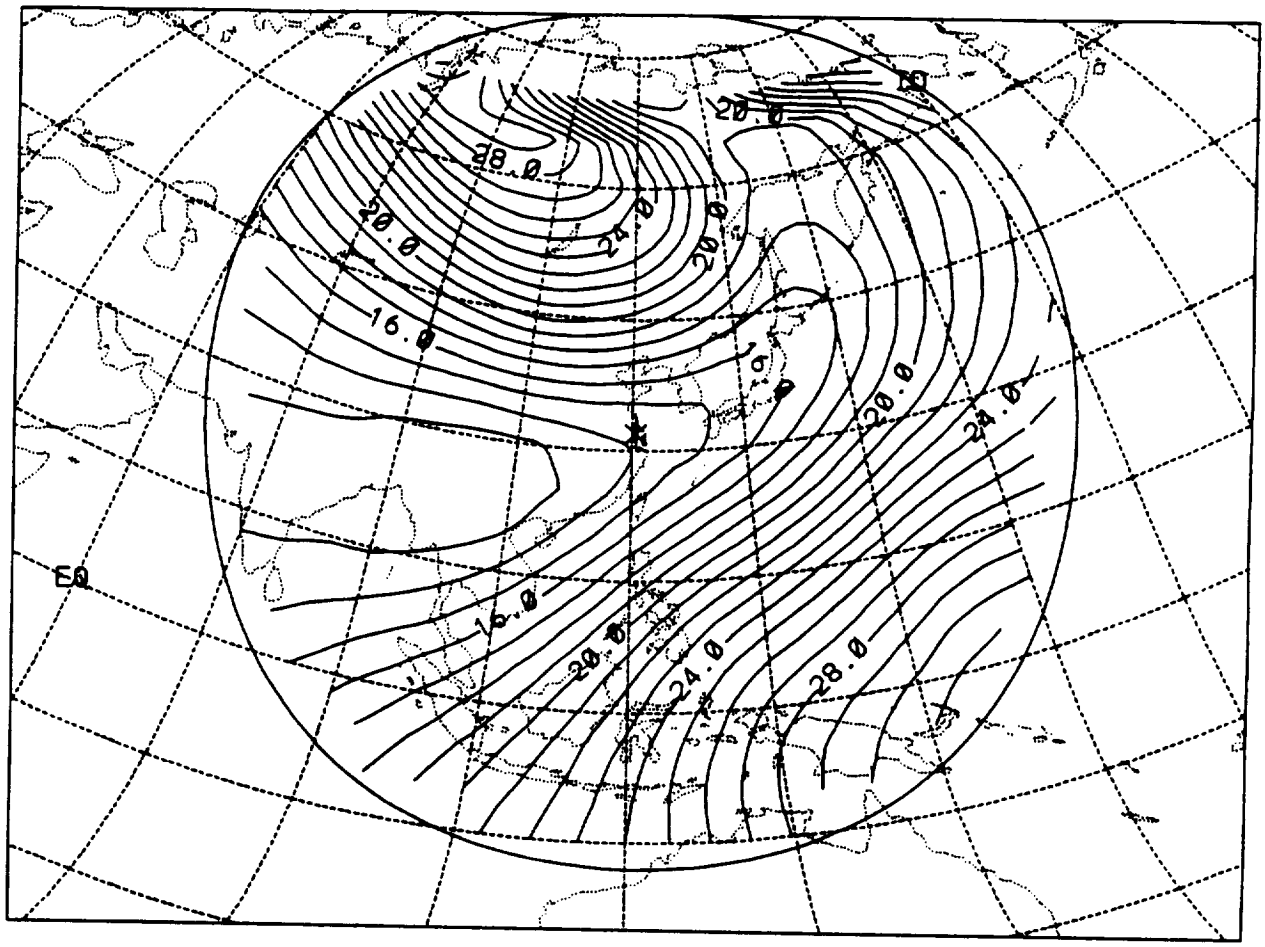

MINIMUM = 12 MM MAXIMUM = 32 MM RMS = 21 MM
CONTOUR INTERVAL = 1 MM

RANGE STANDARD DEVIATION PREDICTED BY GEM-T1
RGO TRACKING LAGEOS ALONG DESCENDING PASSES

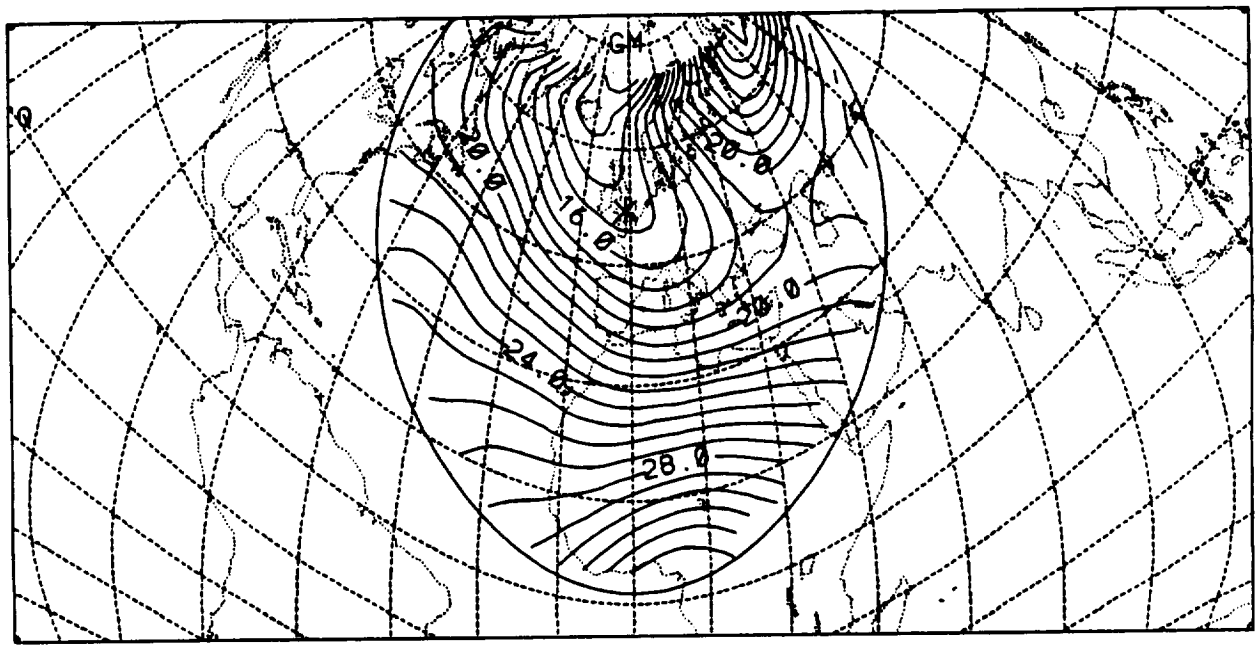

MINIMUM = 11 MM MAXIMUM = 34 MM RMS = 22 MM
CONTOUR INTERVAL = 1 MM

RANGE STANDARD DEVIATION PREDICTED BY GEM-T1
SIMOSATO TRACKING LAGEOS ALONG ASCENDING PASSES

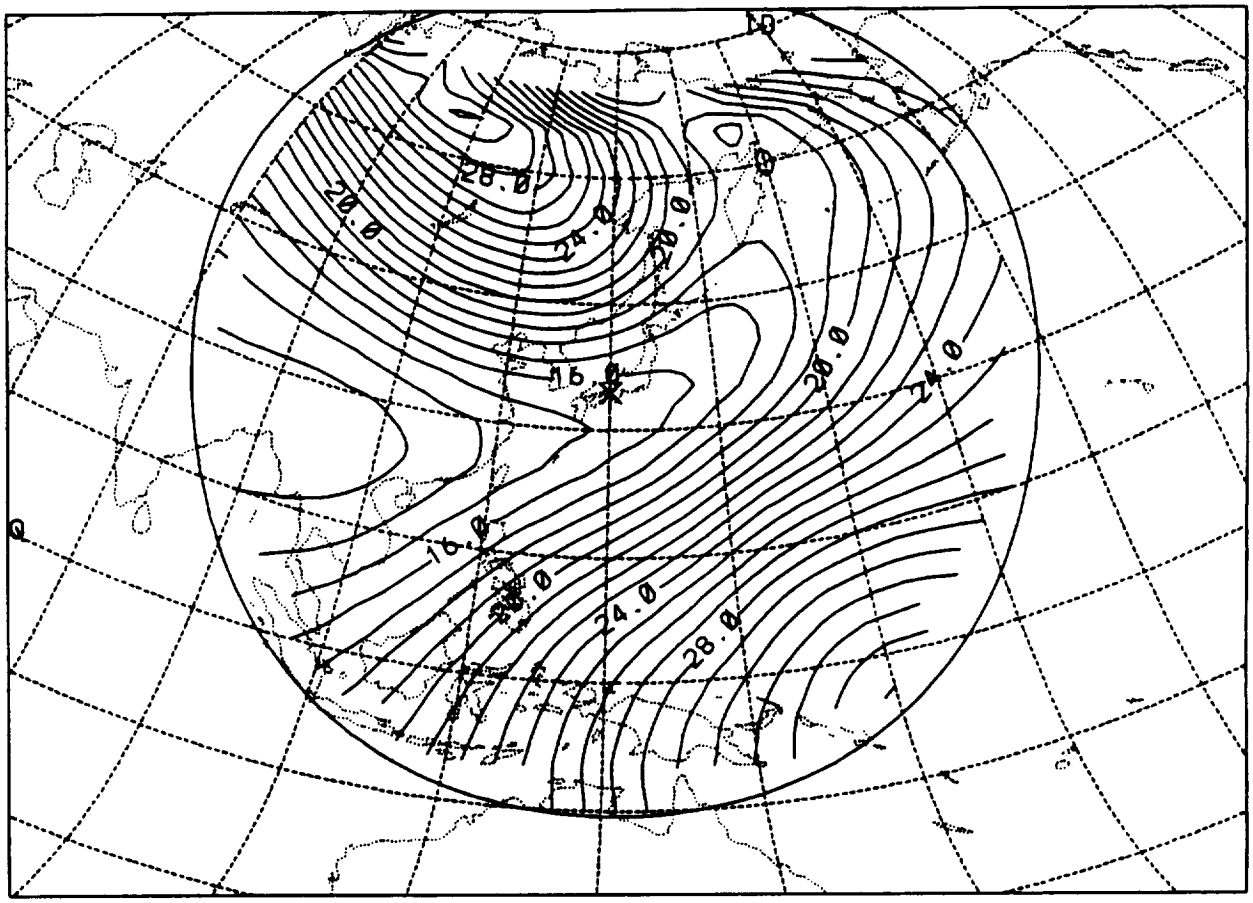

MINIMUM = 12 MM MAXIMUM = 34 MM RMS = 22 MM
CONTOUR INTERVAL = 1 MM

RANGE STANDARD DEVIATION PREDICTED BY GEM-T1
SHANGAHI TRACKING LAGEOS ALONG DESCENDING PASSES

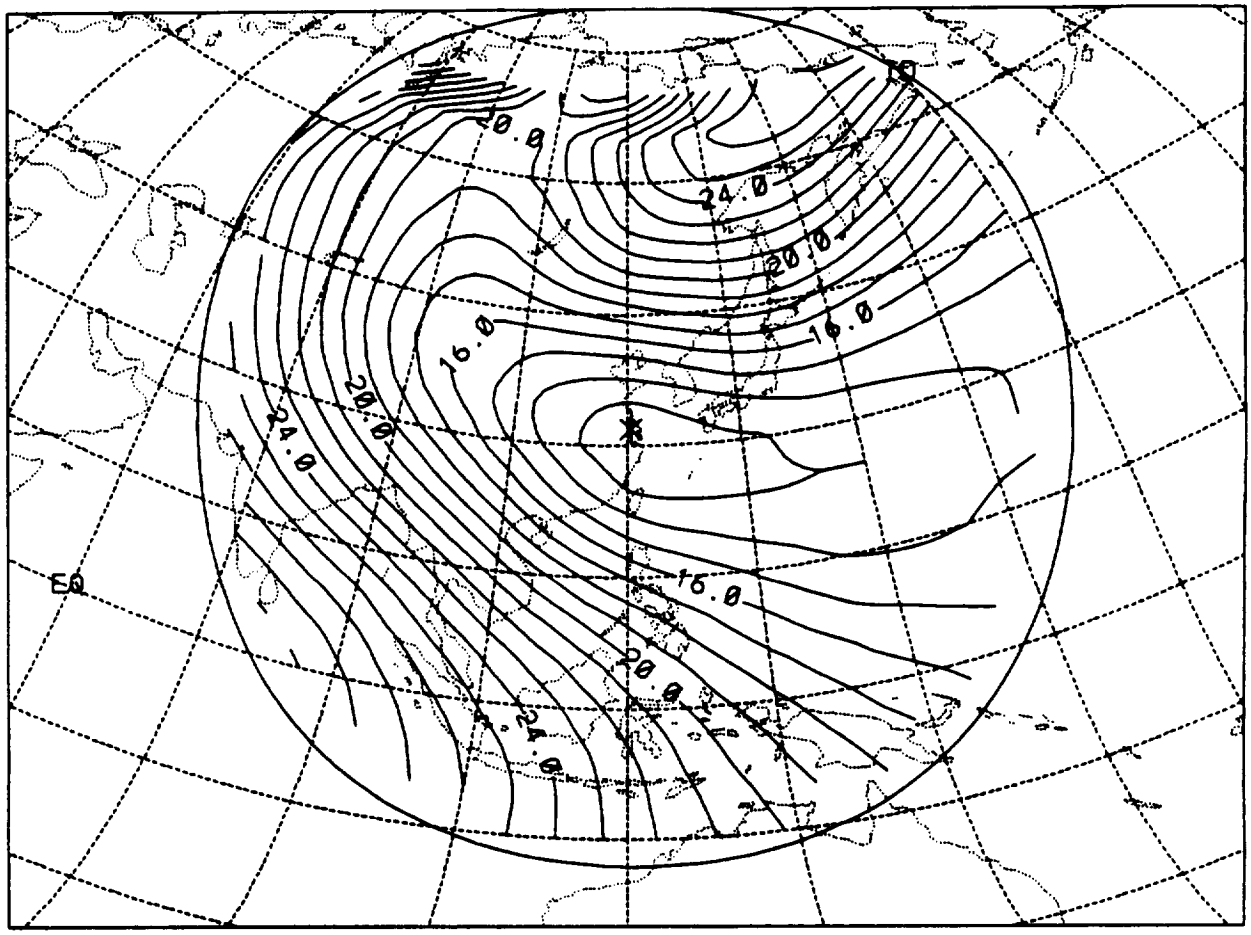

MINIMUM = 12 MM MAXIMUM = 29 MM RMS = 20 MM
CONTOUR INTERVAL = 1 MM

RANGE STANDARD DEVIATION PREDICTED BY GEM-T1
WETTZELL TRACKING LAGEOS ALONG ASCENDING PASSES

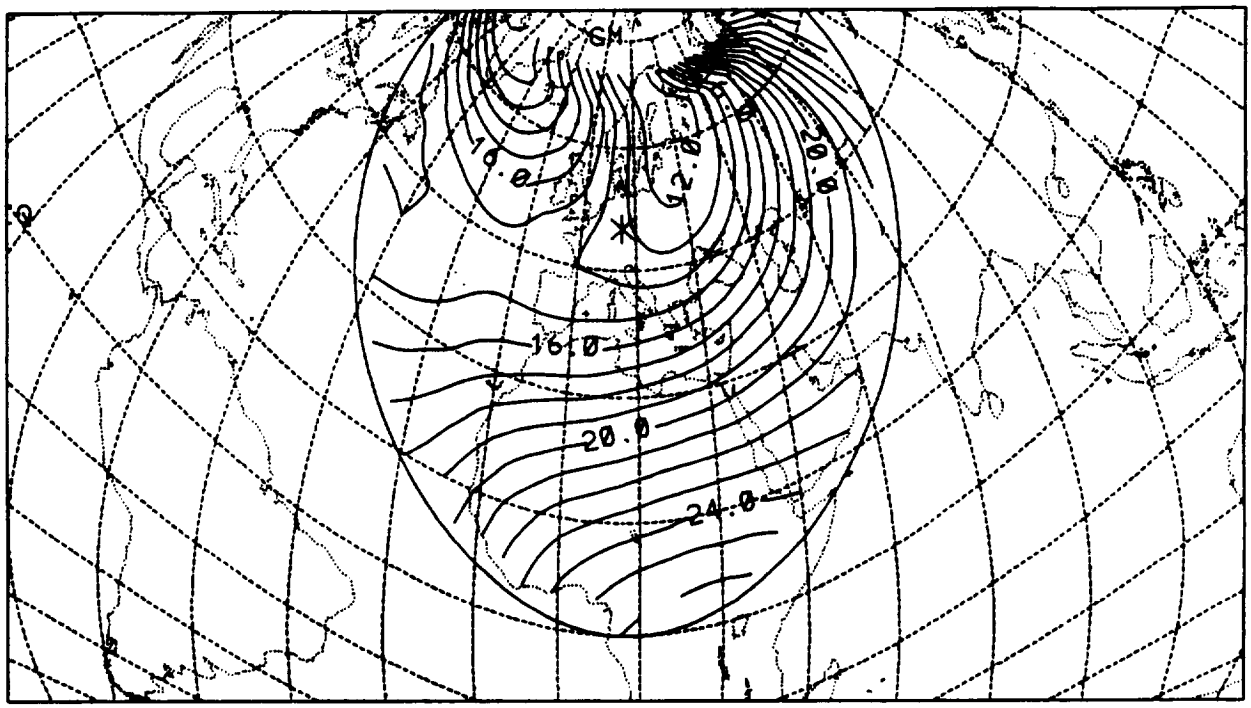

MINIMUM = 11 MM MAXIMUM = 33 MM RMS = 19 MM
CONTOUR INTERVAL = 1 MM

RANGE STANDARD DEVIATION PREDICTED BY GEM-T1
SIMOSATO TRACKING LAGEOS ALONG DESCENDING PASSES

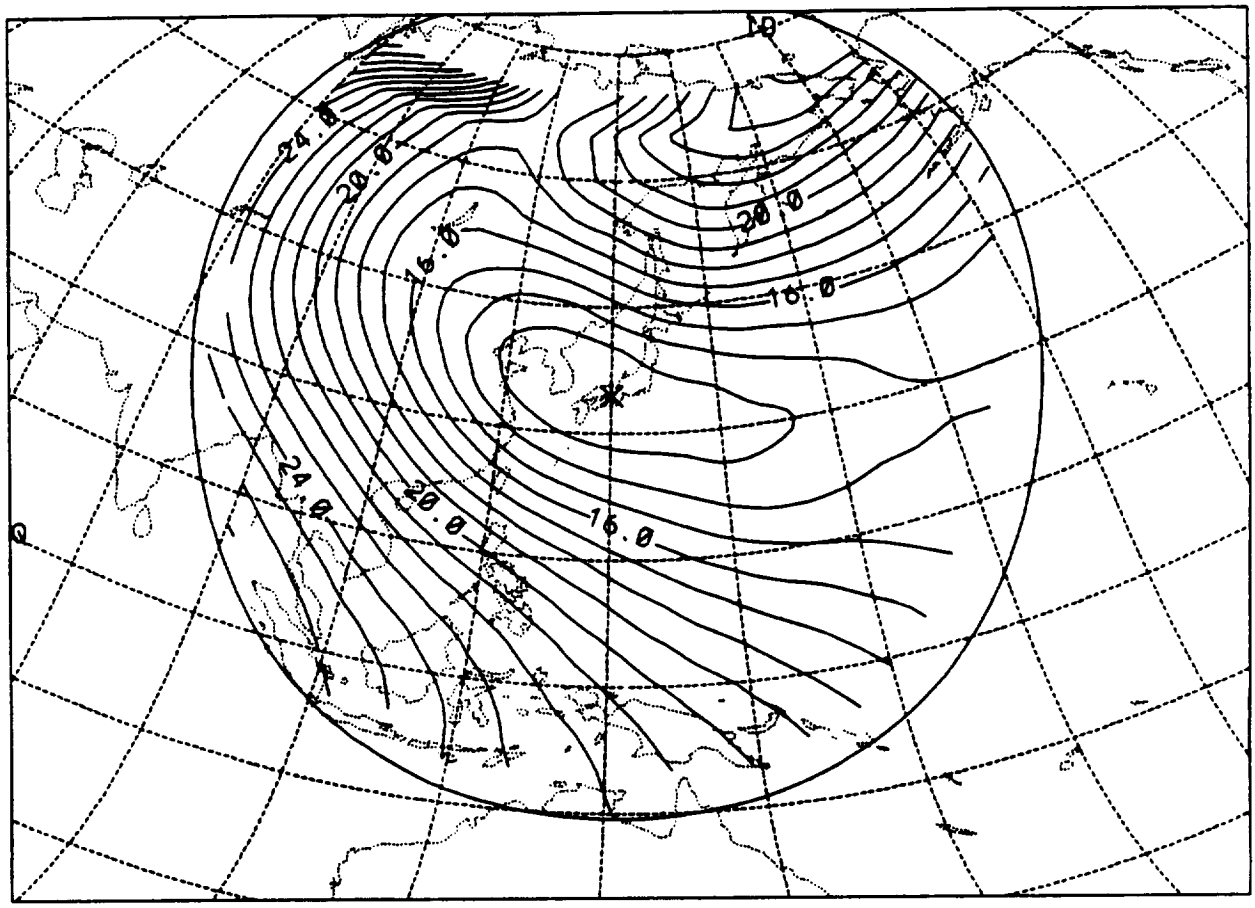

MINIMUM = 12 MM MAXIMUM = 31 MM RMS = 19 MM
CONTOUR INTERVAL = 1 MM

RANGE STANDARD DEVIATION PREDICTED BY GEM-T1
YARAGADEE TRACKING LAGEOS ALONG ASCENDING PASSES

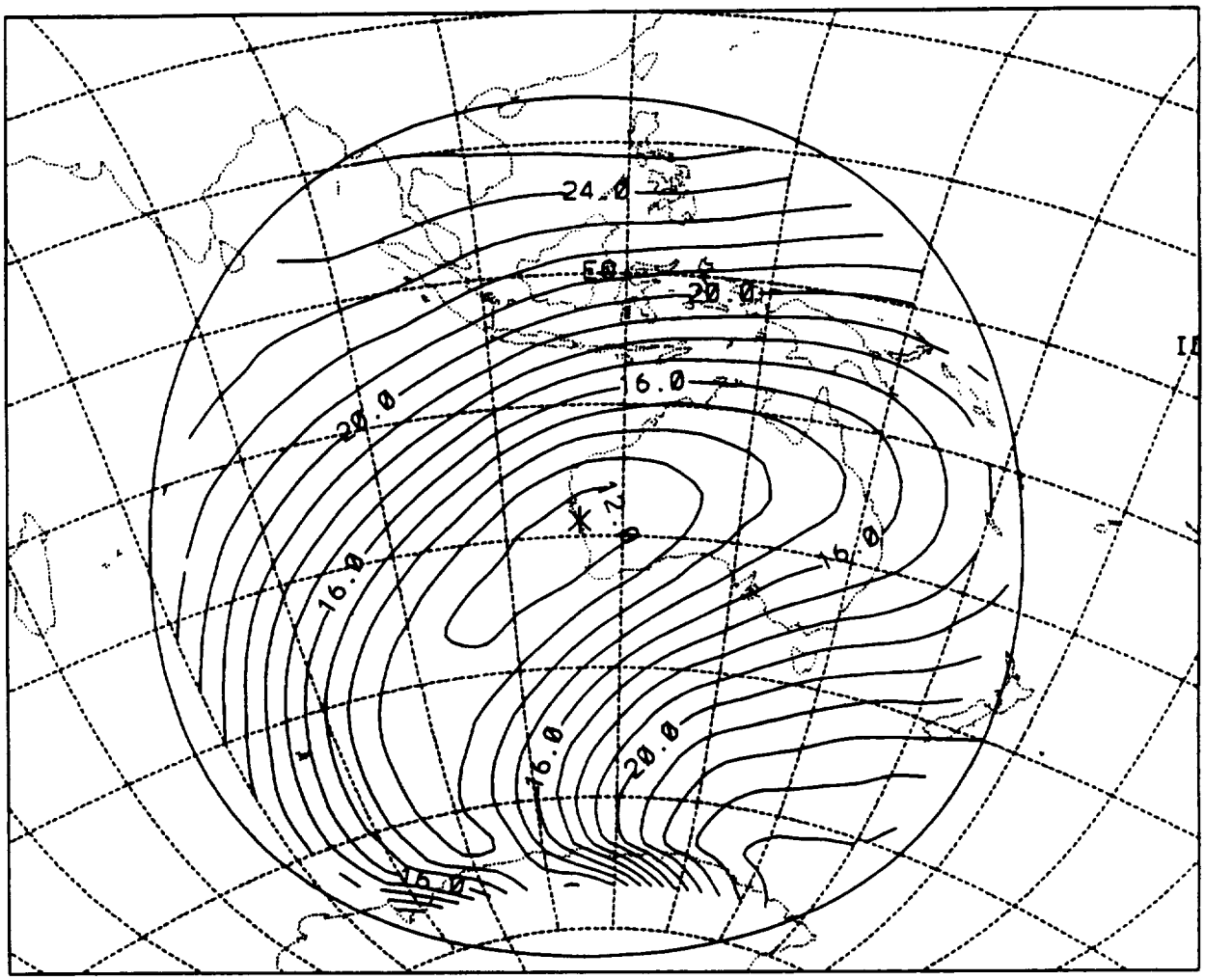

MINIMUM = 11 MM MAXIMUM = 26 MM RMS = 19 MM
CONTOUR INTERVAL = 1 MM

RANGE STANDARD DEVIATION PREDICTED BY GEM-T1
WETTZELL TRACKING LAGEOS ALONG DESCENDING PASSES

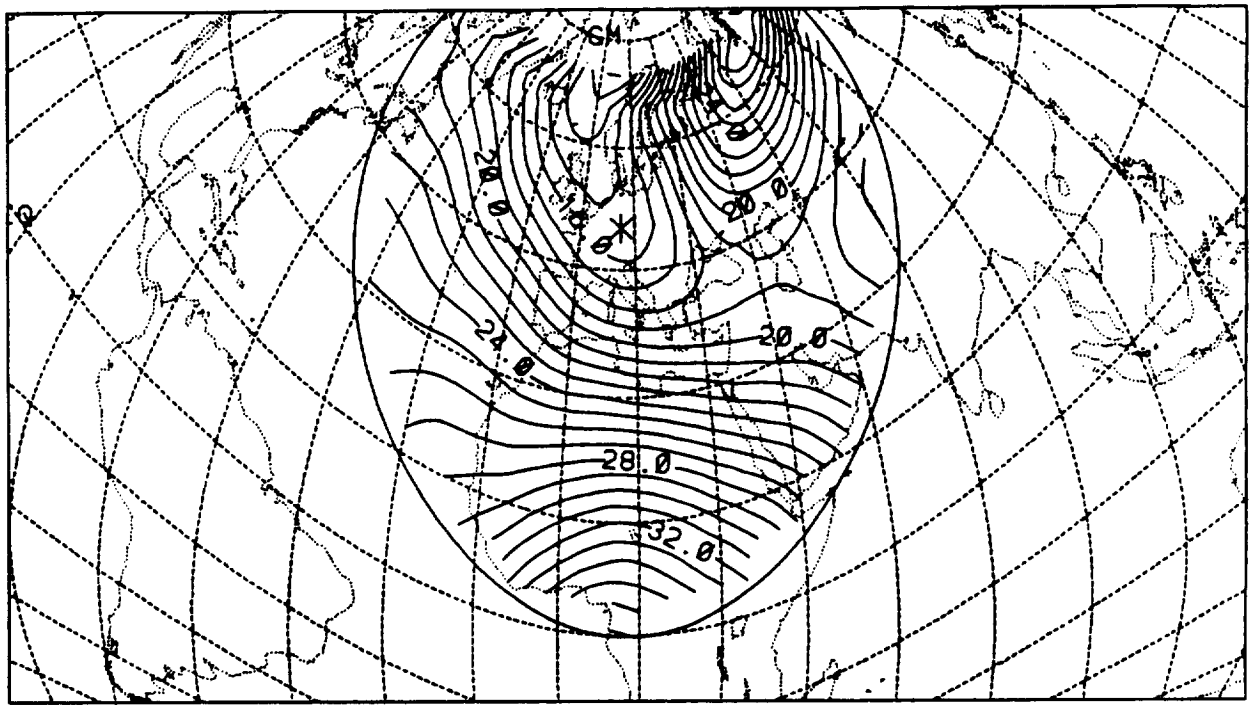

MINIMUM = 12 MM MAXIMUM = 37 MM RMS = 23 MM
CONTOUR INTERVAL = 1 MM

RANGE STANDARD DEVIATION PREDICTED BY GEM-T1
YARAGADEE TRACKING LAGEOS ALONG DESCENDING PASSES

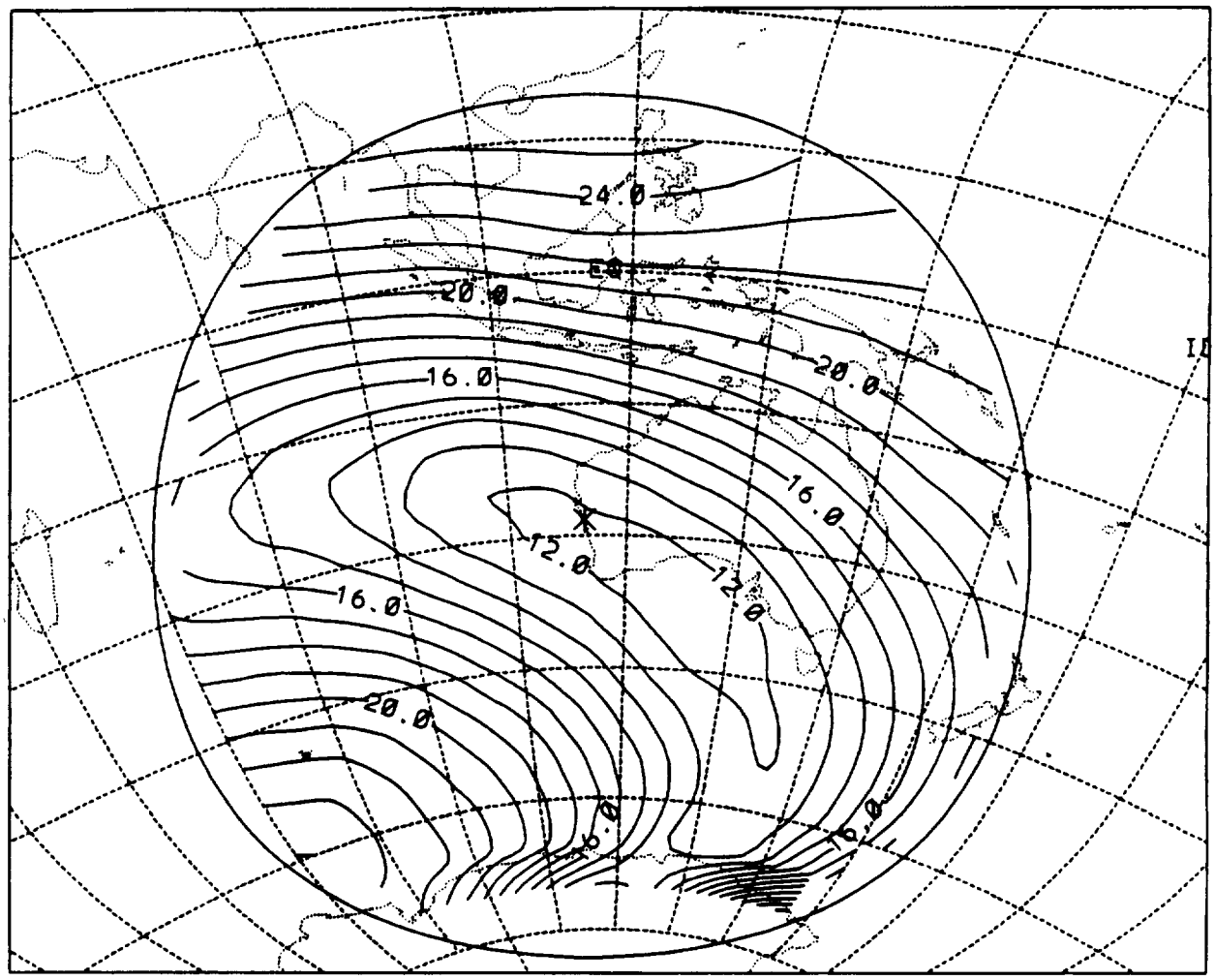

MINIMUM = 11 MM MAXIMUM = 26 MM RMS = 18 MM
CONTOUR INTERVAL = 1 MM